CALVAL / ENVISAT
CLS.DOS/NT/03.733
Issue : 1rev0 **Ramonville, 16 May 2003**
Nomenclature : -

Envisat validation and cross calibration activities during the verification phase. Synthesis Report
ESTEC contract No. 16243/02/NL/FF WP6

		COMPANY	DATE	INITIALS
PREPARED BY	Y. FAUGERE F. MERTZ J. DORANDEU	CLS		
QUALITY VISA	M. DESTOUESSE	CLS		
ACCEPTED BY	J. DORANDEU	CLS		
APPROVED BY	J. BENVENISTE	ESA/ESRIN		

CLS 8-10 Rue Hermès - Parc Technologique du Canal - 31526 Ramonville St-Agne - FRANCE
Telephone 33 5 61 39 47 00 Fax 33 5 61 75 10 14

DISTRIBUTION LIST

COMPANY	NAMES	COPIES
CLS/DOS	J. DORANDEU	1
	Y. FAUGERE	1
	F. MERTZ	1
	M. ABLAIN	1
	G. DIBARBOURE	1
	B. SOUSSI	1
	P.Y. LE TRAON	1
DOC/CLS	N. ROZES	1
ESA	J. BENVENISTE	1
	P. FEMENIAS	1
CNES	N.PICOT	1

List of tables and figures

List of tables :

List of figures :

CONTENTS

1. INTRODUCTION

The near future of altimetry has been recently opened by the successful launch of Envisat. Before data can be used for oceanographic studies and near real-time applications, quality and performances have to be assessed through extensive analyses and comparisons. It is the goal of the verification phase (Benveniste et al., 2002)

This document is the synthesis of the Envisat validation and the cross calibration studies carried out at CLS during the verification phase. This work was performed in the framework of the RA-2/MWR Cross Calibration and Validation Team (CCVT). It was partially funded by the ESTEC contract No. 16243/02/NL/FF, WP6: “EnviSat global statistical analysis”. Cross-calibration results relative to ERS-2 and Jason-1 have also been added as a contribution to the CCVT activities.

Some of the results described here were presented at the CCVT meetings (Frascati, December 2002, March 2003), Validation workshop (Frascati, December 2002) and joint EGS/AGU meeting (Nice, April 2003).

A statistical evaluation of Envisat altimeter data has been carried out to produce a global calibration of this mission. All relevant parameters from altimeter measurements and geophysical corrections are evaluated and tested.

Cross-calibration methods have been developed and applied to assess the consistency of Envisat data with the ERS-2 and Jason-1 missions.

Two specific studies have also been performed: sea ice detection on Envisat data, and a high frequency signal analysis.

2. PROCESSING

2.1. DATA

The data used by the CCVT are GDR cycles 10 to 12 (October 2002 to January 2003). They were produced in February and March 2003, with V4.53 IPF version and the V5.5_02 CMA version.Table 1 shows the data unavailability over these 3 cycles.

	Cycle 10	Cycle 11	Cycle 12
Missing passes (not delivered)	194	195	106
Passes with no radiometer correction	73	116	349
Passes impacted by the F-PAC anomaly (no level 2 processing for some records, all set to default)	26	4	0

Table 1 : Data unavailability

2.2. UPDATES

In order to assess the product quality some updates were necessary:

- Ice flag: The same method as in the ERS-2 OPR quality assessment (e.g. Mertz et al., 2003) has been used for ENVISAT (see algorithm in section 5.1)
- Model ionosphere correction: There is no model available in the product. Thus the Bent and JPL GIM ionosphere corrections are computed to assess the dual frequency and Doris corrections. The GIM model has been computed thanks to the procedures kindly provided by Remko Scharroo to the CCVT (Scharroo, 2002).
- Filtered dual frequency ionosphere correction: A 300-km low pass filter is applied along track on the dual frequency ionosphere correction to reduce the noise of the correction.
- Sigma0 attenuation correction: Indeed, there was an error in the specification of the RAD_PHY_ATT_01 algorithm: the S-Band sigma0 is tested while it should not, and a climatologic value is used when the S-band is not available.

- MWR wet troposphere correction: It is recomputed adding 1dB on Sigma0 as recommended by the MWR community (P. Femenias, E. Obligis, CCVT meeting, March 2003)
- Sea State Bias: different parametric SSB models are computed
- MSS CLS01V1 (Hernandez et al., 2000)

2.3. EDITING

Data editing is necessary to remove altimeter measurements having lower accuracy. There are 3 steps in the editing procedure. The first step is based on flags: the radiometer land/ocean flag and the computed ice flag. Then, measurements are edited using thresholds on several parameters. These thresholds are expected to remain constant throughout the ENVISAT mission, so that monitoring the number of edited measurements allows a survey of data quality. However, these thresholds have been derived from the ERS-2, TOPEX/Poseidon and Jason-1 experience, and may need to be refined for the ENVISAT mission. This is one of the objectives of the verification phase. Table 2 gives for each tested parameter, the minimum and maximum thresholds used in this study.

Parameter	Min threshold	Max threshold
Sea surface height (m)	-130.000	100
Variability relative to MSS (m)	-10	10.
Number of 18Hz valid points	10.	-
Std. deviation of 18Hz range (m)	0	0.2
Off nadir angle from waveform (deg2)	-0.200	0.160
Dry tropospheric correction (m)	-2.500	-1.900
Invert barometer correction (m)	-2.000	2.000
MWR wet tropospheric correction (m)	-0.500	0.001
Bent Ionospheric correction (m)	-0.200	-0.001
Significant wave height (m)	0.000	11.000
Sea state Bias (m)	-0.500	0.000
Backscatter coefficient (dB)	7.000	30.000
Ocean tide height (m)	-5.000	5.000
Long period tide height (m)	-0.500	0.500

Earth tide (m)	-1.000	1.000
Pole tide (m)	-15.000	15.000
RA2 wind speed (m/s)	0.000	30.000

Table 2 : Editing thresholds

The last step uses cublic splines adjustments to the ENVISAT Sea Surface Height (SSH) to detect remaining spurious measurements.

Figure 1 and Figure 2 show respectively valid and edited data. Figure 3 to Figure 13 illustrate the measurements edited by each criterion (threshold method). The maps are given for cycle 11. The thresholds used here seem suitable for ENVISAT. All criteria based on the altimeter measurement quality tend to remove data in areas of strong waves. It is particularly the case for the RMS of Ku range (Figure 7). Wet areas also appear in the maps of edited measurements, probably because of altimeter contamination by rain. Note that we do not use any rain flag in our editing procedure, as this flag had not been tuned in the product during the verification phase. The sea ice edge also appears on this map. This issue is analysed in detail in section 5, dedicated to sea ice detection. Some pass segments in North Atlantic are edited on all altimeter parameter criteria. They correspond to sigma0 passive calibration operations. MWR criteria remove data in wet areas but also at high latitudes. These data have positive radiometer corrections (see 3.2).

From Figure 7 and Figure 16, the 20 cm threshold used for the RMS of elementary Ku-band measurements could be considered too restrictive, particularly in strong sea state conditions. Thus a 25 cm threshold has also been tested. The measurements edited by the RMS of Ku range criterion only, in this 25 cm configuration, are shown on Figure 14. Of course, more points are now kept by this criterion but in areas of strong waves, these measurements are edited due to the other altimeter parameters (e.g. SWH, mispointing) (Figure 15).

3. ALTIMETER AND RADIOMETER QUALITY ASSESSMENT

3.1. ALTIMETER PARAMETERS

3.1.1. Range

Histograms of RMS of Ku and S-band Range are plotted respectively on Figure 16 and Figure 17. The mean of the RMS of 20Hz elementary data is about 9 cm, which corresponds to about 2 cm at 1Hz, assuming uncorrelated 20Hz measurements. It is consistent with the expected value. Figure 18 shows the consistency between the RMS of elementary data of the two bands. Figure 19 shows the wave dependency of the RMS of Ku-band Range.

3.1.2. Sigma0

Histograms of Ku and S-band Sigma0 are plotted respectively on Figure 20 and Figure 21. The Sigma0 has been adjusted on ERS-2 mean to be compliant with the wind speed model (Witter and Chelton, 1991). The histogram in Ku band has a good shape except 2 small peaks on each side of the main peak. The mean value is around 11 dB.

3.1.3. Altimeter wind

The histogram of the Ku-band altimeter wind speed is plotted on Figure 22. There is a local maximum in this histogram at 1.0m/s. This is due to the wind speed model used (Witter and Chelton, 1991). However it is quite consistent with the ECMWF model (Figure 23).

3.1.4. SWH

Histograms of Ku and S-band SWH are plotted respectively on Figure 24 and Figure 25. A new retracking has been implemented in the CMA. The SWH histogram has a good shape. The new retracking has improved the low waves (0-1m) but a zero class has appeared. The locations of these zero values are plotted on Figure 26. The zero class is larger in S-Band.

3.1.5. Dual frequency and Doris ionosphere corrections

Comparisons have been made between the Dual Frequency (DF) ionosphere correction, the Doris one, and two models: Bent and JPL GIM. Figure 27 and Figure 28 show the histogram of DF and Doris corrections. The Doris one is unrealistic, there is clearly a problem on this correction. Figure 29 shows that there is also a problem of calculation over a large area in the south of Australia.

Table 3 shows the differences between the Dual frequency correction and the other corrections.

	Number	Mean (cm)	Standard deviation (cm)
DF-DORIS	782926	-3.8	37.3
DF-BENT	853028	-4.0	2.5
DF-GIM	853028	-1.9	1.7

Table 3 : Ionosphere correction differences on cycle 11

There is a -4 cm bias between DF and Bent corrections. This mean difference was +2.6 cm using the data set produced in November 2002 with the previous IPF version (cycle 10 only). This change is probably due to the use of a wrong value in the characterisation file which impacted the range values in the two bands, and consequently the ionosphere correction. The GIM model seems to be closer to the DF correction than to the Bent model. The 2 scatter plots on Figure 30 and Figure 31 illustrate this result.

3.1.6. Squared mispointing

The histogram of the squared mispointing is plotted on Figure 32. It has a good shape but it has a strong bias of 0.027 deg^2 which corresponds to 0.16 degrees. Investigations are on-going at algorithm level to deal with the bias issue. Figure 33 monitors this parameter through cycles10, 11 and 12. There is an increasing trend, but at this stage, no conclusion can be drawn because of possible seasonal effect in this global mean value. The 3 peaks on the curve are also particular features. They correspond to platform events (manoeuvres, Leonid shower).

3.1.7. S-band anomaly

As mentioned by J. Benveniste (internet communication, November 9, 2002) an anomaly occasionally occurs on the S-Band. This anomaly concerns the “summation of the S-Band power echoes”. It is visible on the Ku-S altimeter parameter differences and particularly for the

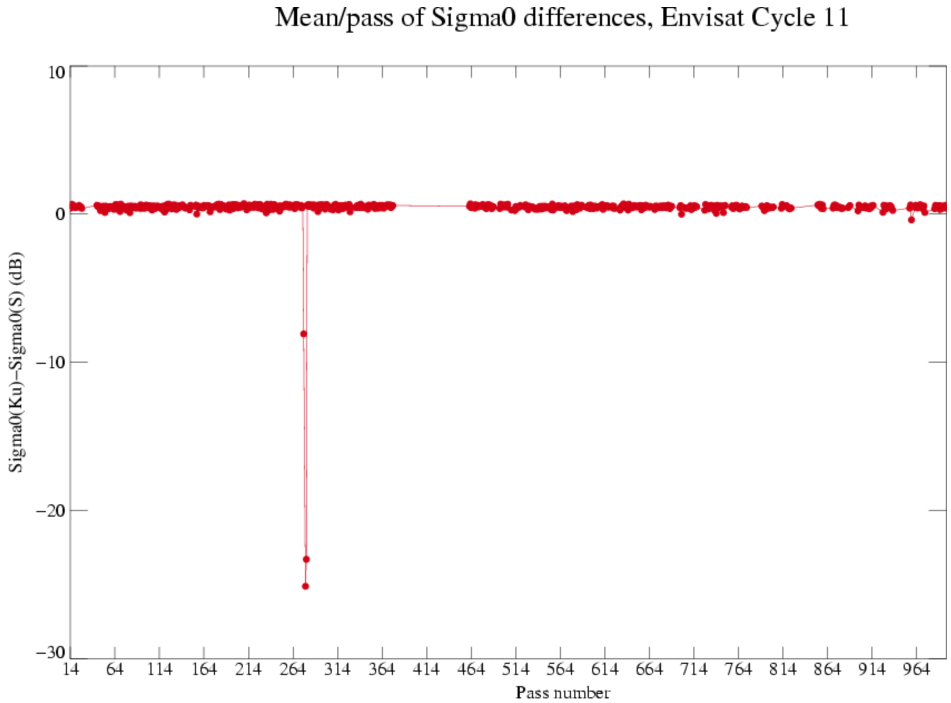

backscatter coefficient (Figure 34,

Figure 35 and Figure 36). A large period is impacted by this anomaly on cycle 10. On cycles 11 and 12, only a few passes are impacted. Consequently the Dual Frequency ionosphere correction is not available during these periods.

<u>Warning</u>: These plots have been performed after data editing. Thus S-band anomalies occurring when no MWR correction is available do not appear.

3.1.8. Time-tag bias

It is computed at crossovers as the regression coefficient of the SSH as a function of the radial velocity. The time tag bias is not significantly different from zero, between -0.2 ms and 0.1 ms on the 3 cycles.

3.2. RADIOMETER CORRECTION

As ENVISAT mean sigma0 value has been adjusted on the ERS-2 one, the MWR correction is quite consistent with the ECMWF model as shown on the scatter plot of Figure 37. But the scatter plot is truncated: positive values of wet troposphere have been removed at the editing step. The differences with the model are plotted on Figure 38. Strong differences are clearly visible at high latitudes. The MWR correction has been recomputed using the same algorithm (parametric) as in the product but by adding 1dB to Sigma0. The new scatter plot is presented on Figure 39. The (MWR-ECMWF) differences have been reduced and there are no more positive values.

3.3. SEA STATE BIAS

The SSB in the product is a 3-parameter SSB with coefficients similar to the ERS-2 mission.

Let us define parametric SSB models as follows:

$SSB=C1*SWH+C2*SWH^2+C3*SWH*U+C4*SWH*U^2$

Where U denotes the wind speed, and SWH the significant wave height.

From cycle 10, different parametric models have been computed: a 1-parameter model (BM1) to estimate directly the wave dependency, another 3-parameter model (BM3) and a 4-parameter model (BM4).

The results for cycle 10 are summarized in Table 4.

	C1	C2	C3	C4
BM1	-0.056022	-	-	-
BM3 from Product	-0.048	-	-0.0026	0.000126
Computed BM3	-0.026664	-	-0.004637	0.000189
BM4	-0.056464	0.004201	-0.003711	0.000130

Table 4 : Parametric SSB coefficients

The BM1 model does not seem significantly different from the ERS-2 one, but this model is too simplistic. Indeed, comparing the BM3 models estimated in this study and from the product (actually the ERS-2 BM3 model) leads to very different results, particularly for the first coefficient (SWH coefficient). This type of parametric estimations will be used for monitoring the ENVISAT SSB behaviour in the long term.

Note that a specific analysis on non-parametric SSB is being performed by Sylvie Labroue. A new non parametric SSB will be soon provided, in order to be implemented in the next GDR version.

3.4. PERFORMANCES AT CROSSOVER

Crossover statistics are calculated using the following algorithms for the SSH:

- ECMWF dry troposphere correction
- Inverted barometer correction with time varying pressure
- Total geocentric GOT99 ocean tide height
- Geocentric pole tide height
- Solid earth tide height
- Wet troposphere correction: product MWR derived, recomputed MWR or ECMWF
- Ionosphere correction: Dual frequency, Doris, Bent, GIM ionosphere correction
- SSB: BM3 from product, BM3 computed , BM1, BM4 or non parametric

Table 5 shows the statistics for different combinations SSB, ionosphere and wet troposphere corrections.

Ionosphere correction	Wet tropo correction	SSB	Cycle 10	Cycle 11	Cycle 12
BENT	MWR product	BM4	10.17 (16012)	9.81 (14286)	8.92 (7826)
DORIS	MWR product	BM4	10.03 (14706)	9.94 (11951)	8.94 (7424)
DUAL	MWR product	BM4	9.80 (5313)	9.38 (14197)	8.64 (7369)
GIM	MWR product	BM4	9.91 (16012)	9.52 (14286)	8.70 (7826)
BENT	MWR product	BM3 product	10.27 (16012)	9.93(14286)	9.01 (7826)
BENT	MWR product	BM3 computed	10.21 (16012)	9.86(14286)	8.98 (7826)
BENT	MWR product	NP	10.30 (16012)	9.91 (14286)	9.03 (7826)
BENT	ECMWF	BM4	10.33 (16012)	9.98 (14286)	9.13 (7826)
BENT	ECMWF	NP	10.41 (16012)	10.02 (14286)	9.18 (7826)
BENT	MWR computed	BM4	10.24 (16774)	9.82 (14660)	9.03 (8269)

Table 5 : Standard deviation of ENVISAT SSH crossover differences, bathymetry < -1000m

The global results are good. The best results are obtained with the Dual frequency, MWR and BM4. However there are more crossover points using the recomputed MWR correction as there are less edited points in this case, especially in dry areas like high latitudes. The non parametric SSB model also leads to good results but is still under development.

The map of the crossover differences using Bent, product MWR and BM4 is plotted on Figure 41.

Different ionosphere corrections have also been tested in terms of performances on a common crossover data set (Table 6).

	Cycle 10 (3153)	Cycle 11 (5808)	Cycle 12 (3333)
DUAL	8.54	7.55	7.33
DUAL filtered	8.51	7.51	7.30
Doris	9.07	8.05	7.46
Bent	9.09	8.00	7.79
GIM	8.71	7.70	7.69

Table 6 : Standard deviation of SSH differences at crossovers on a common data set, bathymetry<-1000m, |ΔT|<10j

Using the Dual frequency gives the lower standard deviation. GIM is the best ionosphere correction model.

3.5. SLA RELATIVE TO MSS

Statistics on [SSH –MSS CLS01] are calculated in different configurations (Table 7). The first line gives the results in the product configuration. This mainly allows estimating the impact of each correction on the ENVISAT bias. In the following results, a constant bias of 73.68 cm has been corrected for, since it comes from an error in the characterisation file used to produce the present ENVISAT dataset.

SSH = Orbit –Range –IB –Dry_Tropo –MWR_Wet_Tropo -DF_Iono –SSB –Earth_Tide –GOT99_Ocean_Tide-Pole_Tide -73.68

The other lines show the impact of each algorithm.

Changes / GDR	Bias (cm)	Std (cm)
-	49.5	10.1
iono Bent	45.1	10.3
Iono GIM	47.6	10.2
wet tropo corrected	50.2	10.1
ECMWF wet tropo	50.9	10.2
BM4	50.7	10.0
NP SSB	46.5	10.1
wet tropo corrected, NP SSB (Optimal configuration ?)	47.2	10.1
Iono GIM, ECMWF wet tropo (Model configuration)	49.0	10.3

Table 7 : (SSH - CLS01 MSS) statistics, bathymetry<-1000m

The Envisat bias is about 45-51 cm depending on the algorithms used.

The map of [SSH –MSS] is plotted on Figure 40.

4. CROSS CALIBRATION

Comparisons with ERS-2 and Jason-1 have been performed by computing, on one hand, along track residuals between ERS-2 and ENVISAT and, on the other hand, crossovers between Jason and ENVISAT. Indeed, ENVISAT and ERS-2 have the same ground track and the time difference between both satellites is about 28 mn. Cycles 78 to 80 and cycles 25 to 37 have been used for ERS-2 and Jason respectively.

4.1. WITH ERS-2

4.1.1. Updates of the ERS-2 OPR product

A preliminary work was to update ERS-2 data to make them homogeneous with ENVISAT ones. We used the following fields from the ERS-2 product:

- DPAF orbit
- Dry troposphere correction from ECMWF
- Bent ionosphere correction
- Earth tide correction from product
- SWH

and the following fields have been computed and/or updated:

- Range corrected for time tag bias, SPTR2000 and OSU drift (Martini and Féménias, 2000)
- Inverse barometer with time varying pressure
- Radiometer wet troposphere correction corrected for gain drop and TB drift (Obligis et al., 2003)
- GIM ionosphere correction (following Remko Scharroo procedure).
- Sigma0 bias applied corrected (Dorandeu et al, 2000)
- BM3 sea state bias (Wind Speed recomputed from Sigma0 corrected)
- GOT99 oceanic tide correction
- Polar tide correction

4.1.2. SWH comparisons

The (ERS-2 – ENVISAT) SWH difference is –21 cm (Table 8). Figure 42 shows the histogram of SWH values for the whole ERS-2 cycle 79. The noticeable point is the number of 0-values measurements, also high in the ENVISAT histogram (Figure 24). Figure 43 and Figure 44 show scatter plots respectively of ERS-2 SWH versus ENVISAT SWH and (ERS-2 – ENVISAT) SWH differences versus ENVISAT SWH. The last plot indicates that in strong wave height areas, the difference between the two satellites is higher than in weaker areas: SWH differences are 20 cm higher at 8m-waves than at 1m-waves as evidenced on Figure 45: the differences are higher in regions of strong sea states.

	Cycle 10	Cycle 11	Cycle 12
Number of measurements	973646	941859	761327
Mean (cm)	-21	-21.2	-20.7
Standard deviation (cm)	26.8	27	26.8

Table 8 : (ERS-2 – ENVISAT) SWH statistics in cm for cycles 10 to 12.

4.1.3. SIGMA0 comparisons

ERS-2 Sigma0 has been corrected for the recommended bias (Dorandeu et al., 2000). Statistics are very close (Table 9) but the shape of the histogram for ENVISAT is significantly better than that of ERS-2 (Figure 20 compared to Figure 46). Figure 47 and Figure 48 show scatter plots respectively of ERS-2 Sigma0 versus ENVISAT Sigma0 and (ERS-2 – ENVISAT) Sigma0 differences versus ENVISAT Sigma0. Particular features on the scatter plot (Figure 48) may come from the shape of ERS-2 histogram (Figure 46).

Figure 49 and Figure 50 respectively present maps of Sigma0 differences with and without the contribution of the atmospheric attenuation for both satellites. A tropical zone appears in Figure 49 explained by the computation of ERS-2 attenuation correction. Indeed contrary to ENVISAT, it only takes into account the cloud liquid water delay and neglects the contribution from water vapor and oxygen.

	Cycle 10	Cycle 11	Cycle 12
Number of measurements	973646	941859	761327
Mean (dB)	0.059	0.063	0.04
Standard deviation (dB)	0.28	0.26	0.29

Table 9 : (ERS-2 – ENVISAT) SIGMA0 statistics in dB for cycles 10 to 12.

4.1.4. Comparison of ionosphere corrections from models

Comparisons have been performed on BENT ionosphere correction. The mean difference is -3.4 mm (Table 10). Most of the difference is obtained in the geomagnetic equatorial region (Figure 51). A large band is visible in this region and indicates that the bias is systematic. Such differences are not surprising since there is a variation of the local hour (28 mn) between the two satellites.

An update of both products has been performed with the GIM model correction. As shown in Table 10, the mean difference value is now 1.3 mm. The major differences are also located in geomagnetic equatorial region (Figure 52).

		Cycle 10	Cycle 11	Cycle 12
BENT Model	Number of measurements	973646	941859	761327
	Mean (mm)	-4.4	-3.3	-2.5
	Standard deviation (mm)	4.5	3.9	3.1
GIM model	Number of measurements	973646	941859	761327
	Mean (mm)	1.5	1.3	1.2
	Standard deviation (mm)	6.05	4.9	4.8

Table 10 : (ERS-2 – ENVISAT) BENT and GIM ionosphere corrections statistics in mm for cycles 10 to 12.

4.1.5. Comparisons of wet troposphere corrections

Two kinds of ECMWF outputs are used to compute the model wet troposphere corrections: Gaussian grids are used for ENVISAT while rectangular grids are used for ERS-2. A 7 mm bias is obtained for the mean difference (Table 12) but discrepancies are not homogeneous (Figure 53). Geographical patterns appear depending on wet and dry areas, and near the coasts.

	Cycle 10	Cycle 11	Cycle 12
Number of measurements	973646	941859	761327
Mean (mm)	7.1	7.03	6.88
Standard deviation (mm)	9.2	9.1	9.1

Table 11 : (ERS-2 – ENVISAT) ECMWF model wet troposphere corrections statistics for cycles 10 to 12.

To perform radiometer wet troposphere corrections comparisons, a TB drift correction was applied on ERS-2 (Obligis et al., 2003), and the ENVISAT radiometer correction was computed applying +1 dB on sigma0. The global mean is -4.7 mm (Table 12) and the scatter plot (Figure 54) shows a good consistency between the two corrections except for dry regions, where ERS-2 underestimates this correction.

	Cycle 10	**Cycle 11**	**Cycle 12**
Number of measurements	973646	941859	761327
Mean (mm)	-4	-4.7	-5.32
Standard deviation (mm)	10.7	10.8	10.6

Table 12 : (ERS-2 – ENVISAT) MWR wet troposphere correction differences statistics in mm for cycles 10 to 12. ERS-2 corrected.

4.1.6. SSH comparisons

The SSH comparisons have also been performed by repeat-track analysis. An initial configuration has been computed as described in

initial configuration	**ENVISAT**	**ERS-2**
Orbit	CNES (product)	DPAF (product)
Range	product	Product + SPTR2000 + USO drift + time tag bias
Inverse barometer	time varying pressure (product)	Time varying pressure (computed)
Dry troposphere	product	Product
Wet troposphere	ECMWF (product)	ECMWF (product)
Ionosphere	GIM	GIM
SSB	BM4 (computed)	BM3 (computed)
Ocean tide	GOT99	GOT99
Earth tide	product	Product
Pole tide	product	Computed

Table 13.

initial configuration	ENVISAT	ERS-2
Orbit	CNES (product)	DPAF (product)
Range	product	Product + SPTR2000 + USO drift + time tag bias
Inverse barometer	time varying pressure (product)	Time varying pressure (computed)
Dry troposphere	product	Product
Wet troposphere	ECMWF (product)	ECMWF (product)
Ionosphere	GIM	GIM
SSB	BM4 (computed)	BM3 (computed)
Ocean tide	GOT99	GOT99
Earth tide	product	Product
Pole tide	product	Computed

Table 13 : Initial parameters used to compute SSH for ENVISAT and ERS-2.

The standard deviation obtained for SSH residuals is around 8 cm (Table 14). A great part of this high value may be explained by large ERS-2 orbit errors as illustrated in section 4.1.7. A global mean bias of –41.95 cm is obtained for the initial configuration (the results are corrected for the 73.68 cm bias introduced in the characterisation file). In order to reduce as much as possible the differences between both SSH, the ENVISAT dry troposphere correction was updated using the rectangular grids as for ERS-2: the SSH difference is then reduced to –41.25 cm (Table 14).

Several configurations have been tested: for each configuration, one of the corrections is changed in the ENVISAT SSH computation (e.g. non parametric SSB) or for both ENVISAT and ERS-2 (BENT ionosphere correction and wet troposphere radiometer correction). Statistics are then calculated in each case and the results are summarised in Table 14.

Configuration		Cycle 10	Cycle 11	Cycle 12
Initial	Number of measurements	973646	941859	761327
	Mean (cm)	-42.02	-41.82	-41.92
	Standard deviation (cm)	7.9	8.3	8.2
ENVISAT ECMWF tropo with rectangular grids (EN)	Mean (cm)	-41.42	-41.12	-41.22
NP SSB (EN)	Mean (cm)	-38.42	-38.02	38.12

Radiometer wet tropo (EN/E2)	Mean (cm)	-40.92	-40.62	40.7
Bent Iono (EN/E2)	Mean (cm)	-41.52	-41.12	41.43

Table 14 : Statistics of (ERS-2 – ENVISAT) SSH differences for several configurations.

With the NP SSB, the mean is 38.18 cm, but further investigations are still on-going: a new NP SSB model estimation will be implemented in the next GDR version.

The global mean with the radiometer correction is –40.75 cm and it is -41.36 cm with the BENT ionosphere correction model. These results are consistent with those obtained from the comparisons relative to the MSS (section 3.5).

4.1.7. Comparisons of SSH after orbit error correction

Orbit error corrections have been performed using adjustments relative to Jason as described in Le Traon and Ogor, 1998. Large orbit errors induce a high standard deviation in along-track SSH comparisons (section 4.1.6): about 8 cm, mainly due to ERS-2 DPAF orbit error. Indeed, correcting for the adjusted orbit error leads to reduce the ERS-2 RMS from 13.9 to 11.7 cm and ENVISAT RMS from 11.5 to 10.8 cm. The major improvement is obtained for ERS-2, as the ENVISAT orbit is more precise.

The orbit error correction also makes the ENVISAT / ERS-2 differences more consistent: the standard deviation of the (ERS-2 – ENVISAT) SSH differences is reduced to 3.8 cm. This improvement is clearly evidenced on maps of along-track SSH differences in Figure 56 and Figure 57: many passes appear in Figure 56 and the differences in Figure 57 have been much improved. There are still some discrepancies located in the tropical zone due to the ERS-2 geographically correlated orbit error compared to JGM3 orbits (Le Traon and Ogor, 1998).

4.2. WITH JASON

4.2.1. Jason – ENVISAT dual-crossovers

Dual crossovers are computed with a 10-day time lag for SSH differences, and with a 3-hour time lag for altimeter parameters in order to reduce geophysical variability. The geographical coverage is homogeneous (Figure 58): no particular region is systematically removed from statistics.

4.2.1.1. SWH and SIGMA0 comparisons

The global SWH mean value is 14 cm, Envisat being higher than Jason. The standard deviation is 26.1 cm. Sigma0 global mean value is 0.65 dB and the standard deviation is 0.4 dB. The scatter plots (Figure 59 and Figure 60) show a good consistency.

		Cycle 10	Cycle 11	Cycle 12
SWH	Number of measurements	723	1166	645
	Mean (cm)	15.	13.21	13.8
	Standard deviation (cm)	26.3	25.4	26.6
SIGMA0	Number of measurements	723	1166	645
	Mean (dB)	-0.71	-0.62	-0.62
	Standard deviation (dB)	0.4	0.4	0.4

Table 15 : Crossover statistics for (Jason – Envisat) SWH crossover differences.

4.2.1.2. Ionosphere and troposphere comparisons

Dual-Frequency and DORIS ionosphere corrections have been compared (Table 16). As shown is section 3.1.5, there is clearly a problem in the ENVISAT DORIS ionosphere correction which explains the high standard deviation in cycle 10. The Dual-Frequency corrections are close together.

		Cycle 10	Cycle 11	Cycle 12
Dual-Frequency /Dual-Frequency	Number of measurements	396	1162	628
	Mean (cm)	-1.4	-1.4	-0.62
	Standard deviation (cm)	1.9	2.1	2.66
DORIS/ DORIS	Number of measurements	639	1068	621
	Mean (cm)	-1.5	1.36	0.06
	Standard deviation (cm)	16.8	3.34	2.02

Table 16 : Crossover statistics for (Jason – Envisat) Dual-Frequency and DORIS ionosphere corrections differences.

The mean difference between the two radiometer corrections is about 1 cm (Table 17) and the consistency is rather good (Figure 62) also indicated by the low standard deviation value.

	Cycle 10	Cycle 11	Cycle 12
Number of measurements	723	1166	645
Mean (cm)	1.53	0.98	1.44
Standard deviation (cm)	1.25	1.51	1.15

Table 17 : Crossover statistics for (Jason – Envisat) radiometer wet troposphere corrections.

4.2.1.3. SSH comparisons

SSH comparisons have been computed on dual-crossover differences with a 10-day time lag, in deep ocean areas (bathymetry < -1000 m). The following table summarises the corrections used on the two satellites for SSH computation in the initial configuration:

initial configuration	**ENVISAT**	**JASON**
Orbit	CNES (product)	CNES (product)
Range	product	product
Inverse barometer	time varying pressure (product)	time varying pressure (product)
Dry troposphere	product	Product
Wet troposphere	ECMWF (product)	ECMWF (product)
Ionosphere	GIM	Dual Frequency
SSB	BM4 (computed)	BEM NP (updated)
Ocean tide	GOT99	GOT99
Earth tide	product	product
Pole tide	product	product

Table 18 : Parameters used to compute SSH for ENVISAT and Jason.

Statistics have been computed for the initial configuration and for several other cases, changing one the ENVISAT corrections (e.g. MWR radiometer wet troposphere correction, non parametric SSB). The Jason-1 configuration remains the same. The results are given in the following table after correcting for the 73.68 constant bias (from characterization file).

Configurations		Cycle 10	Cycle 11	Cycle 12
Initial	Number of measurements	59103	58354	54854
	Mean (cm)	34.12	34.22	33.68
	Standard deviation (cm)	8.21	7.9	7.5
MWR wet tropospere	Mean (cm)	32.92	33.12	32.68
computed (Envisat)	Standard deviation (cm)	8.15	7.81	7.48
NP SSB (Envisat)	Mean (cm)	29.92	29.92	29.81
	Standard deviation (cm)	8.28	7.96	7.57

Table 19 : Statistics of (ENVISAT – Jason-1) SSH crossover differences for several configurations of ENVISAT corrections.

For the initial configuration, the global mean is 34.22 cm and standard deviation is 8 cm. The dual crossover performances are very good compared to individual results. With the MWR wet troposphere correction, the mean is 32.9 cm and standard deviation is 7.8 cm and with non parametric SSB (NP SSB), the mean is 29.9 cm and standard deviation 7.9 cm. Applying the NP SSB correction strongly reduces the mean value as in Envisat/ERS-2 comparisons. The standard deviation is also reduced in the two last configurations, as expected.

Note that the NP SSB correction is not the final SSB solution since it will be further investigated by Sylvie Labroue (CLS).

A map of SSH 10-day dual crossovers has been plotted (Figure 63). Good overall consistency is obtained, even if some discrepancies appear due to residual orbit errors.

4.2.2. General comparisons on same time/space sampling

It is interesting to compute statistics from the same geographic area and from the same time period, since both satellites should give comparable general results. ENVISAT data are selected from a 10 day period corresponding to Jason-1 cycle 31, over the same geographic area (-66°S < latitude < 66°N). Performances at crossovers are compared, for the two satellites, in the following table:

	ENVISAT	JASON
Number of crossovers	2232	6555
Standard deviation of crossovers	8.1 cm	8.1 cm

POE orbit, filtered iono, BM4 (ENVISAT) NP SSB (Jason)		
Standard deviation of crossovers Bathy < -1000m	7.1 cm	6.7 cm

Table 20 : Crossover statistics from Jason cycle 31 and a comparable selection of ENVISAT data.

The quality of the ENVISAT data is nearly at the same level than that of Jason at crossovers (8.1 cm) though it is a bit lower when selecting only deep ocean areas. However this kind of comparison results will have to be confirmed because in this particular dataset the number of ENVISAT crossovers is very small due to S-band and MWR data unavailability.

5. SEA ICE DETECTION

The purpose of this study is to define a simple, straightforward, empirical method to detect sea ice. First the method used on ERS-2 is applied on ENVISAT data. Then the peakiness parameter, available in the GDR product is tested. Finally an algorithm combining these two methods is proposed.

5.1. ERS-2 ALGORITHM

This algorithm has been developed by J. Stum for ERS-2 OPR quality assessment. The ice flag is set if at high latitude one of the 2 conditions is true:

- |Latitude| >50
- **N_{20Hz} criterion**: the number of 20Hz valid data < 17
  Or
  MWR criterion: |MWR–ECMWF| > 10cm
  Where MWR is the radiometer wet troposphere correction and ECMWF the model one.

Figure 66 and Figure 67 illustrate the “efficiency” of these two criteria. The N_{20Hz} criterion only flags a few points whereas the MWR criterion flags a large amount of data in the north and in the south. Thus all the work is done by the MWR criterion. That seems specific to ENVISAT. So it can be a problem when the MWR correction is not available.

The sea ice measurements retrieved by the ERS-2 full method are plotted on Figure 68. This method seems to work well on ENVISAT data. However it is not perfect: there are measurements which have been missed in the middle of the pack ice.

Figure 69 points out another drawback of this method. It shows the ocean data where RMS of Ku range is greater than 20cm. There is a band of data along the ice/ocean transition. The waveforms have apparently been corrupted by sea ice. These data should have been ice-flagged.

Figure 70 illustrates this problem on a particular pass. South of 61.7S, the altimeter measurements are corrupted by sea ice. There is no impact on N_{20Hz}. On the ocean/ice transition, the MWR/ECMWF difference increases gradually to exceed 10 cm at 62S. 5-10 of points have been missed by the ERS-2 method between 61.7S and 62S

5.2. PEAKINESS INFORMATION

On Envisat there is a parameter which does not exist on ERS-2, the peakiness parameter. This parameter is derived from the waveforms. It is proportional to the maximum/mean ratio of the waveform. Figure 71 shows the histogram of peakiness valueson ocean data. The peakiness ranges between 1.6 and 1.8 and the mean is about 1.7.

Figure 72 shows the map of this peakiness parameter. Red points correspond to peakiness >1.9. The sea-ice signature is clearly evidenced. However the zoom over Antarctic shows values around 1.7 in the middle of the pack ice. Depending on the season, 0 to 5 % of the sea ice shows an “ocean-like peakiness” (Seimour Laxon, March 2003, Internet communication).

We tried to apply a threshold on peakiness to see how ice is retrieved. Figure 73, Figure 74 and Figure 75, show respectively the ice and the ocean data for a threshold of 1.8, 1.9 and 2.0. It is globally efficient but for thresholds of 1.8 and 1.9, many points in open ocean are ice-flagged. On the other hand, even with a 1.8 threshold, not all the sea-ice is retrieved, as said previously.

But on the particular pass (Figure 79), we can see that the ice/ocean is better described with the peakiness than with the MWR-ECMWF differences. As soon as the waveform is corrupted, the peakiness value is immediately higher than 2.

5.3. COMBINATION OF ALTIMETER AND RADIOMETER CRITERIA

The 2 methods seem to be complementary. The MWR criterion is quite reliable except on ice/ocean transitions. Adding a peakiness criterion, with a 2.0 threshold, improves the sea ice detection in these areas. Figure 77 shows this improvement for cycle 10 to 12. 5000 to 10000 (1 to 2%) points have been detected thanks to the addition of the peakiness criterion.

Finally, the proposed algorithm for Envisat is defined as follows. The ice flag is set if:

- |Latitude| >50
- **N_{20Hz} criterion**: the number of 20Hz valid data < 17
  Or
  MWR criterion: |MWR–ECMWF| > 10cm
  Or
  Peakiness criterion: Peakiness>2

6. NOISE AND HIGH FREQUENCY ANALYSIS

6.1. INTRODUCTION

The present study is based on user products and aims at analysing the high frequency signals. Two types of methods are used: spectral analysis and high pass filtering. The two methods are presented in the diagram below. They are applied to the $SLA_{nc/MSS}$ signal of Envisat where:

$SLA_{nc/MSS}$= Raw SSH – MSS CLS 01V1

Raw SSH means not corrected for any geophysical correction. We have selected 10 days of cycle 11 (November 9, 2002 to November 19, 2002) and compared the results with the same period of Jason-1 (Cycle 11) and ERS-2 (cycle 79). A selection on latitude (<60°) and on bathymetry (<-500m) has been performed to get 3 consistent datasets.

The two methods have been applied on elementary 20Hz data and 1Hz data.

Analysis of High Frequency Signals

We use a high-pass filtering technique (Tran et al., 2001) to estimate a HF signal on the Sea Level Anomaly.

SLA relative to a MSS or from repeat-track analysis

Lanczos low-pass filter

Low frequency signal S_{LF}

High frequency signal $S_{HF} = SLA - S_{LF}$

STD of HF signal integrates:
- instrumental noise
- residual geoid signal
- and possibly HF ocean signals

Spectral Analysis

The power spectrum of $\varepsilon(t)$, a pure white noise (i.e a random variable with Gaussian distribution) with standard deviation equal to σ is :

$$S_{\varepsilon}(k) = \alpha = 2\,\Delta t\,\sigma^2$$

where Δt is the resolution of the signal sample

Therefore, if the signal to analyze is $X(t) = s(t) + \varepsilon(t)$, the power spectrum will be composed of :

- the spectrum of the oceanic signal s
+
- the spectrum of the noise ε (i.e α)

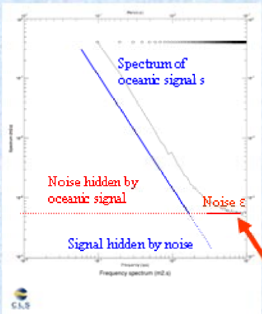

Plateau α

A plateau on a power spectrum can be the signature of a white noise. The STD of its distribution can be obtained by :

$$\sigma = \sqrt{\frac{\alpha}{2.\Delta t}} \quad \text{(I)}$$

Two methods for a single result

Computing the variance of high frequency filtered signals is equivalent to integrating the power spectrum of the original signal from the cut-off frequency fc to the Shannon frequency fs (highest frequency available on a signal).

If the original signal contains white noise, the high frequency part of the power spectrum is constant (plateau) and equal to α, hence :

$$V(fc) = \int_{fc}^{1/2\Delta x} Sp(f).\delta f \rightarrow V(fc) = \alpha\left(\frac{1}{2\Delta x} - fc\right) \quad \text{(II)}$$

The HF method gives the value of V(fc), i.e the energy of HF signal. But, the slope of V(fc) is a direct measurement of the spectral plateau α.

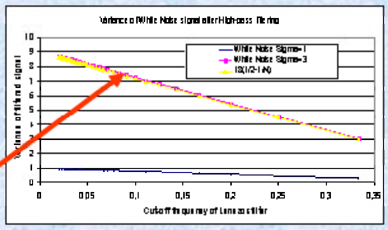

Slope α

6.2. ANALYSIS ON 20HZ DATA

6.2.1. Global results

Figure 78 shows the power spectrum of ENVISAT. It decreases until 3Hz with a swelling around 0.4Hz. At frequencies greater than 3Hz the signal is hidden by a plateau at 10^{-3} m²/cps which corresponds to a white noise of

$$\sigma_{20Hz} = \sqrt{\frac{\alpha}{2 * \Delta t}} = \sqrt{\frac{10^{-3}}{2 * 0.0557}} = 9.5cm$$

Assuming uncorrelated 20Hz measurements, it is equivalent at 1Hz to

$$\sigma_{equiv.1Hz} = \frac{\sigma_{20Hz}}{\sqrt{20}} = 2.1cm$$

Warning: This is only computed to give an order of magnitude at 1 Hz. As explained below this formula is not relevant.

Figure 79 shows the power spectrum of Jason. It has a similar shape as ENVISAT with a plateau at 6.10^{-4} m²/cps which corresponds to a white noise of 7.3cm (1.6cm at 1Hz). The swelling is still more pronounced. Using residuals (SLA relative to a mean profile), to remove short wave length of Geoid, does not change the shape of the spectrum. This feature has no explanation so far.

The plateau we observe on 20Hz data will not be visible on 1Hz data because it begins at frequencies higher than 1Hz. So, even if there is a plateau on 1Hz-spectrum, the equation $\sigma_{1Hz} = \sigma_{20Hz}/\sqrt{20}$ should not be used.

Now, using the high pass filtering method, we plot the energy of the high frequency according to the cut-off wavelength (Figure 80) and the cut-off frequency (Figure 81). On this last plot, we can see that the curves become linear at 0.4 km^{-1} (2Hz). The noise is estimated from the slope of each straight line. The last two points of each curve are used for the computation of the slope. Results are summarized in Table 21.

	Envisat 20Hz	Jason 20Hz
Mean of SWH (m)	2.77	2.71
Noise estimated by high pass filtering method, deduce from the slope (cm)	9.2 (2.1)	7.3 (1.6)
Noise estimated by spectral analysis, deduced from the slope (cm)	9.5 (2.1)	7.3 (1.6)

Table 21 : Noise estimation of $SLA_{nc/mss}$ using 20 Hz elementary data

6.2.2. Geographic distribution

The geographic distribution of this high frequency signal is mapped on Figure 82 for ENVISAT and Figure 83 for Jason. Each box contains the standard deviation of the high frequency signal in a 4°x4° bin. As expected, there is a strong correlation with the SWH (Figure 84). Figure 85 shows the difference between the two standard deviation maps. The ENVISAT standard deviation is larger than the Jason one almost every where.

6.3. ANALYSIS ON 1HZ DATA

6.3.1. Global results

Figure 87 shows the 1Hz ENVISAT spectrum. With 1Hz data fewer samples are available than with 20Hz data. The accuracy is then reduced and it makes the spectrum noisier. There is a sort of small plateau at 0.3Hz. But it is not enough pronounced to assert that it is a white noise signature. From the 20Hz study, it can be stated that it is not white noise. But assuming it was the case, the standard deviation corresponding to the plateau would be 3.2 cm. The ERS-2 (Figure 88) spectrum gives higher results: the standard deviation corresponding to the plateau would be 5 cm which is much higher than the ENVISAT value. On the Jason spectrum (Figure 88) the plateau is still less visible. The standard deviation corresponding to the plateau would be 3.9 cm.

As previously, the energy of the high frequency is plotted according to the cut-off wavelength (Figure 89) and the cut-off frequency (Figure 90). With 1Hz data, no linear trend is visible. It confirms that we cannot estimate a white noise on 1Hz data. Calculating a slope is not meaningful with 1 Hz data. We can only calculate the standard deviation of the high pass filtered signal.

	Envisat Cycle 11	**ERS-2 Cycle 79**	**Jason Cycle 31**
Number of points $\sigma(HF[SLA_{nc/mss}])$ (cm) (using a 3 points cut-off wave length)	294416 1.61	-	429749 2.11
Noise of $SLA_{nc/mss}$ estimated by spectral analysis (cm)	3.2	5.0	3.9

Table 22 : HF energy and noise estimation of $SLA_{nc/mss}$ using 1Hz data

Table 22 summarizes the results. As expected, the results obtained with the high pass filtering method are lower than those obtained by spectral analysis. But the two methods show the same tendency: 1Hz ENVISAT high frequency content is lower than Jason, while opposite results are obtained with 10 Hz data. It is not consistent.

Figure 91 and Figure 92 illustrate this problem. These plots show the HF[$SLA_{nc/mss}$] at 20Hz (red) and 1Hz (blue) according to latitude on Jason and ENVISAT particular passes in the Pacific ocean. Unlike at 20Hz, the 1Hz Jason signal is visually and statistically more energetic than the ENVISAT one: it has larger peaks all along the pass, and seems strongly noisy at several times like for example at -16° of latitude.

In order to explain these differences, one should consider the ENVISAT and Jason compression algorithms, that is to say the computation of 1Hz averaged measurements from 20Hz elementary data. These algorithms are not the same due to different regression methods. Moreover, an anomaly has been detected in the Jason algorithm. It has been recently corrected and improved by adding the MQE criteria (P Thibaut, Jason SWT, New Orleans, October 2002). Reprocessed Jason data will be soon available and this analysis will have to be performed again. It would also be interesting to compare the ENVISAT and Jason 1Hz signals, computed with the same compression algorithm.

6.3.2. Distribution

6.3.2.1. Geographic distribution

The geographic distribution of this high frequency σ(HF[$SLA_{nc/mss}$]) is mapped on Figure 93 for ENVISAT and Figure 94 for Jason. Each box contains the standard deviation of the high frequency signal in a 4°x4° bin. Figure 95 shows the difference between the two standard deviation maps. The ENVISAT standard deviation is lower almost every where, especially in the wet areas.

6.3.2.2. As a function of SWH

Figure 96 and Figure 97 show the scatter plot of σ(HF[$SLA_{nc/mss}$]) according to waves. On the ENVISAT plot, we see clearly the wave dependency whereas on Jason there are strong HF values even for low waves.

7. CONCLUSION

The ENVISAT Ra-2 and MWR data show good general results. Statistics and performances of altimeter and radiometer parameters are consistent with expected values:

- mean of RMS of 20Hz: ~9cm
- Sigma0 and SWH: histogram well shaped
- Time tag bias not significantly different from zero
- Standard deviation of SSH differences at crossovers: ~9 cm
- The SSH-MSS standard deviation around 10 cm and the mean is around 45-51 cm (after removing 73.68 cm due to an error in the characterization file)

Compared to the previous ERS-2 mission, substantial improvements have been evidenced: higher orbit precision, better precision of altimeter and radiometer parameters at both instrumental and algorithm levels. Furthermore, cross-calibration activities have allowed linking the ENVISAT mission with ERS-2 and Jason-1 missions, as it is essential in the purpose of multi-mission altimetry.

From this study it can be concluded that the altimeter ENVISAT data are compliant with the requirements of the scientific applications for which they were designed. However some algorithms still have to be tuned : the altimeter wind model may have to be improved between 0 and 1ms-1. The waveform-deduced mispointing bias has to be investigated. A new non parametric SSB will be provided and implemented in the new GDR version. The S-band anomaly needs to be solved or at least flagged in the product.

In this study, a sea ice flag algorithm has also been proposed, based on the combination |MWR-ECMWF| differences and peakiness criteria. These two criteria are complementary and allow efficient flagging of sea ice measurements.

Precision and resolution of ENVISAT data have been analysed using two high frequency estimation methods: spectral analysis and high pass filtering. The two methods converge to the same estimated noise: 9.cm for ENVISAT and 7.3cm for Jason at 20 Hz. On 1Hz data, less HF energy is obtained with the ENVISAT signal than with Jason.

This work serves as a basis for the Cal/Val and cross-calibration studies routinely conducted at CLS as part of the ENVISAT F-PAC activities. A cyclic ENVISAT quality assessment report will be produced and disseminated to users. These activities will also contribute to the long term quality analysis in the framework of the ENVISAT Quality Working Group.

8. BIBLIOGRAPHY

Benveniste J., and the ENVISAT RA-2/MWR Cross-Calibration and Validation Team: Radar Altimeter and Microwave Radiometer Cross-Calibration and Validation Plan. PO-PL-ESR-RA-0005. Issue 1.1. February 14, 2002.

Dorandeu J., F. Mertz and J. Stum 2000: Note on ERS-2 Sigma0 variations since January 2000. August 2000. CLS/DOS/NT/00.286. Available on internet at http://www.ifremer.fr/cersat.

Le Traon P. Y., F. Ogor, 1998: “ERS-1/2 orbit improvement using TOPEX/POSEIDON: the 2 cm challenge.” *J. G. Res*., VOL 103, p 8045-8057, April 15, 1998.

Mertz, F., Y. Faugere and J. Dorandeu, Validation of ERS-2 OPR cycle 080. CLS.OC.NT/03.702 issue 080. April 17, 2003.

Hernandez, F. and P. Schaeffer, 2000: Altimetric Mean Sea Surfaces and Gravity Anomaly maps inter-comparisons AVI-NT-011-5242-CLS, 48 pp. CLS Ramonville St Agne.

Martini A. and P. Féménias, 2000: The ERS SPTR2000 Altimetric Range Correction: Results and Validation. ERE-TN-ADQ-GSO-6001. 23 November 2000.

Obligis E., L. Eymard and N. Tran, 2003: "ERS-2/MWR drift evaluation and correction", CLS/DOS/NT/03.688

Scharroo R., Routines for iono corrections, internet communication to the CCVT community, December 12, 2002

Witter, D. L., D. B. Chelton, 1991, “A Geosat altimeter wind speed algorithm development”, J. of. Geophys. Res. (oceans), 96, 8853-8860, 1991.

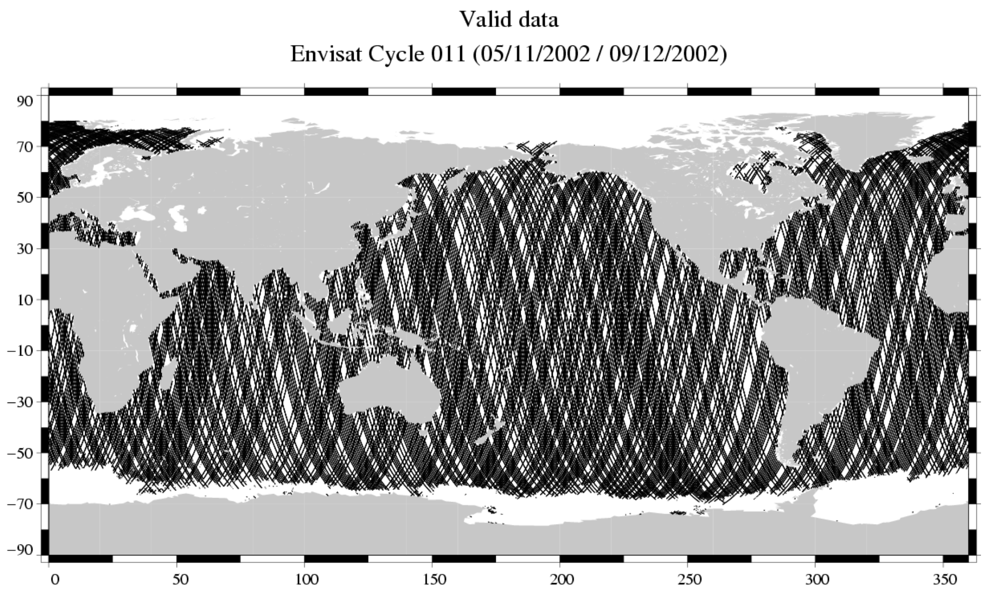

Figure 1 : Map of selected measurements on cycle 11

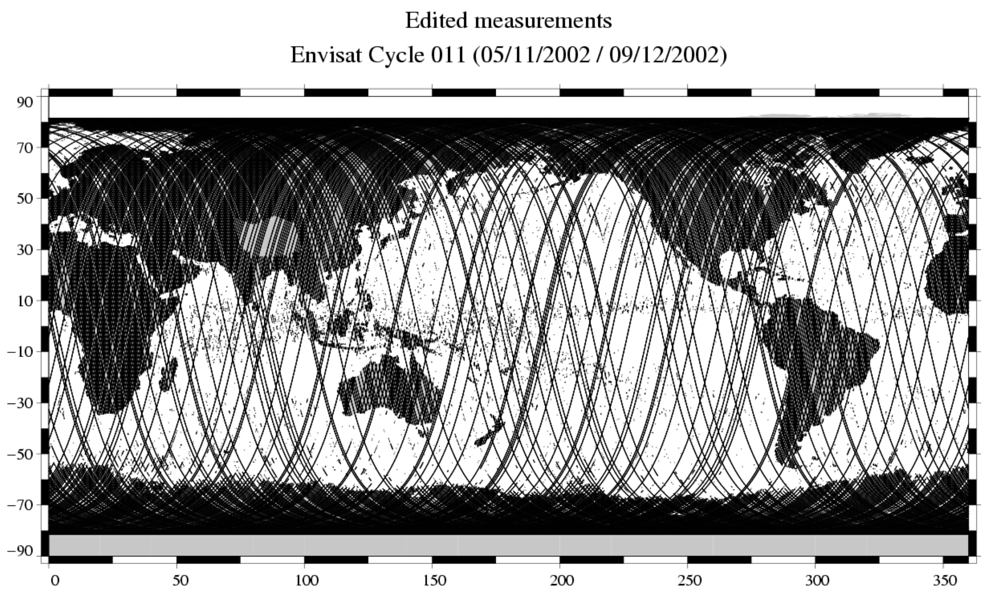

Figure 2 : Map of edited measurements on cycle 11

Edited parameter : Radiometer surface type
Envisat Cycle 011 (05/11/2002 / 09/12/2002)

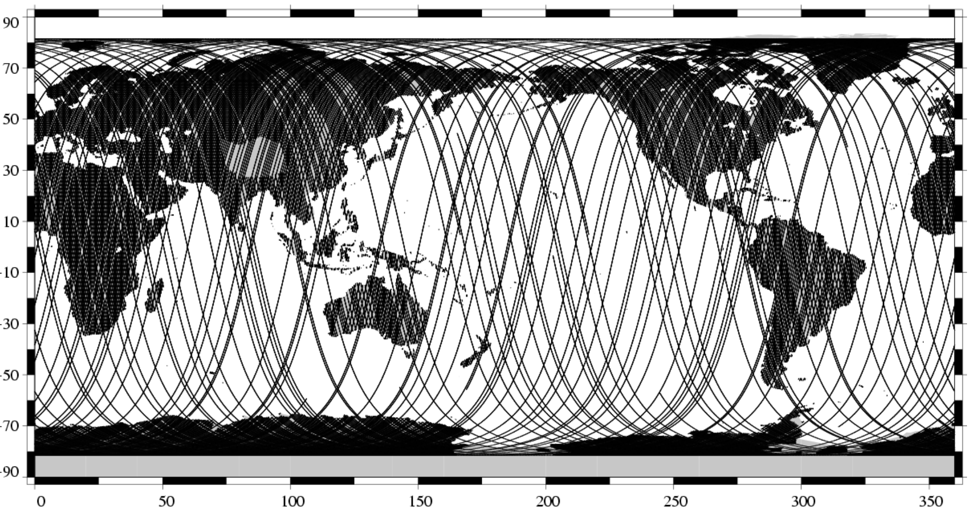

Figure 3 : Map of edited measurements due to radiometer land ocean flag on cycle 11

Edited parameter : ice flag
Envisat Cycle 011 (05/11/2002 / 09/12/2002)

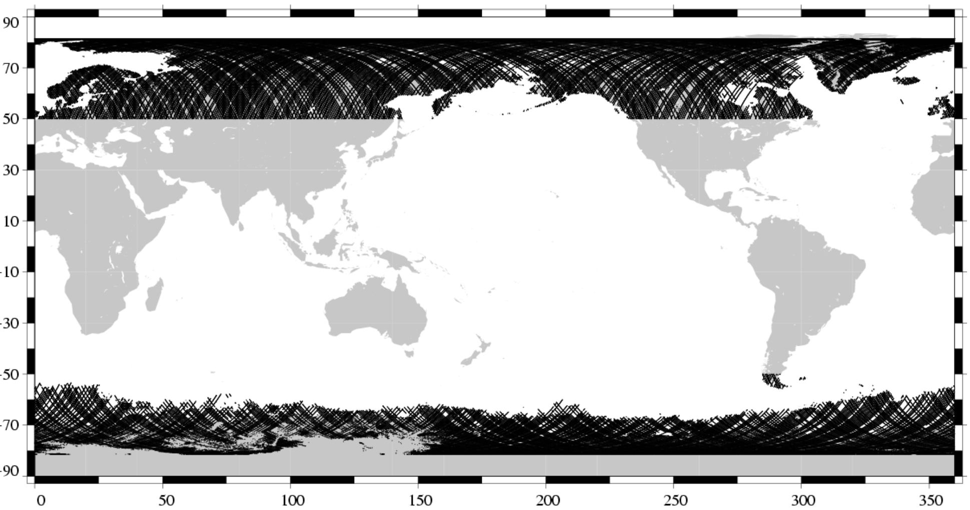

Figure 4 : Map of edited measurements due to ice flag on cycle 11

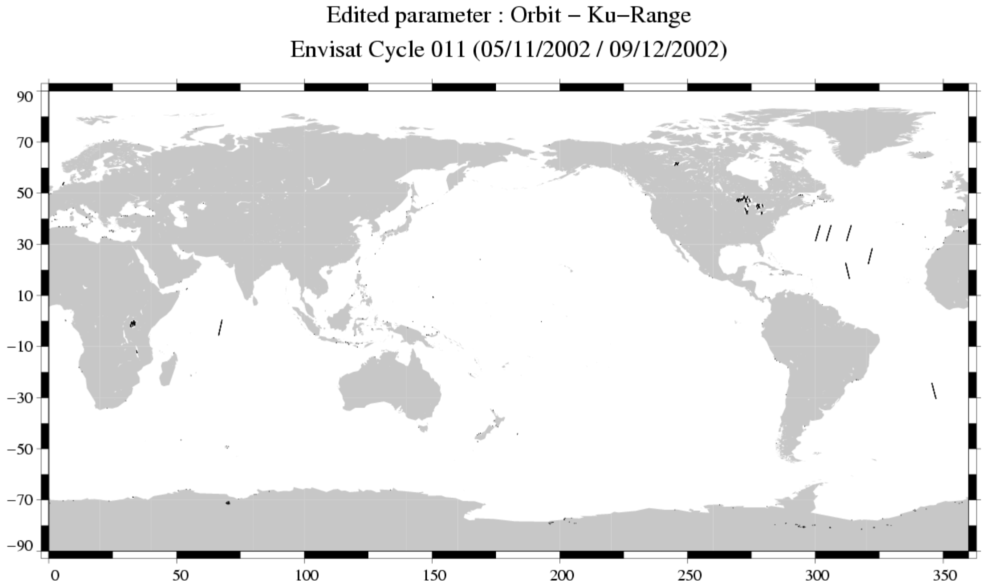

Figure 5 : Map of edited measurements due to [orbit – Range] threshold on cycle 11

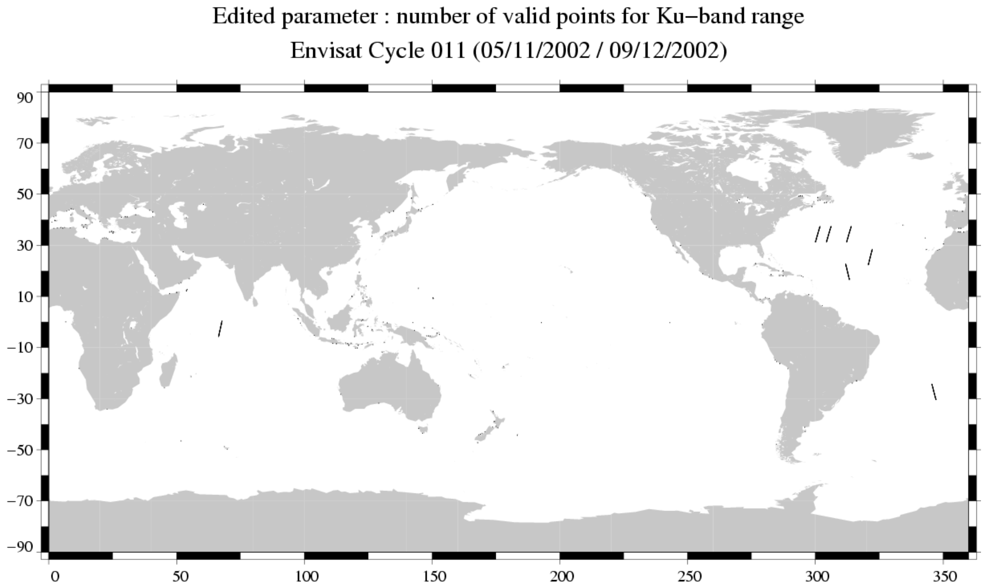

Figure 6 : Map of edited measurements due to [number of Ku range] threshold on cycle 11

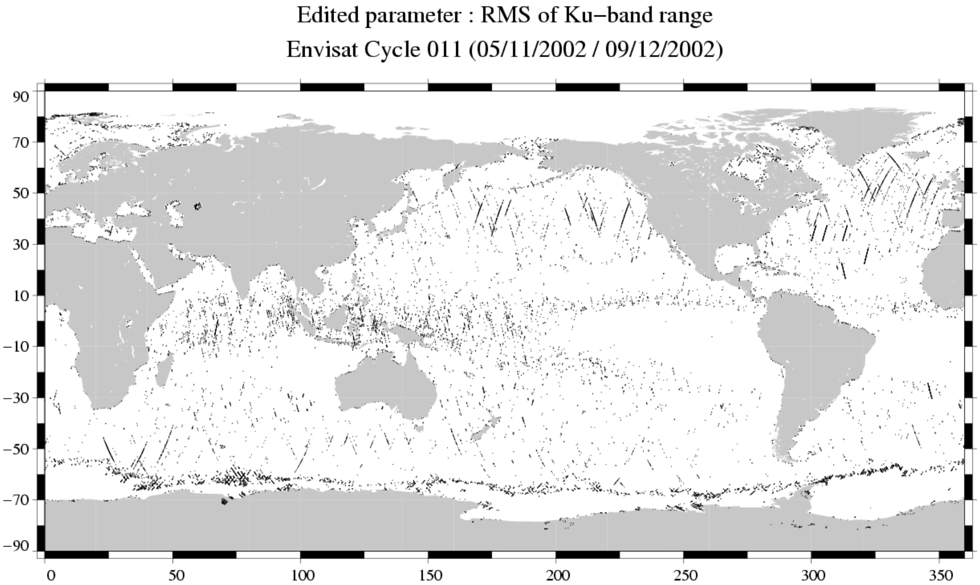

Figure 7 : Map of edited measurements due to [RMS of Ku range] threshold on cycle 11

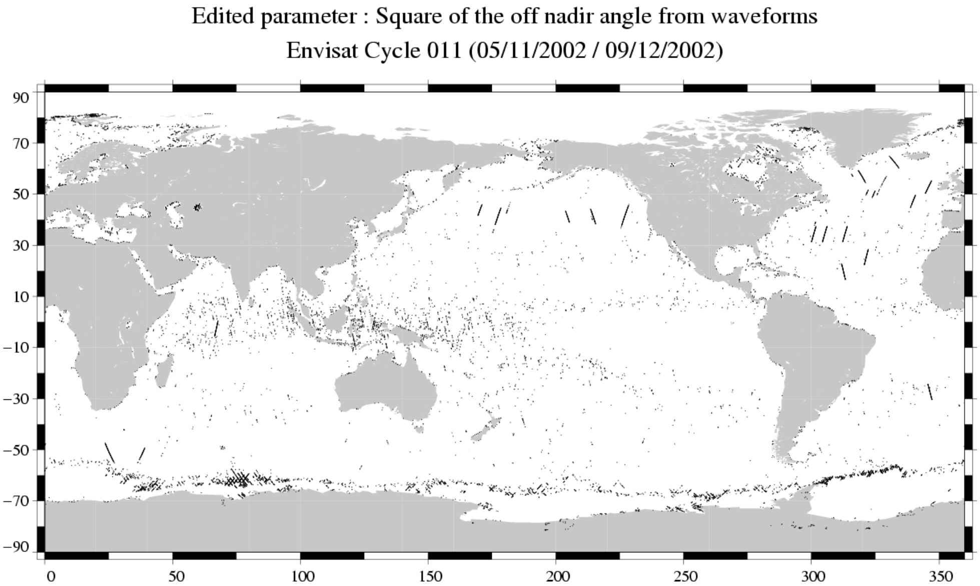

Figure 8 : Map of edited measurements due to [mispointing] threshold on cycle 11

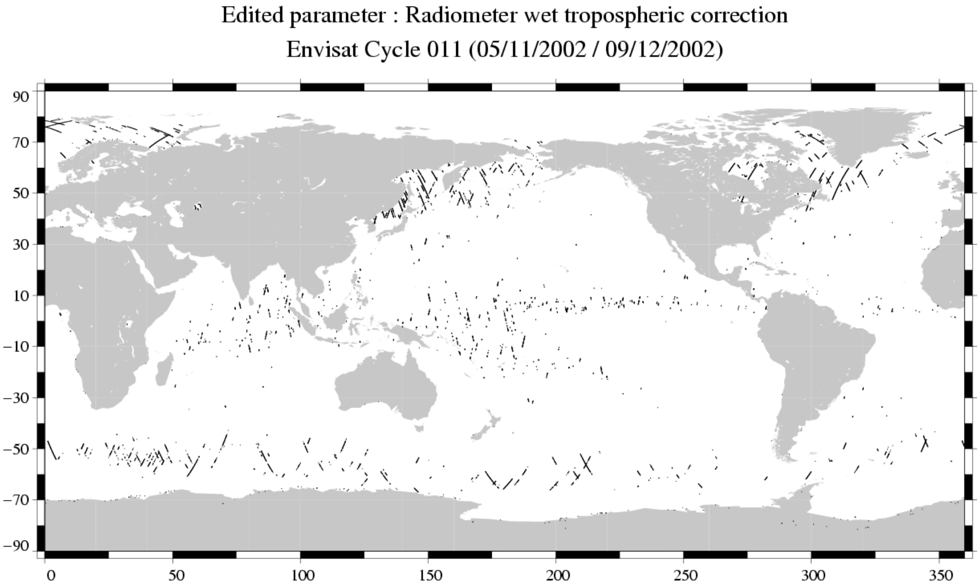

Figure 9 : Map of edited measurements due to [MWR correction] threshold on cycle 11

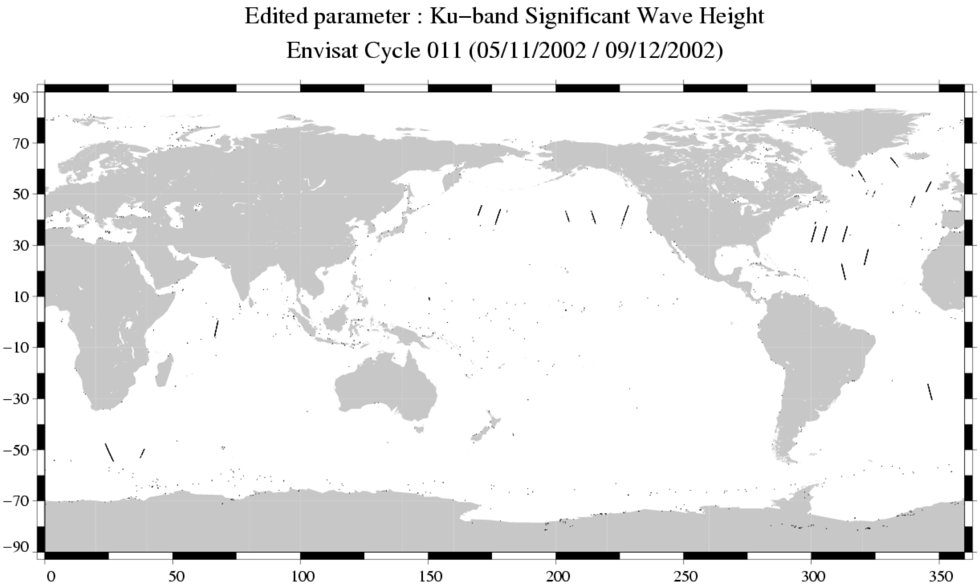

Figure 10 : Map of edited measurements due to [SWH] threshold on cycle 11

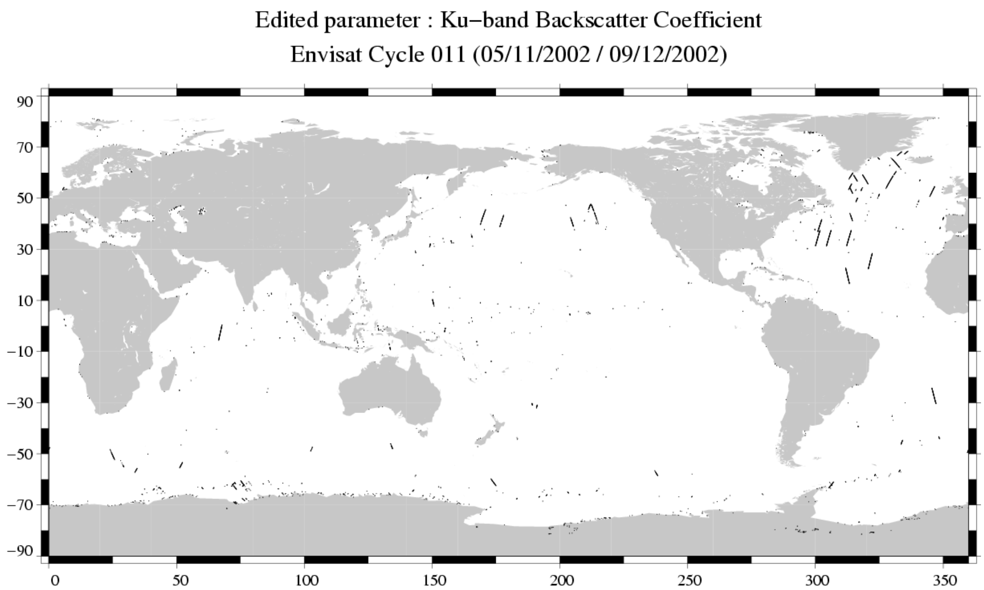

Figure 11 : Map of edited measurements due to [Sigma0] threshold on cycle 11

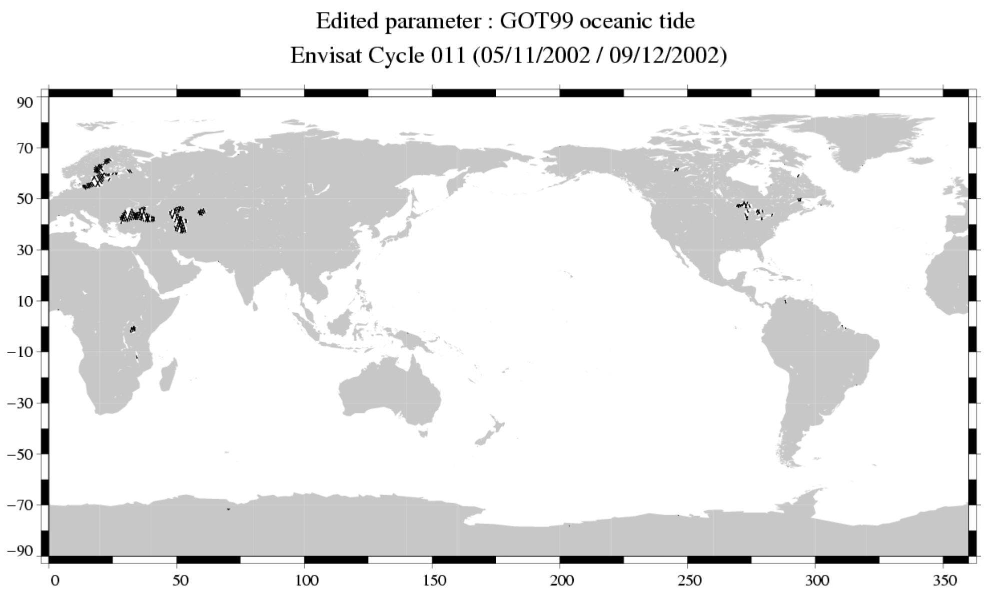

Figure 12 : Map of edited measurements due to [GOT99 ocean tide] threshold on cycle 11

Edited parameter : VENT_ALT
Envisat Cycle 011 (05/11/2002 / 09/12/2002)

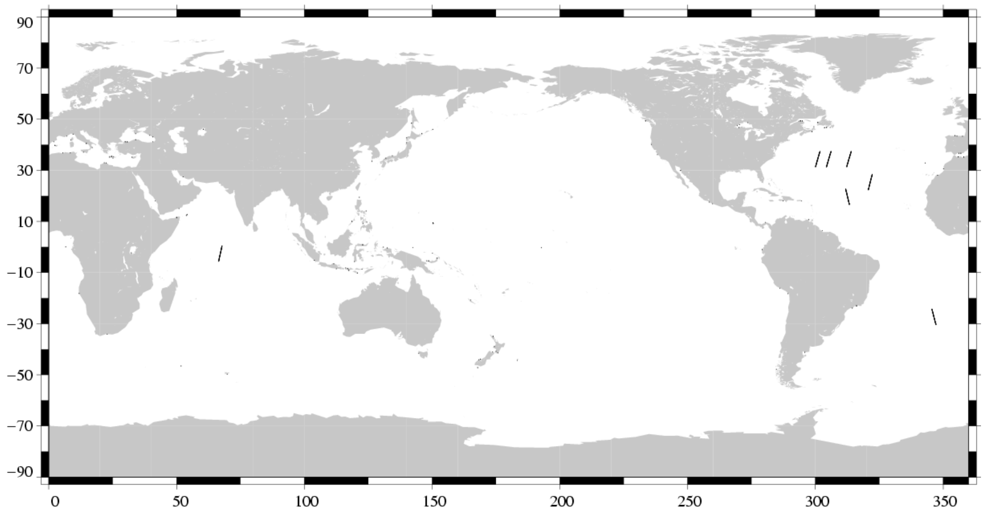

Figure 13 : Map of edited measurements due to [altimeter wind] threshold on cycle 11

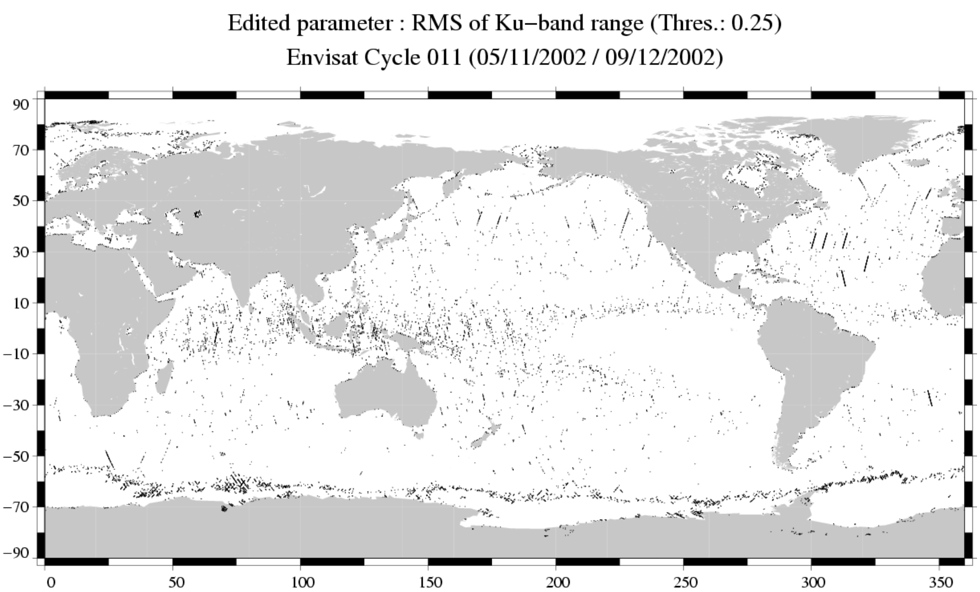

Figure 14 : Map of edited points by the [RMS of Ku range] criterion only, when set to 25cm (same as figure 7 but with a 25 cm threshold instead of 20 cm).

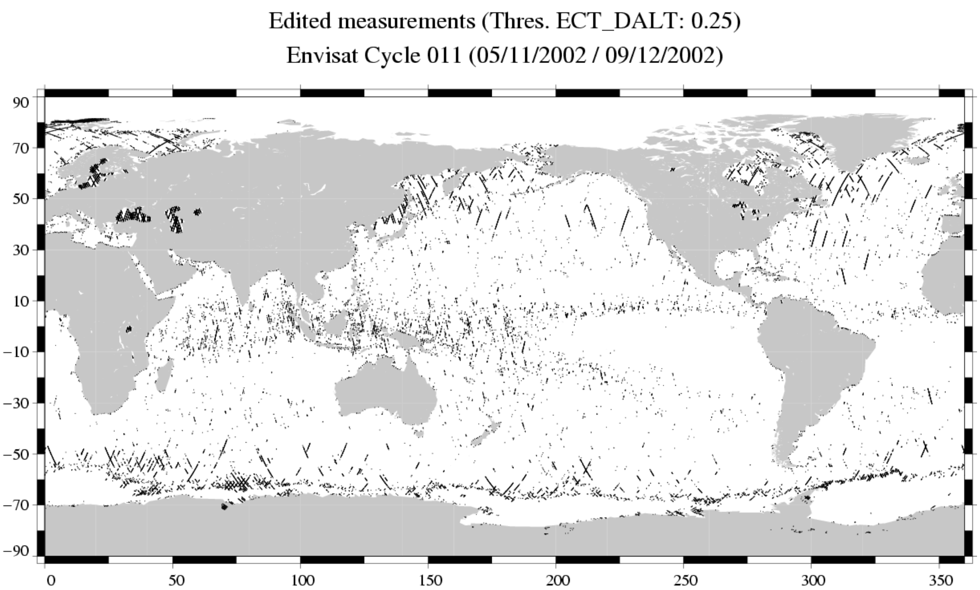

Figure 15 : Same as figure 2, except the RMS of Ku range threshold which is 25 cm instead of 20 cm

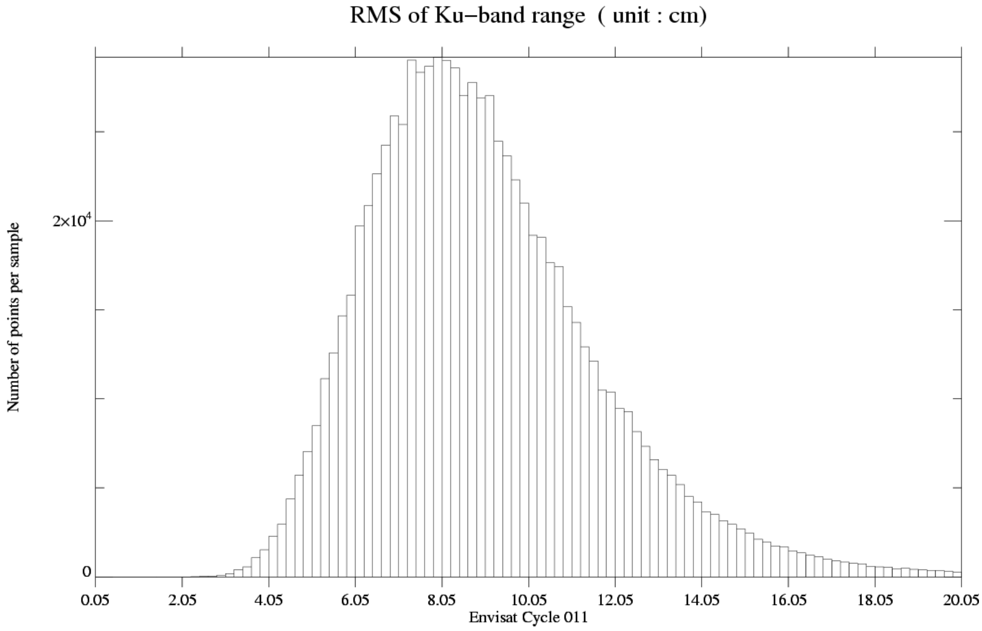

Global nb of points	:	856047	Sel. nb of points	:	856047	Sample interval	:	0.200
Global mean	:	9.015	Selected mean	:	9.015	Maximum value	:	20.000
Global Std	:	2.624	Selected std	:	2.624	Minimum value	:	1.800

Figure 16 : Histogram of RMS of Ku-Band range on cycle 11 (cm)

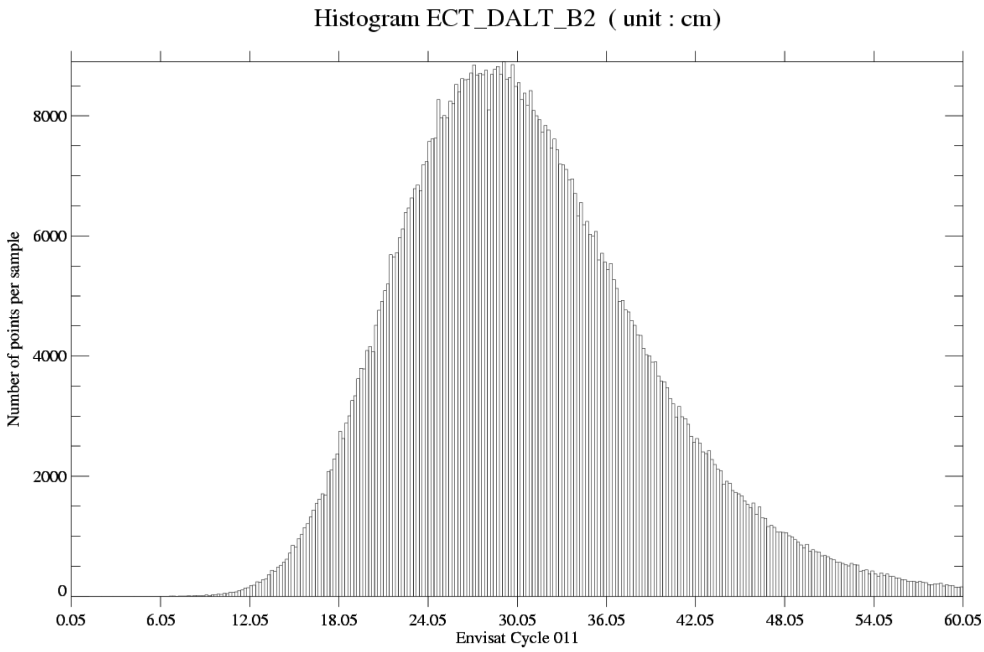

Global nb of points	:	852337	Sel. nb of points	:	846114	Sample interval	:	0.200
Global mean	:	31.071	Selected mean	:	30.701	Maximum value	:	976.000
Global Std	:	10.461	Selected std	:	8.162	Minimum value	:	6.000

Figure 17 : Histogram of RMS of S-Band range on cycle 11 (cm)

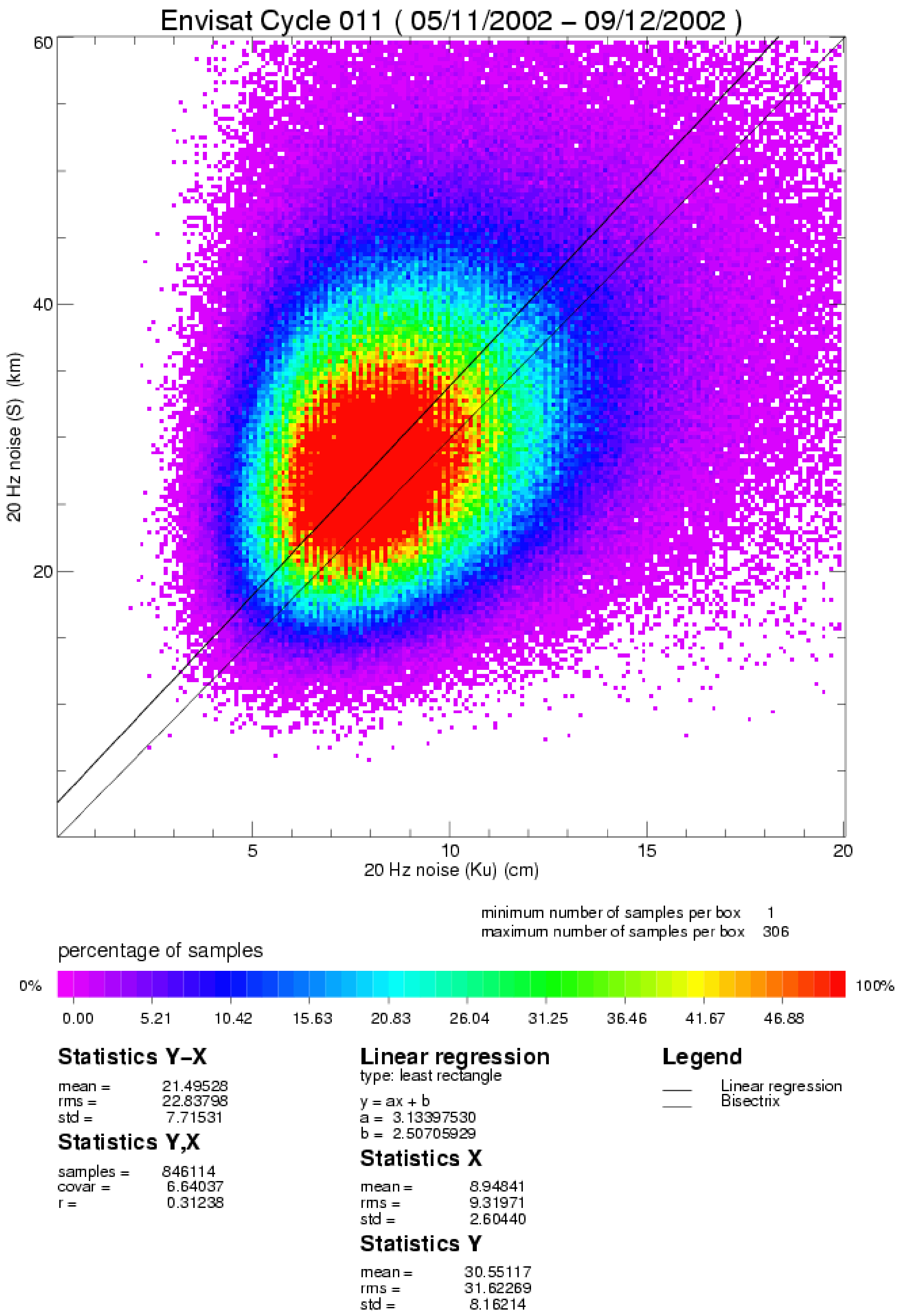

Figure 18 : Scatter plot of Ku and S-band RMS on cycle 11 (cm)

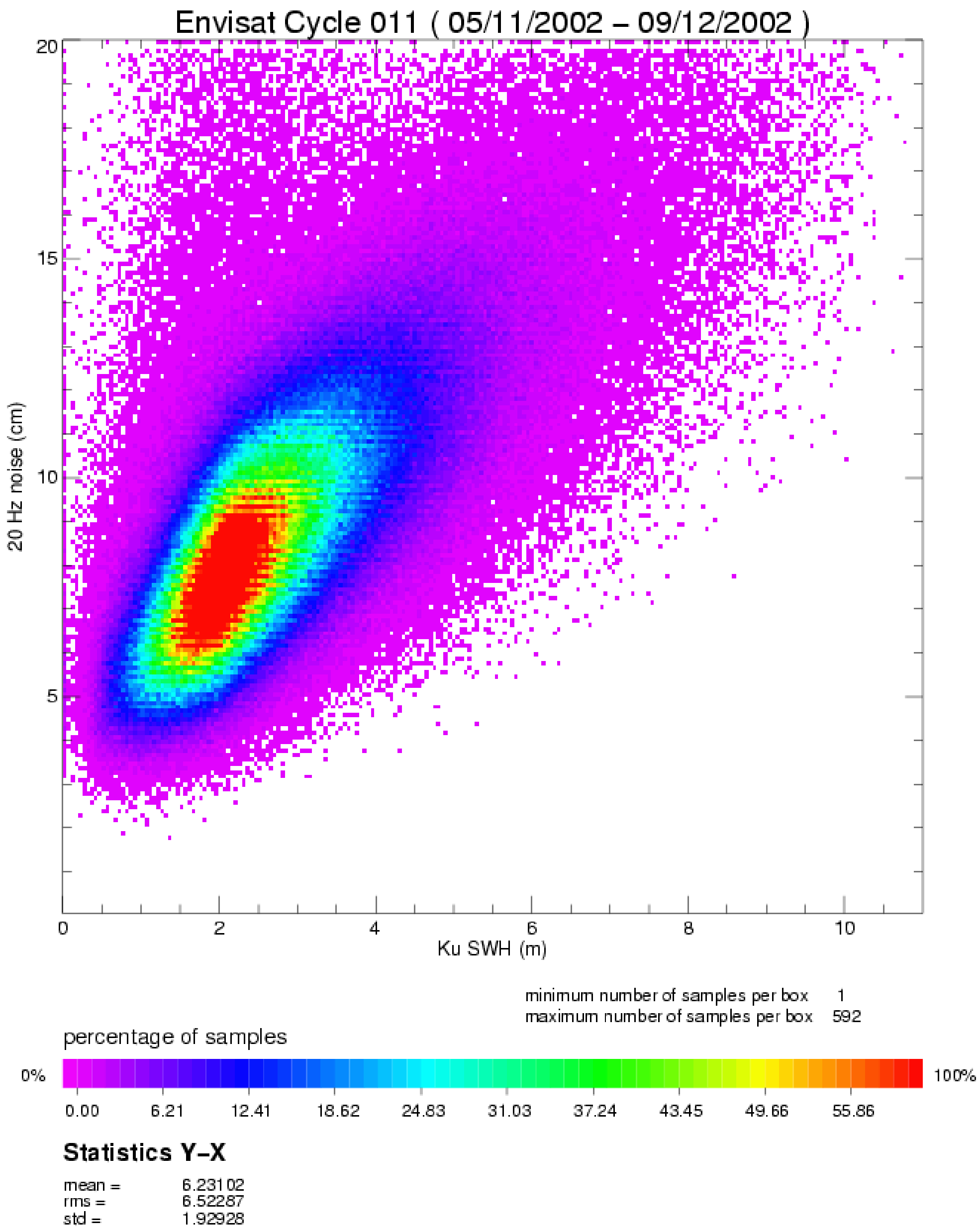

Figure 19 : Scatter plot of RMS of Ku -Band range as a function of Ku SWH, on cycle 11 (cm)

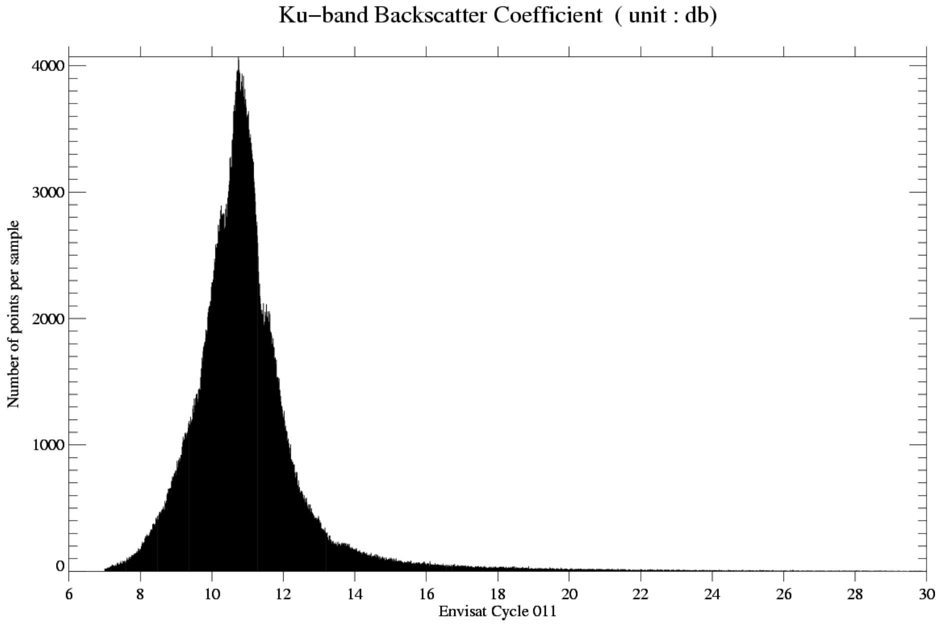

Global nb of points	:	856047	Sel. nb of points	:	856047	Sample interval	:	0.010
Global mean	:	10.981	Selected mean	:	10.981	Maximum value	:	29.970
Global Std	:	1.754	Selected std	:	1.754	Minimum value	:	7.000

Figure 20 : Histogram of Sigma0 in Ku Band on cycle 11 (dB)

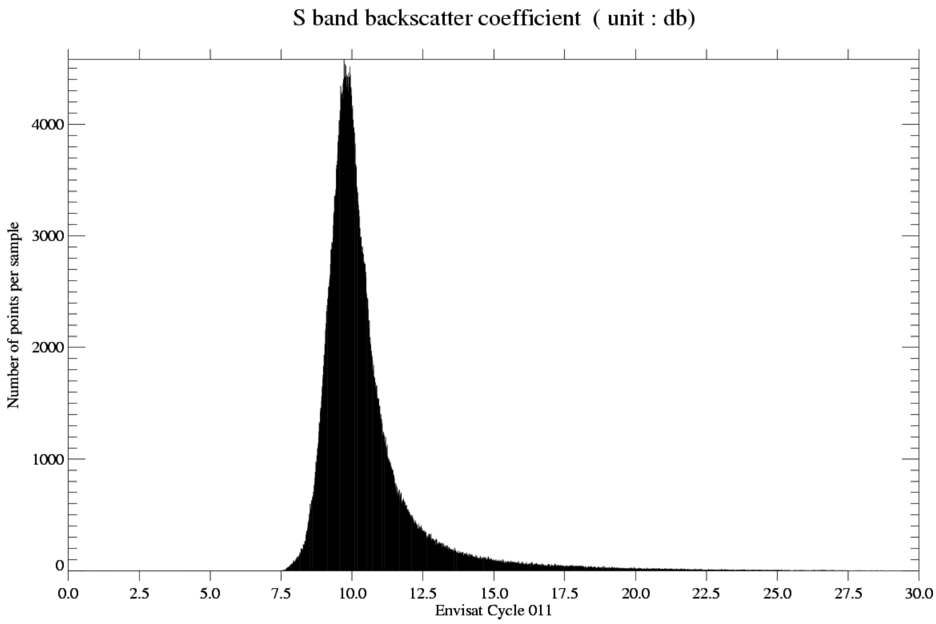

Global nb of points	:	852337	Sel. nb of points	:	852329	Sample interval	:	0.010
Global mean	:	10.473	Selected mean	:	10.473	Maximum value	:	31.560
Global Std	:	1.816	Selected std	:	1.815	Minimum value	:	7.480

Figure 21 : Histogram of Sigma0 in S Band on cycle 11 (dB)

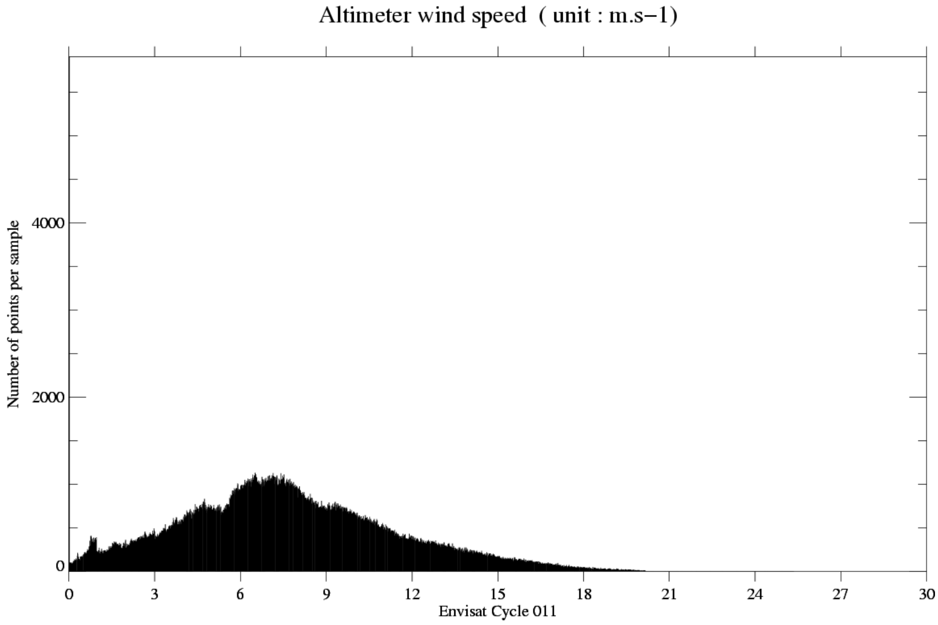

Global nb of points	:	856047	Sel. nb of points	:	856047	Sample interval	:	0.010
Global mean	:	7.645	Selected mean	:	7.645	Maximum value	:	20.150
Global Std	:	3.739	Selected std	:	3.739	Minimum value	:	0.010

Figure 22 : Histogram of altimeter wind in Ku Band on cycle 11 (m/s)

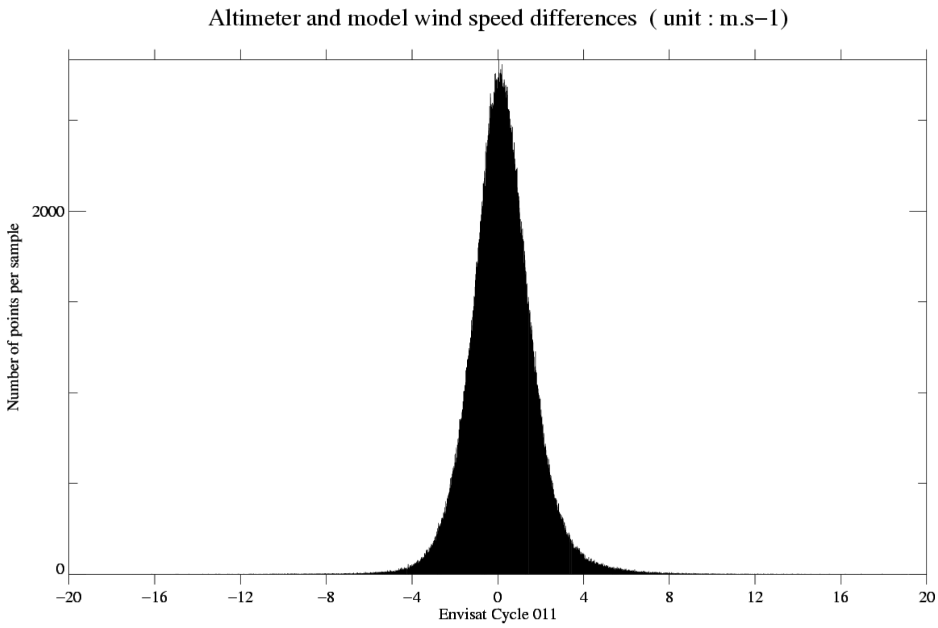

Global nb of points	:	856047	Sel. nb of points	:	856047	Sample interval	:	0.010
Global mean	:	0.210	Selected mean	:	0.210	Maximum value	:	17.924
Global Std	:	1.507	Selected std	:	1.507	Minimum value	:	−16.130

Figure 23 : Histogram of [altimeter-Model wind] differences on cycle 11 (m/s)

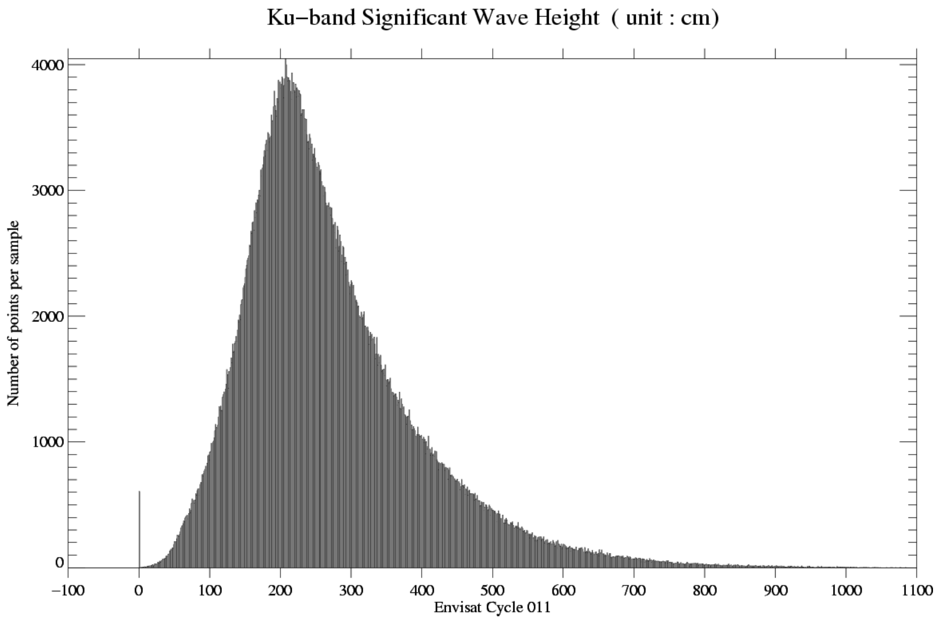

Global nb of points :	856047	Sel. nb of points :	856047	Sample interval :	1.000
Global mean :	270.437	Selected mean :	270.437	Maximum value :	1084.100
Global Std :	124.380	Selected std :	124.380	Minimum value :	0.000

Figure 24 : Histogram of SWH in Ku band (m)

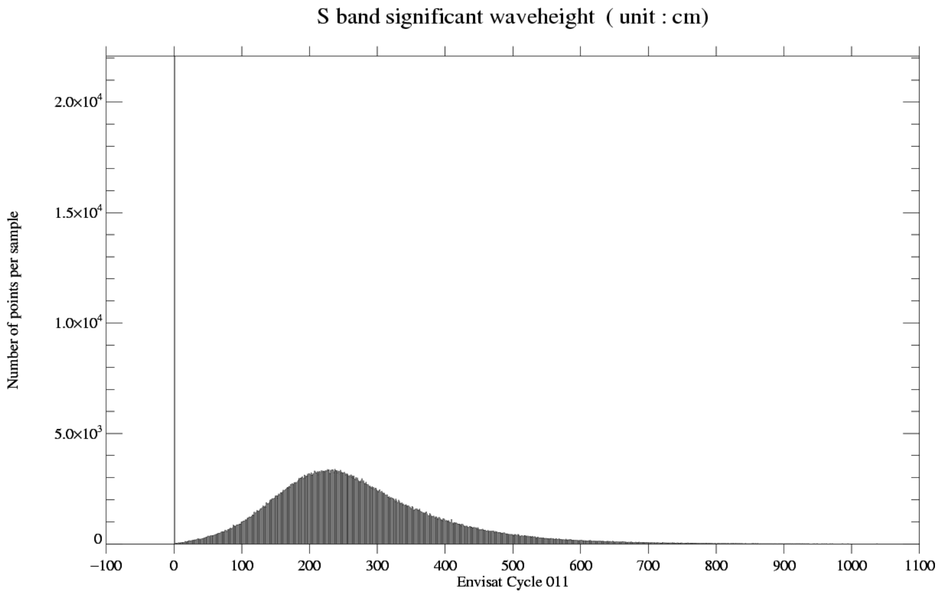

Global nb of points :	852337	Sel. nb of points :	852229	Sample interval :	1.000
Global mean :	263.406	Selected mean :	263.270	Maximum value :	2527.900
Global Std :	129.263	Selected std :	128.681	Minimum value :	0.000

Figure 25 : Histogram of SWH in S band (m)

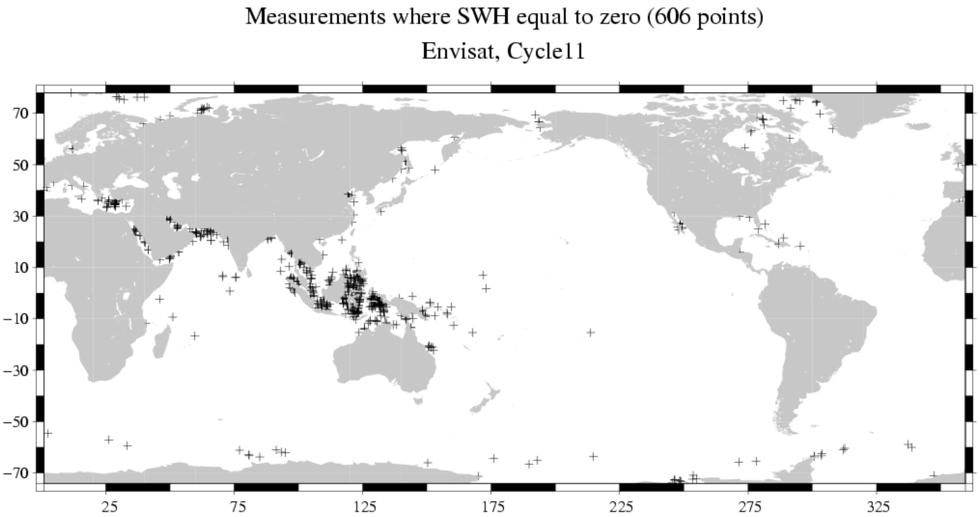

Figure 26 : Location of the zero-clipping SWH measurements on cycle 11

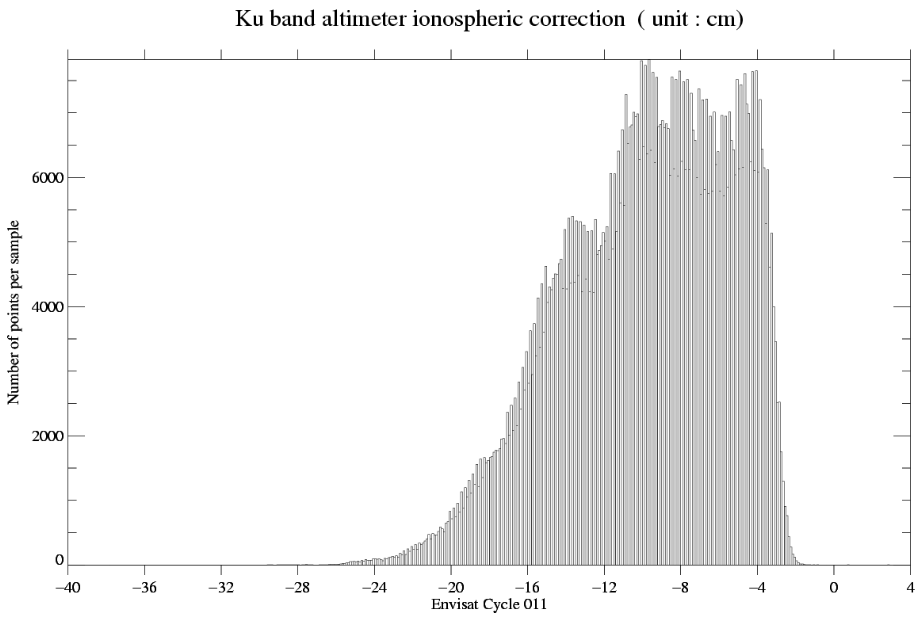

Global nb of points	:	852337	Sel. nb of points	:	852327	Sample interval	:	0.100
Global mean	:	−9.766	Selected mean	:	−9.766	Maximum value	:	7.400
Global Std	:	4.404	Selected std	:	4.402	Minimum value	:	−68.000

Figure 27 : Histogram of dual frequency ionosphere correction on cycle 11

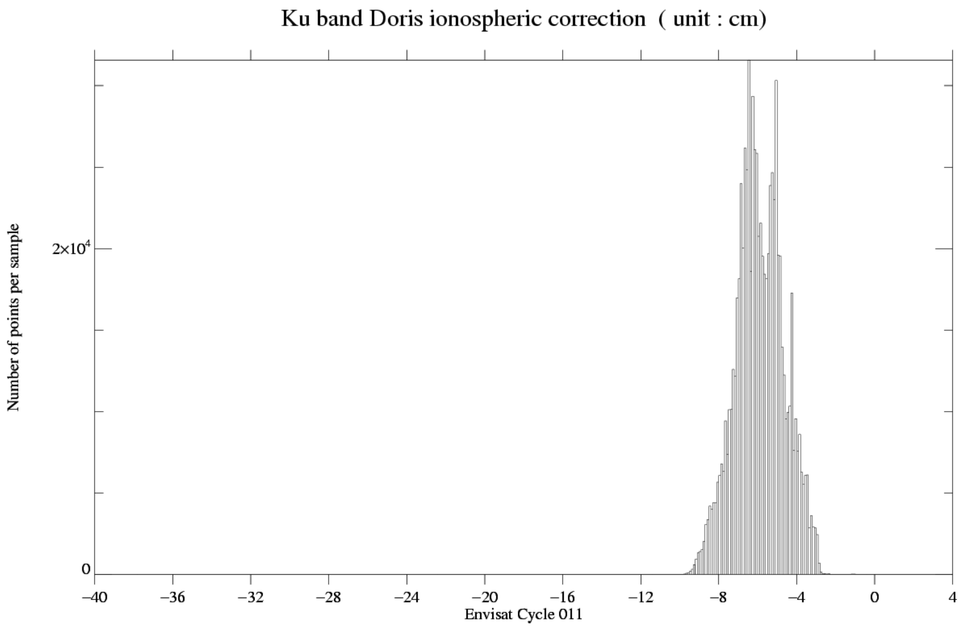

Global nb of points	:	785535	Sel. nb of points	:	785205	Sample interval	:	0.100
Global mean	:	−6.188	Selected mean	:	−5.832	Maximum value	:	3254.600
Global Std	:	37.031	Selected std	:	1.237	Minimum value	:	−3257.700

Figure 28 : Histogram of DORIS ionosphere correction on cycle 11

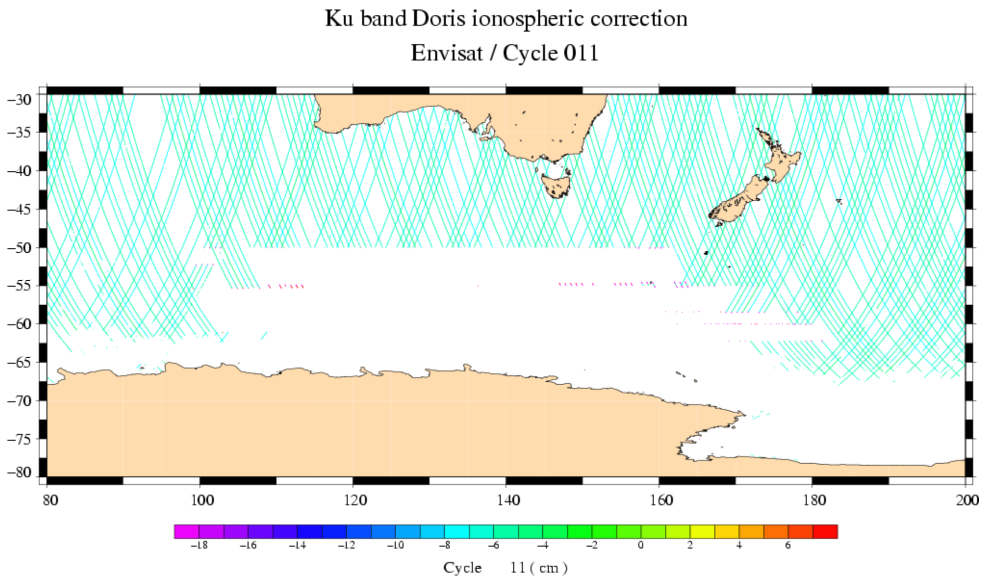

Figure 29 : Location of missing DORIS ionosphere correction on cycle 11

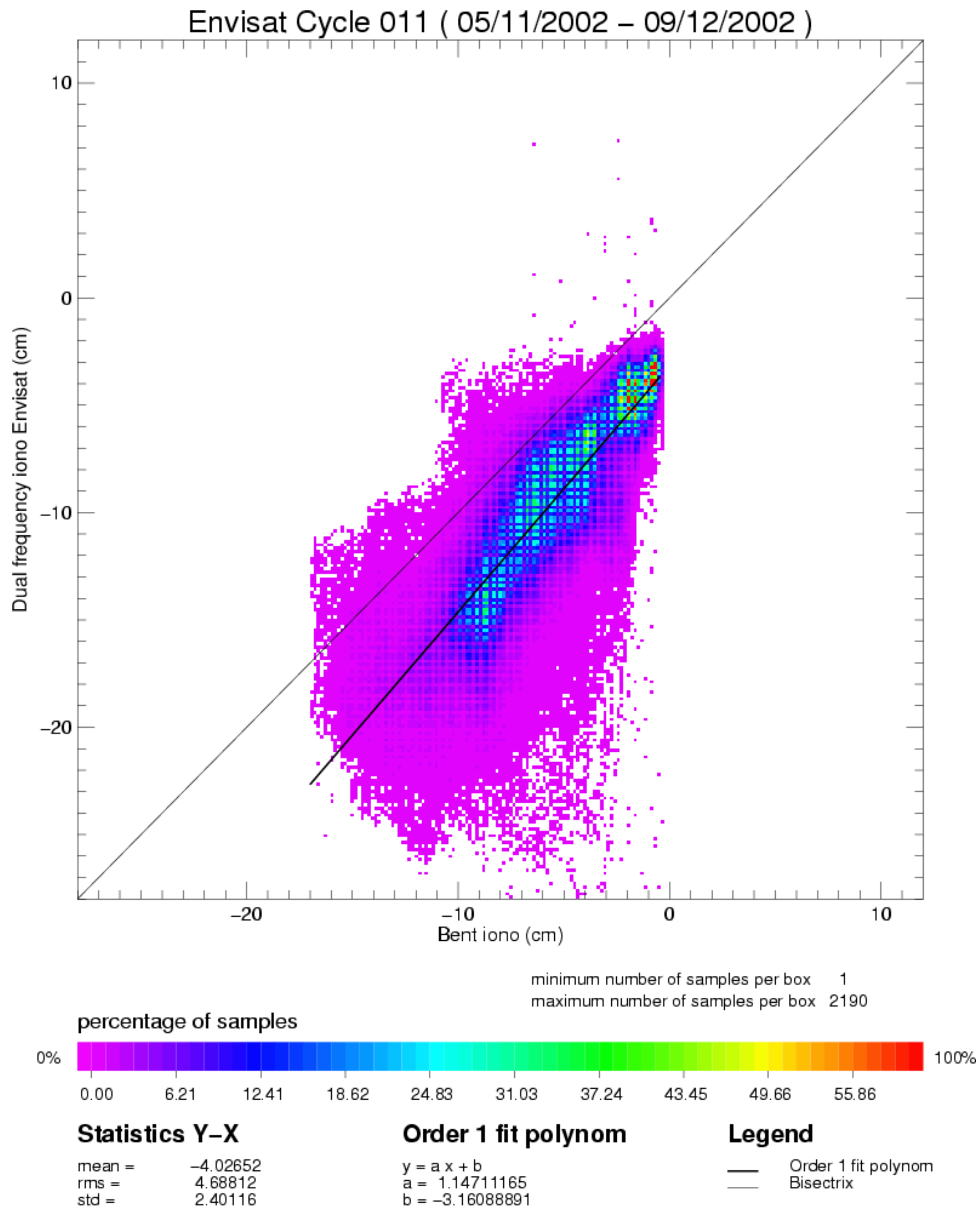

Figure 30 : Scatter plot of Dual-Frequency/Bent ionosphere corrections on cycle 11

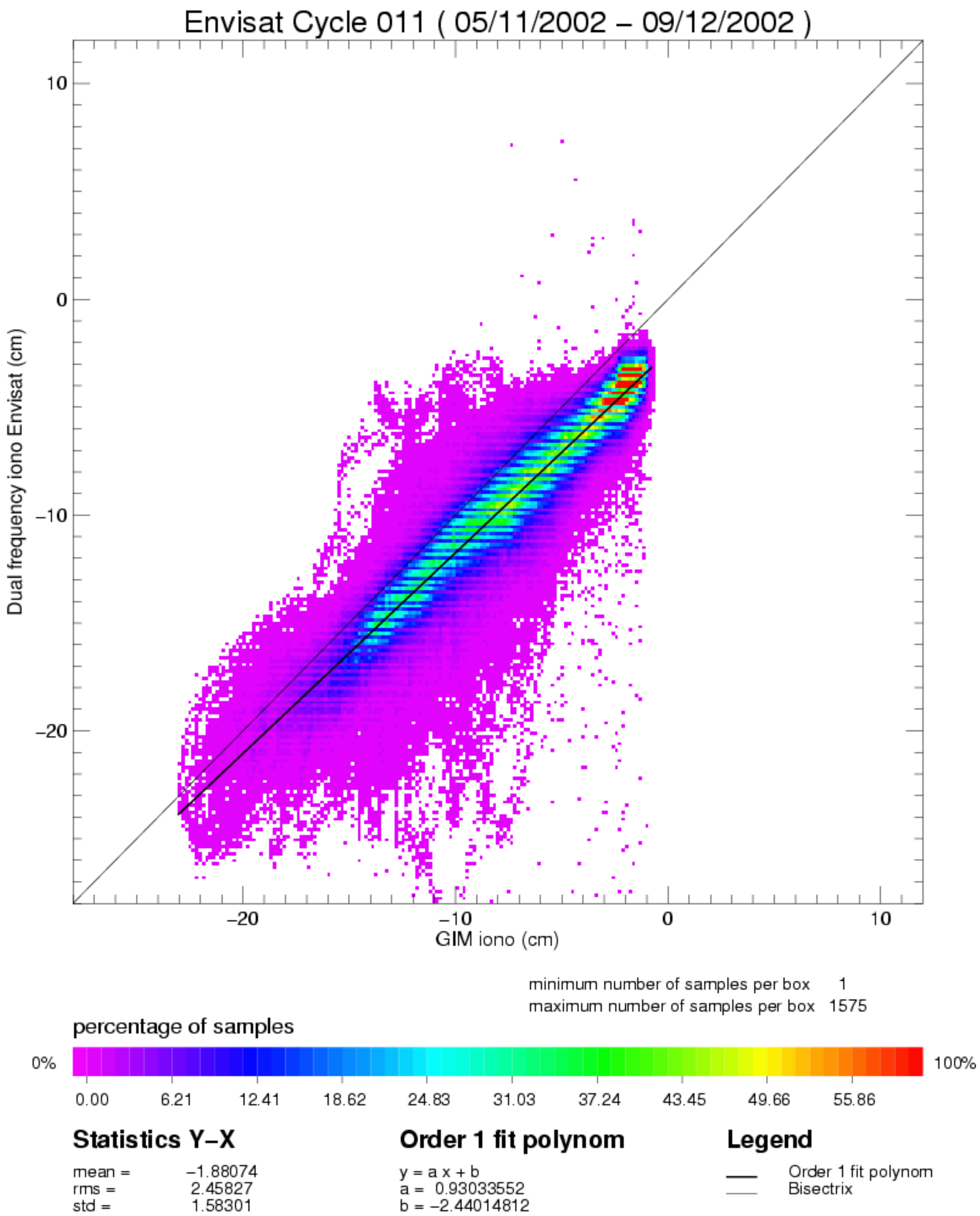

Figure 31 : Scatter plot of Dual-Frequency/GIM ionosphere corrections on cycle 11

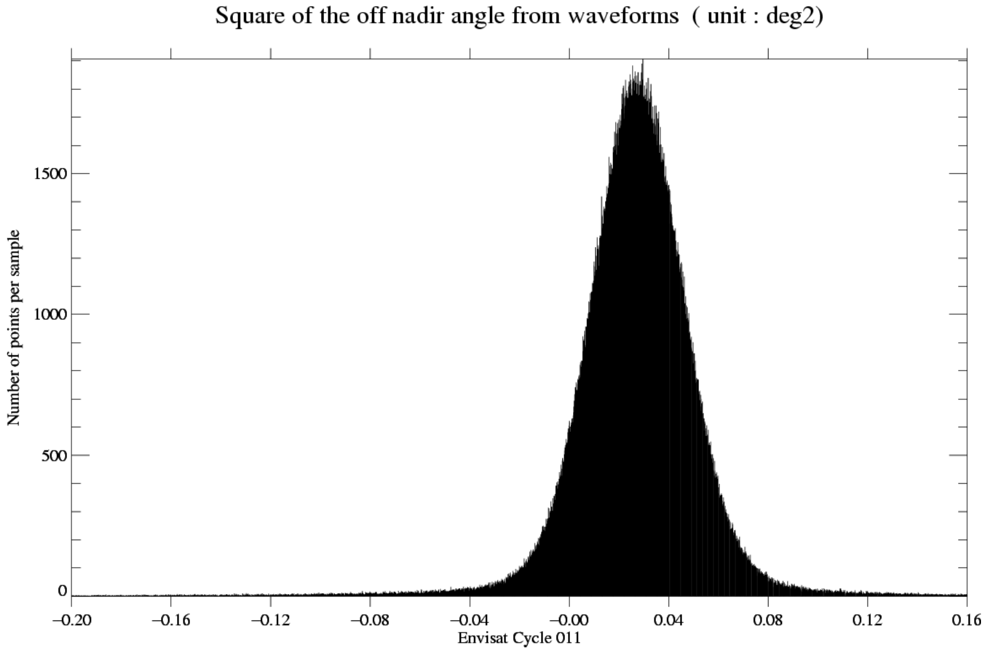

Global nb of points	:	856047	Sel. nb of points	:	856044	Sample interval	:	0.000
Global mean	:	0.027	Selected mean	:	0.027	Maximum value	:	0.160
Global Std	:	0.024	Selected std	:	0.024	Minimum value	:	−0.200

Figure 32 : Histogram of squared mispointing on cycle 11 (deg2)

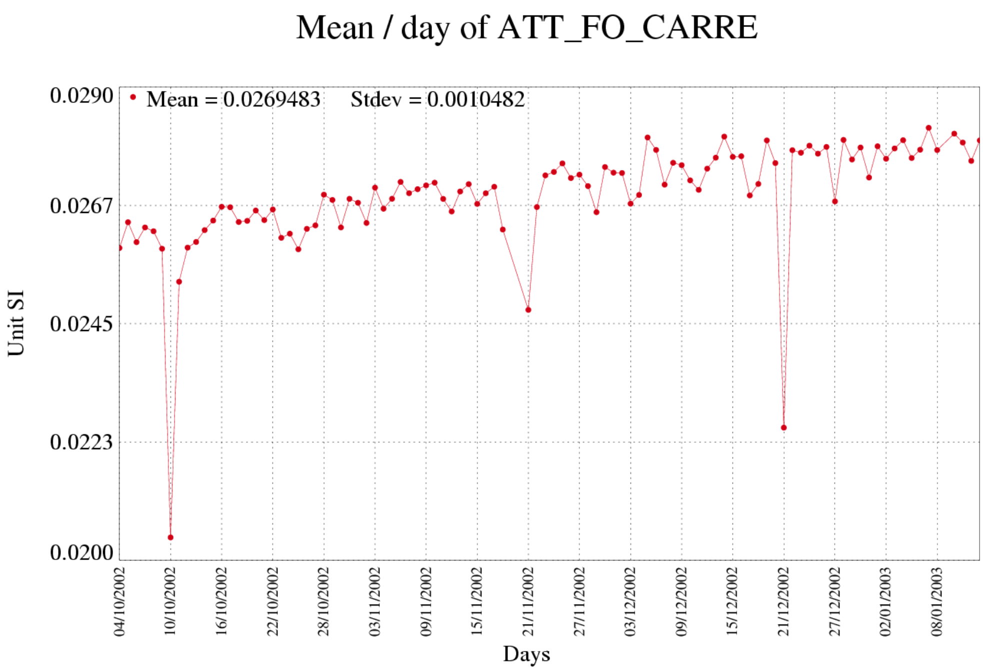

Figure 33 : Daily mean of squared mispointing (deg2)

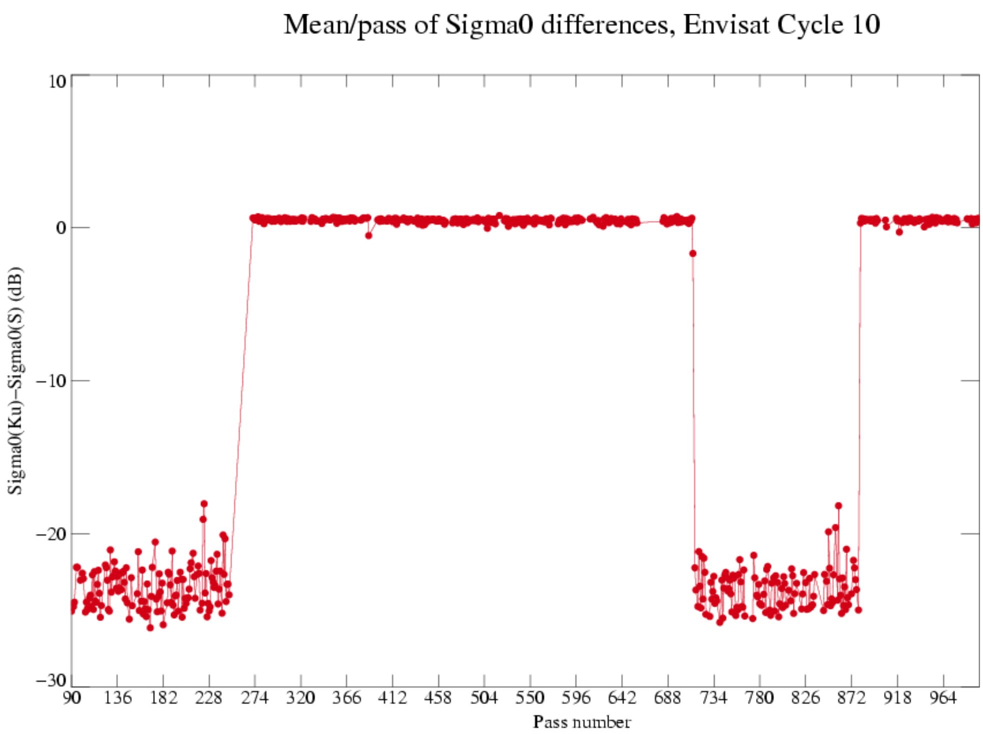

Figure 34 : Pass mean of [Ku-S] Sigma0 differences (dB), cycle 10

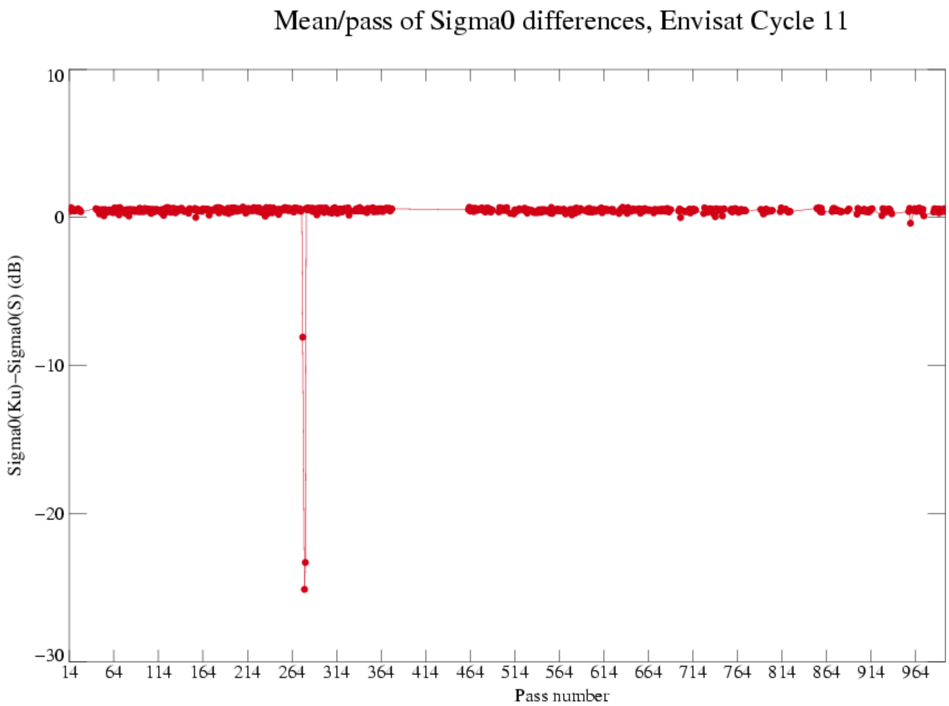

Figure 35 : Pass mean of [Ku-S] Sigma0 differences (dB), cycle 11

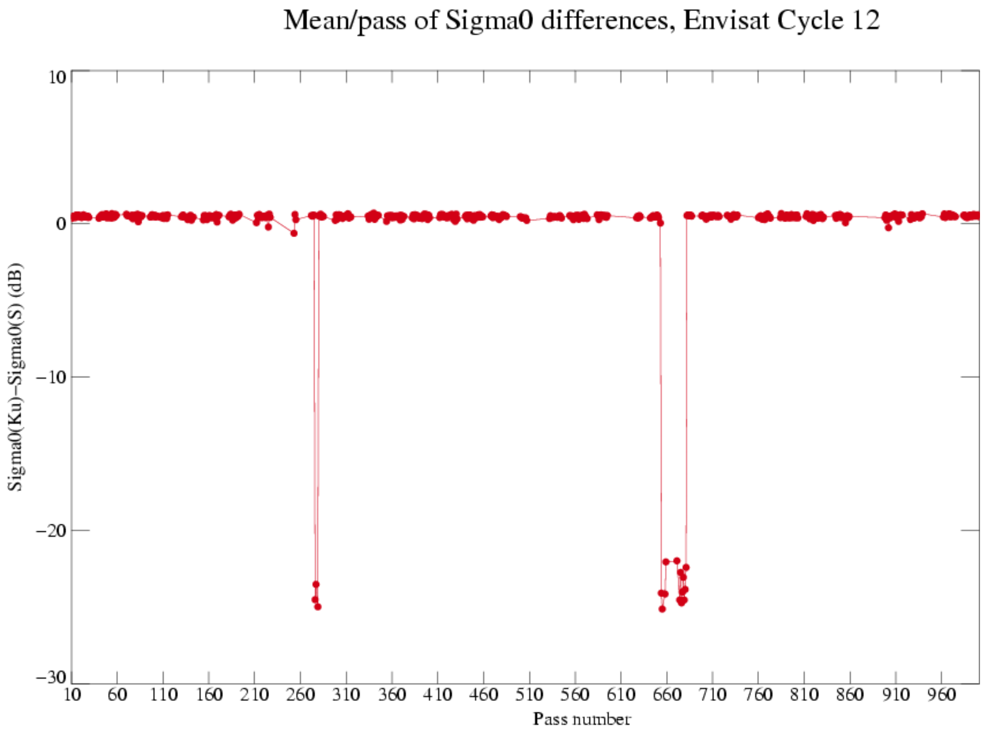

Figure 36 Pass mean of [Ku-S] Sigma0 differences per pass (dB), cycle 12

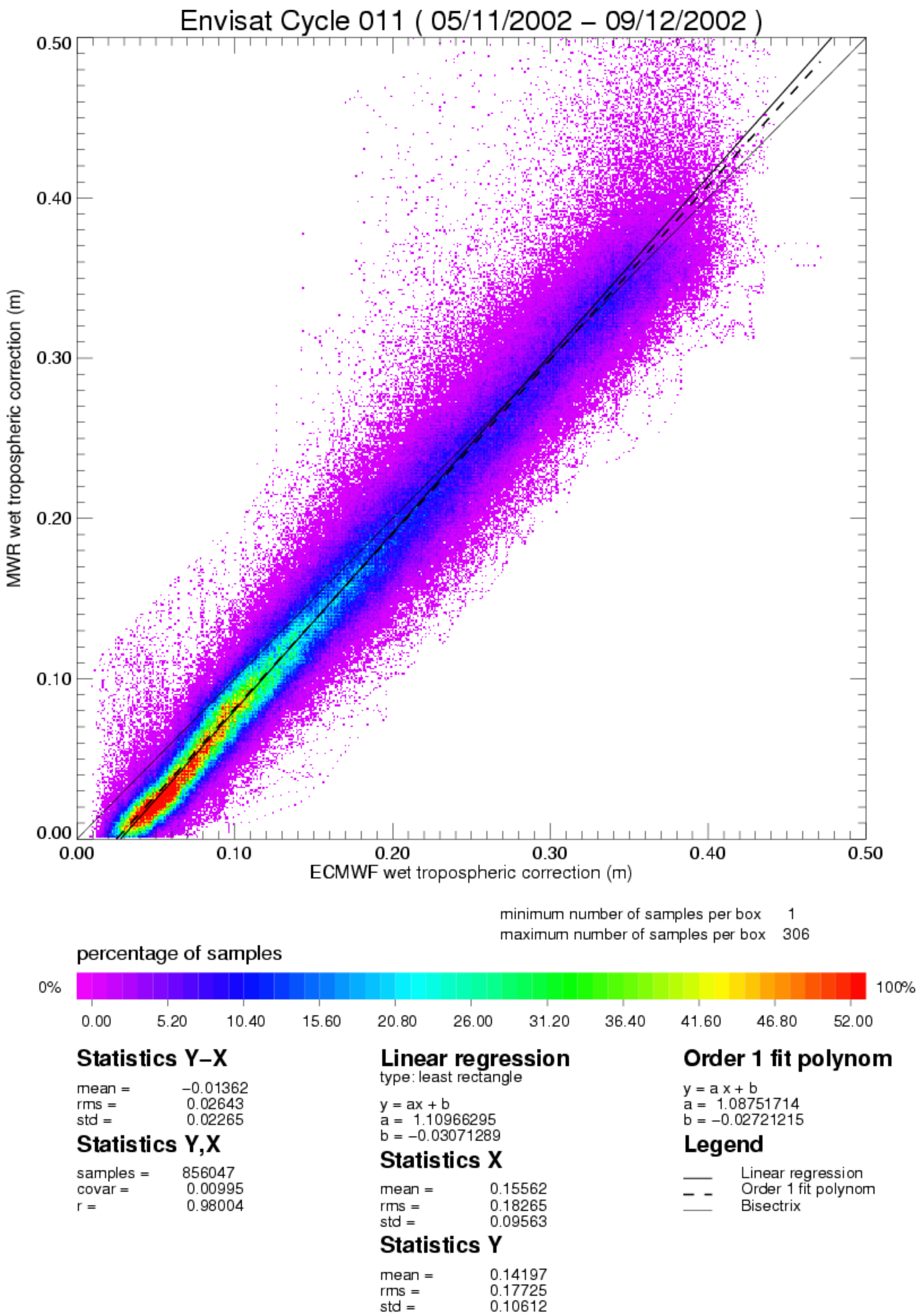

Figure 37 : Scatter plot of MWR(product)/ECMWF wet troposphere corrections (m) on cycle 11

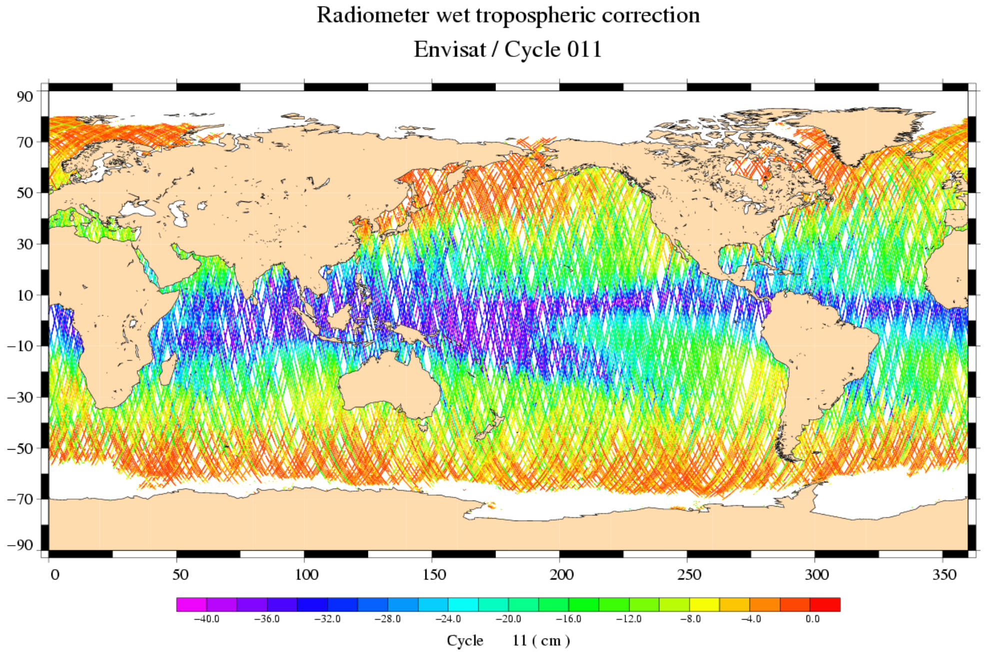

Figure 38 : Map of MWR(product) wet troposphere correction (cm) on cycle 11

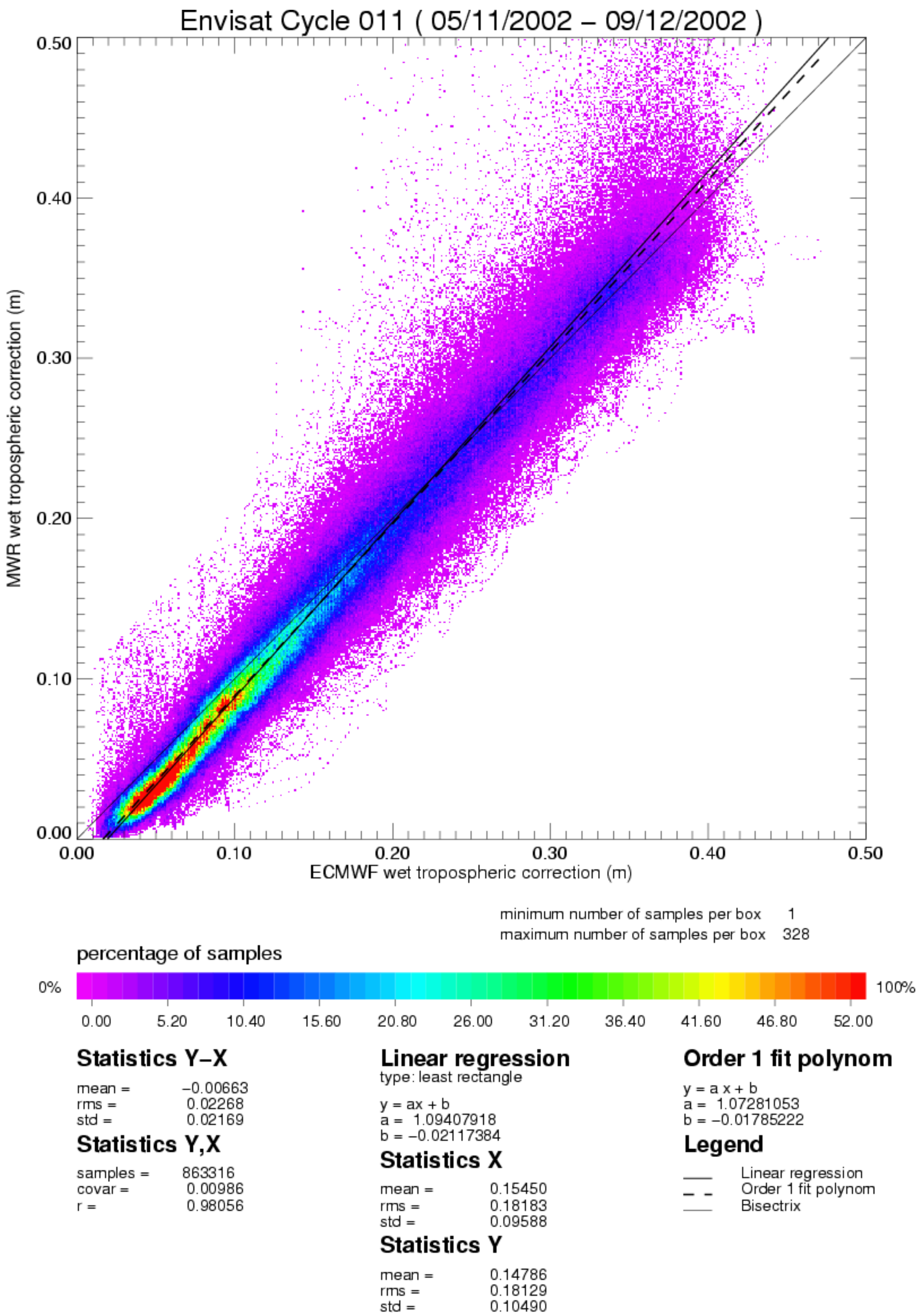

Figure 39 : Scatter plot of MWR(computed)/ECMWF wet troposphere corrections (m) on cycle 11

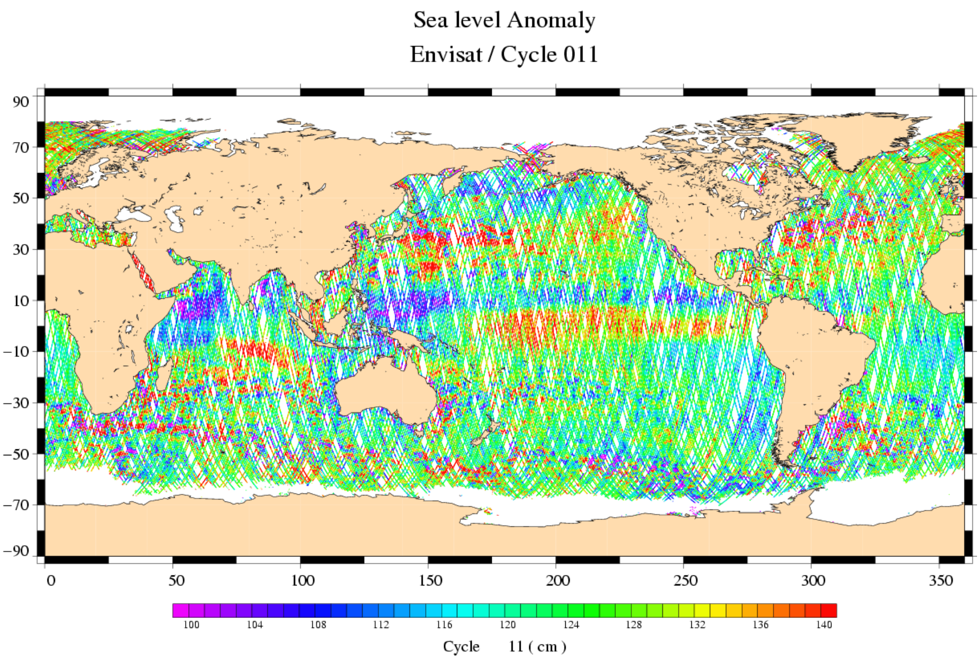

Figure 40 : Map of [SSH-MSS] (cm) on Cycle 11

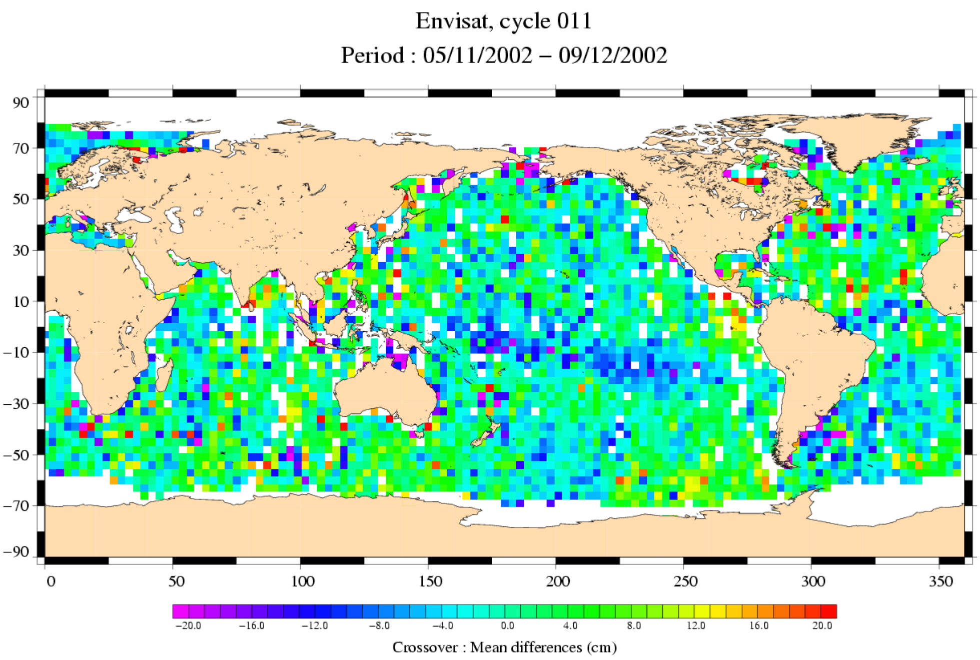

Figure 41 : Map of mean crossover differences (cm) on cycle 11

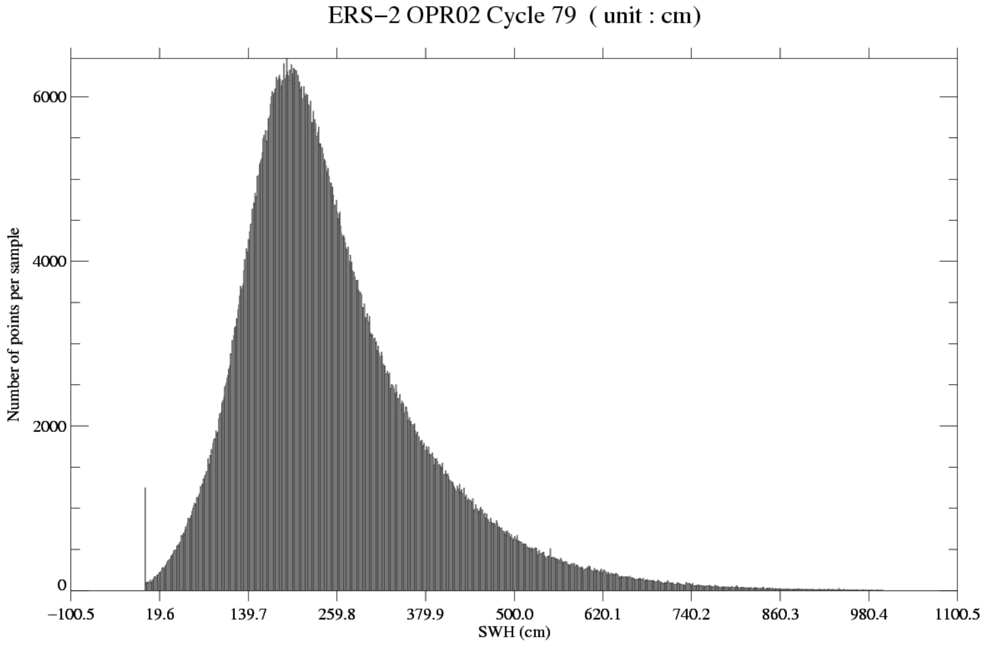

Global nb of points	:	1431708	Sel. nb of points	:	1431708	Sample interval	:	1.000
Global mean	:	254.027	Selected mean	:	254.027	Maximum value	:	1000.000
Global Std	:	124.963	Selected std	:	124.963	Minimum value	:	0.000

Figure 42: ERS-2 SWH histogram for cycle 79

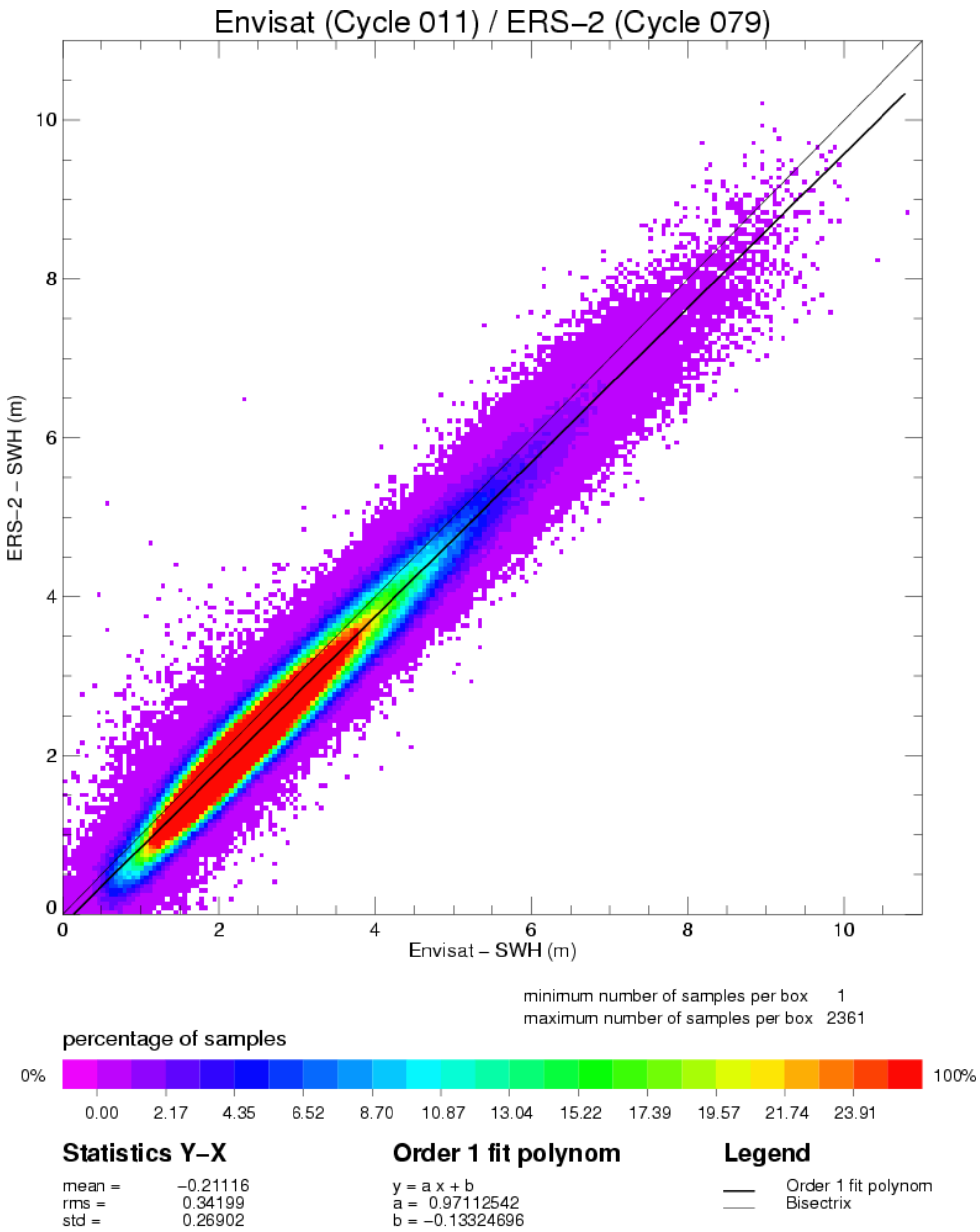

Figure 43: Scatter plot of ERS-2 SWH versus ENVISAT SWH in meters.

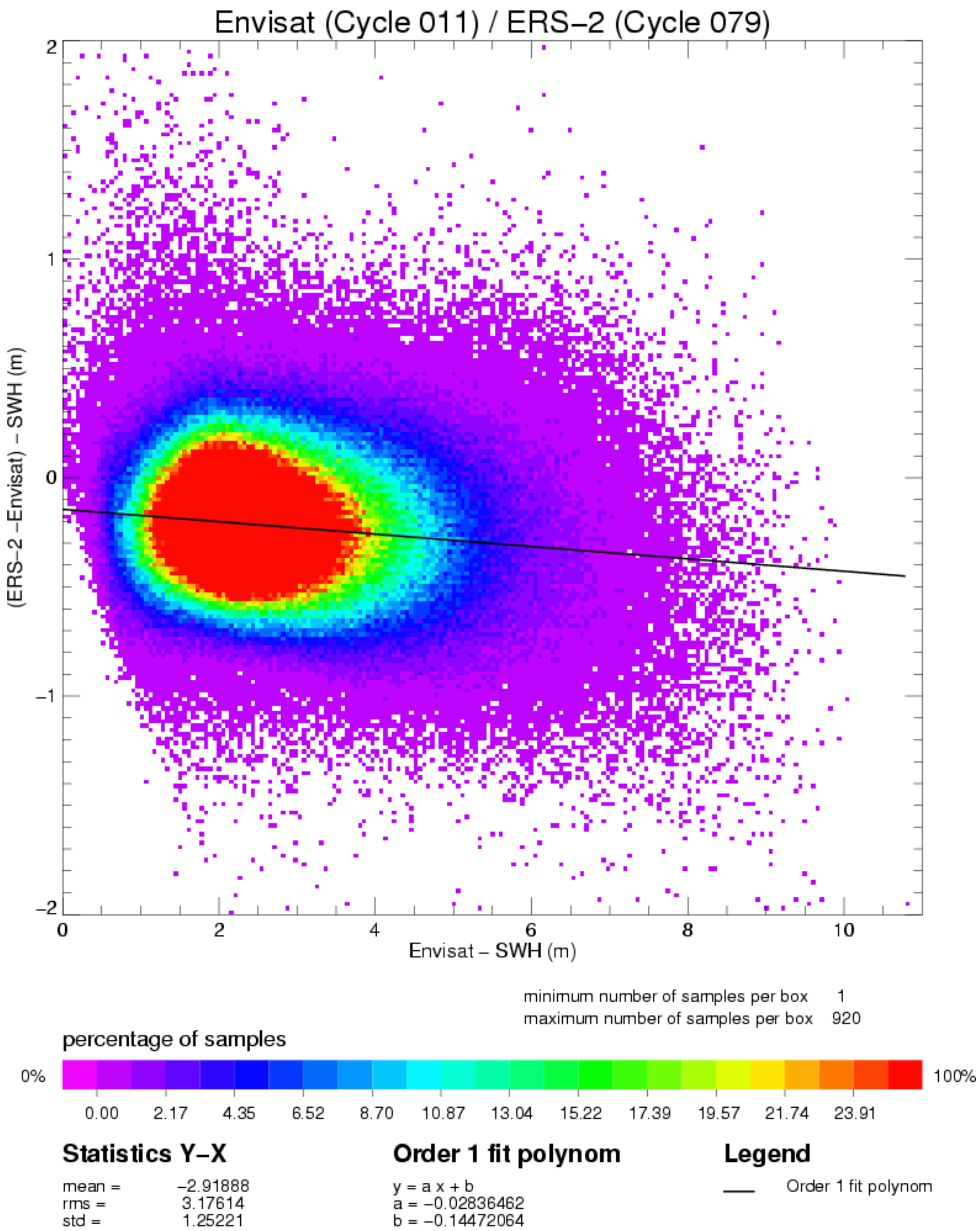

Figure 44: Scatter plot of (ERS-2-ENVISAT) SWH differences (m) versus ENVISAT SWH.

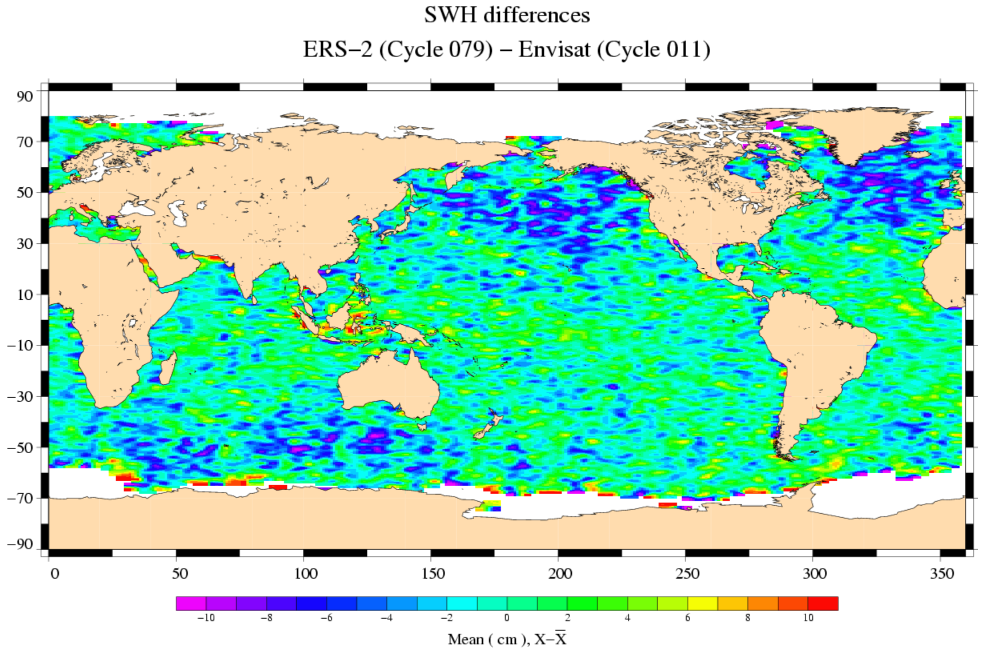

Figure 45: Map of (ERS-2 – ENVISAT) SWH differences (cm). Values are centred about the mean.

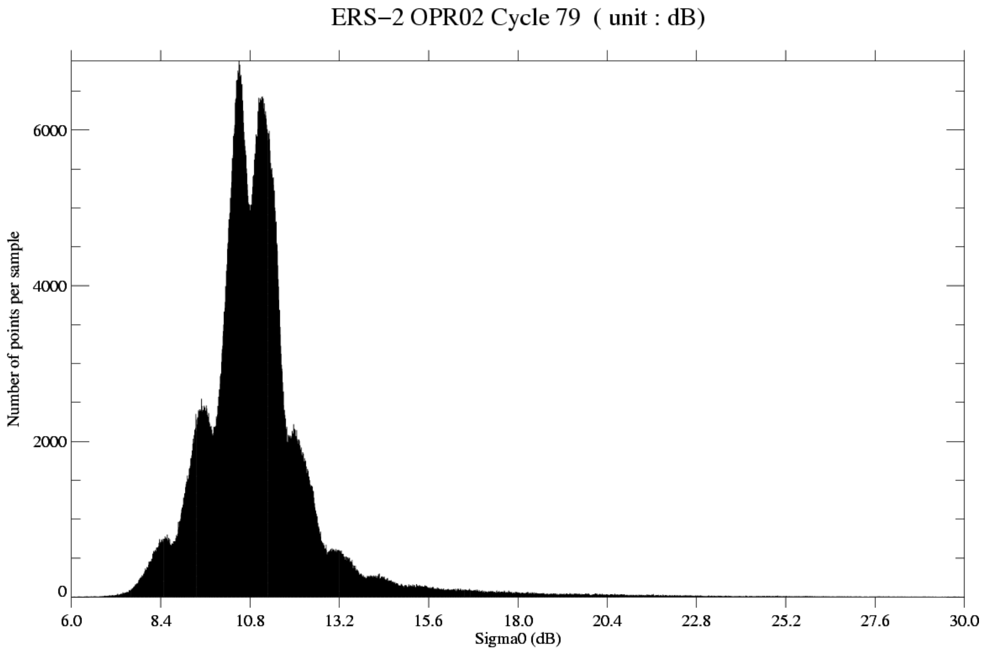

Global nb of points :	1480104	Sel. nb of points :	1480104	Sample interval :	0.010
Global mean :	11.034	Selected mean :	11.034	Maximum value :	30.000
Global Std :	1.718	Selected std :	1.718	Minimum value :	6.000

Figure 46: ERS-2 Sigma0 (dB) histogram for cycle 79.

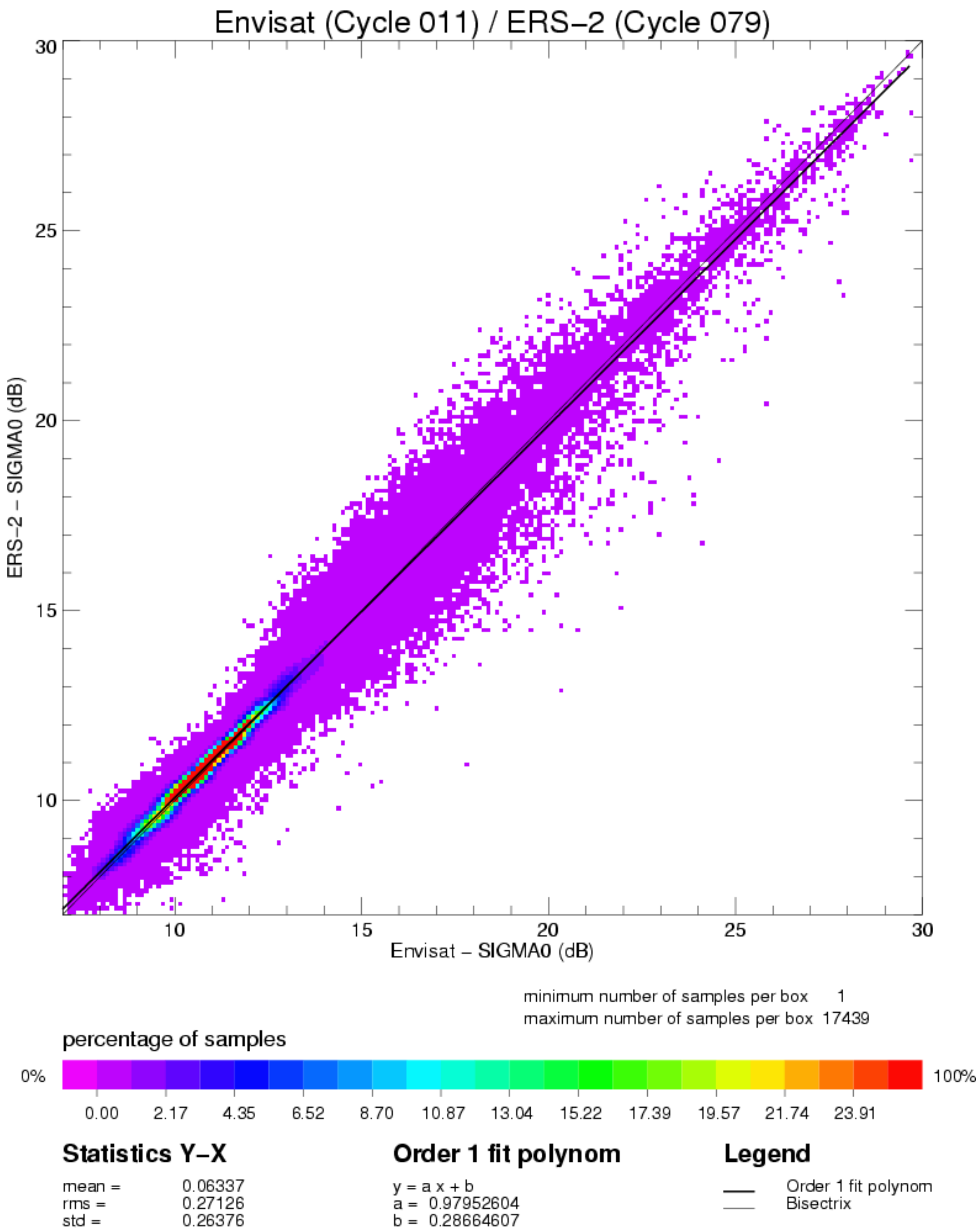

Figure 47: Scatter plot of ERS-2 Sigma0 versus ENVISAT Sigma0 (dB).

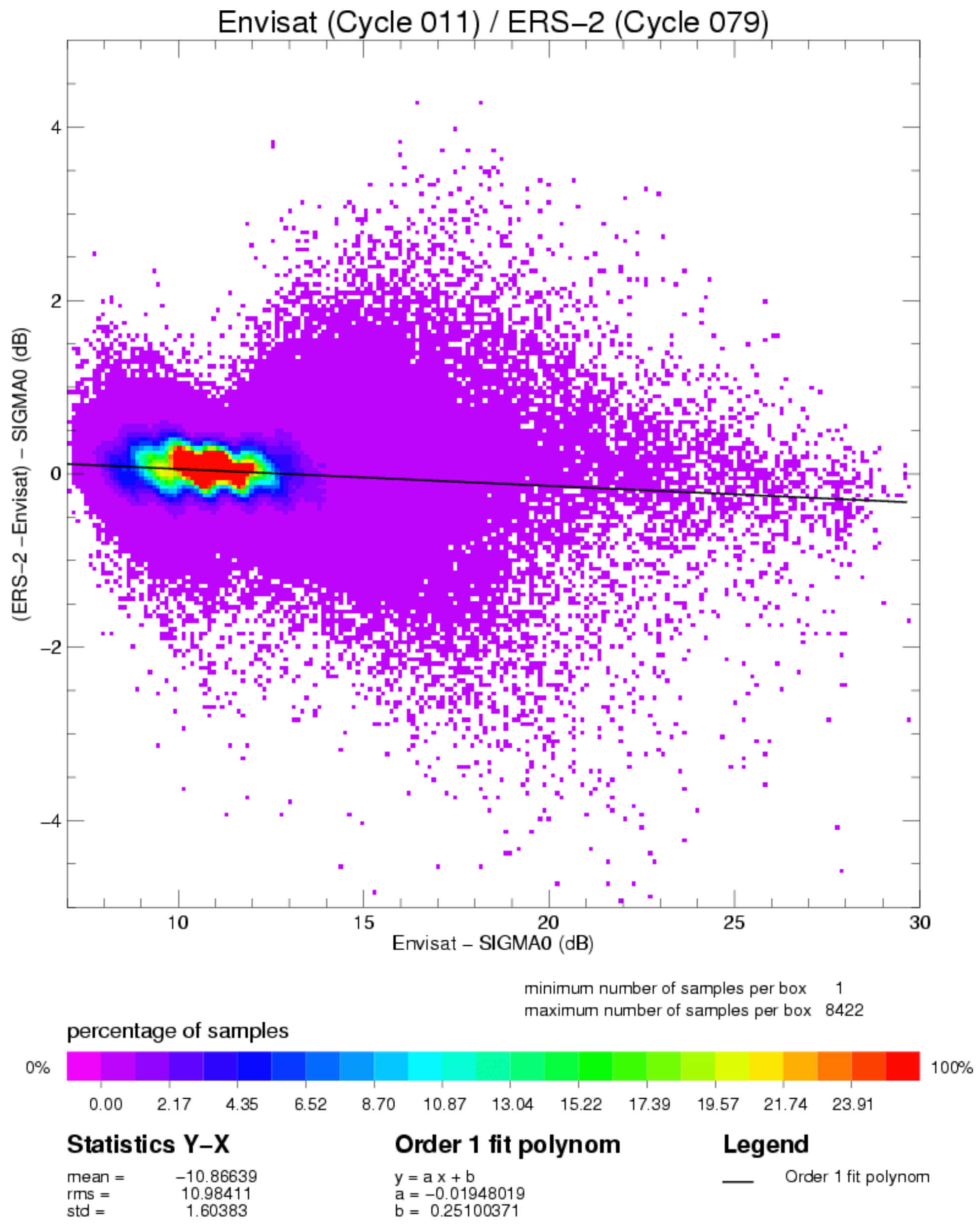

Figure 48: Scatter plot of (ERS-2-ENVISAT) Sigma0 differences versus ENVISAT Sigma0 (dB).

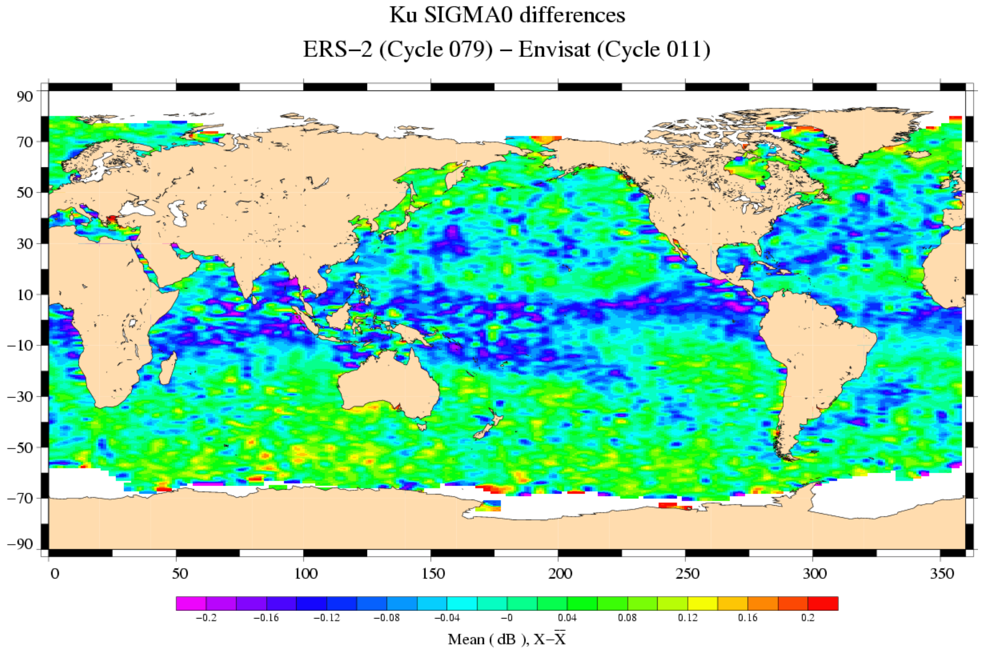

Figure 49: Map of Sigma0 differences (dB). Values are centred about the mean value.

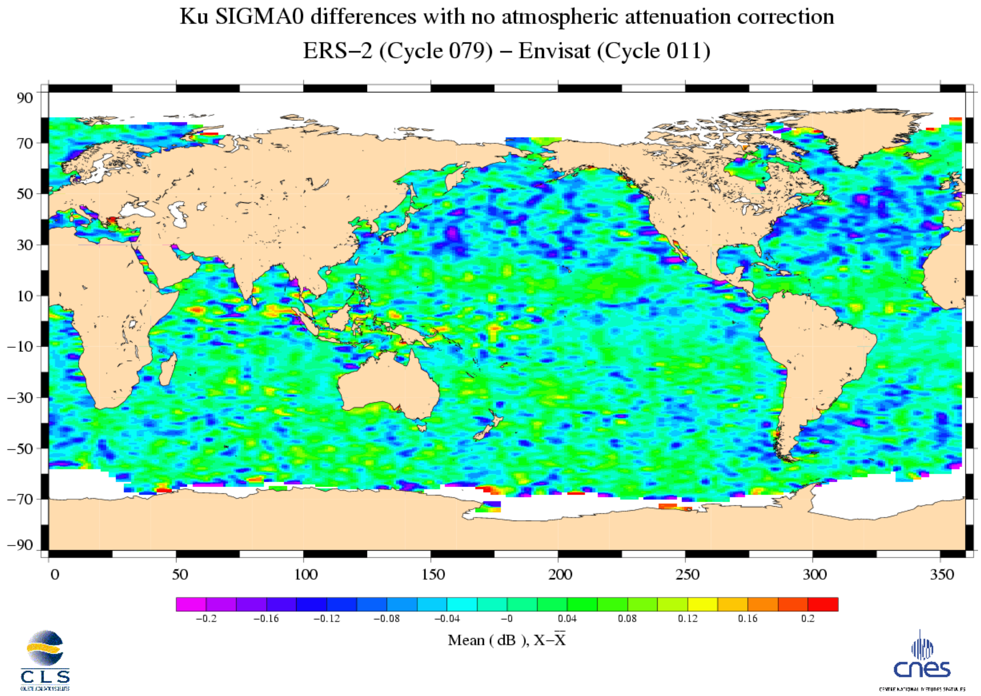

Figure 50 : Map of Sigma0 differences (dB) without any correction of atmospheric attenuation.

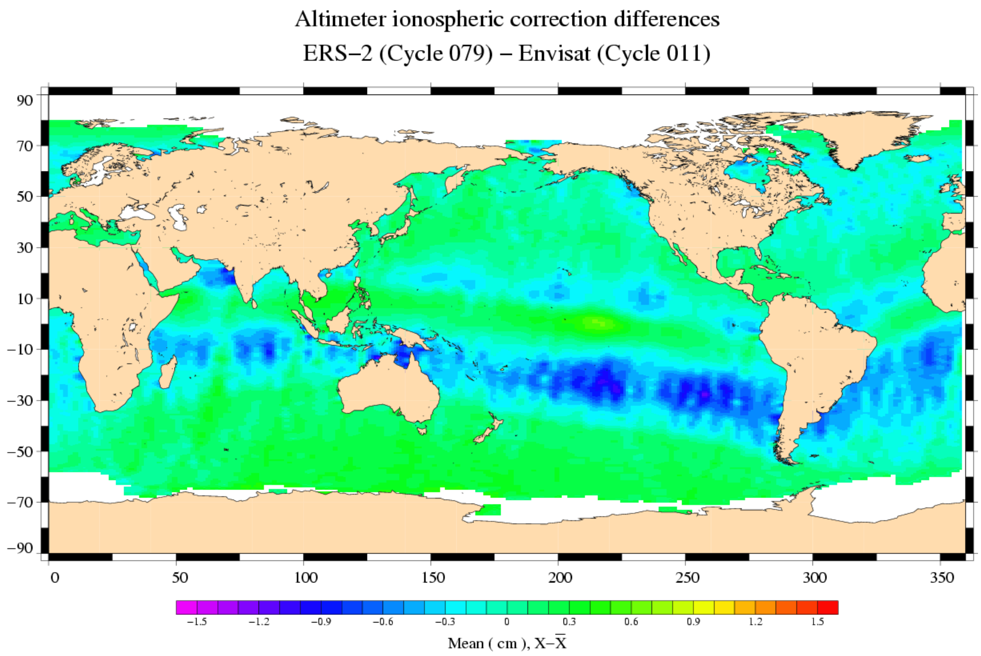

Figure 51: BENT ionosphere correction differences in cm. Values are centred about the mean.

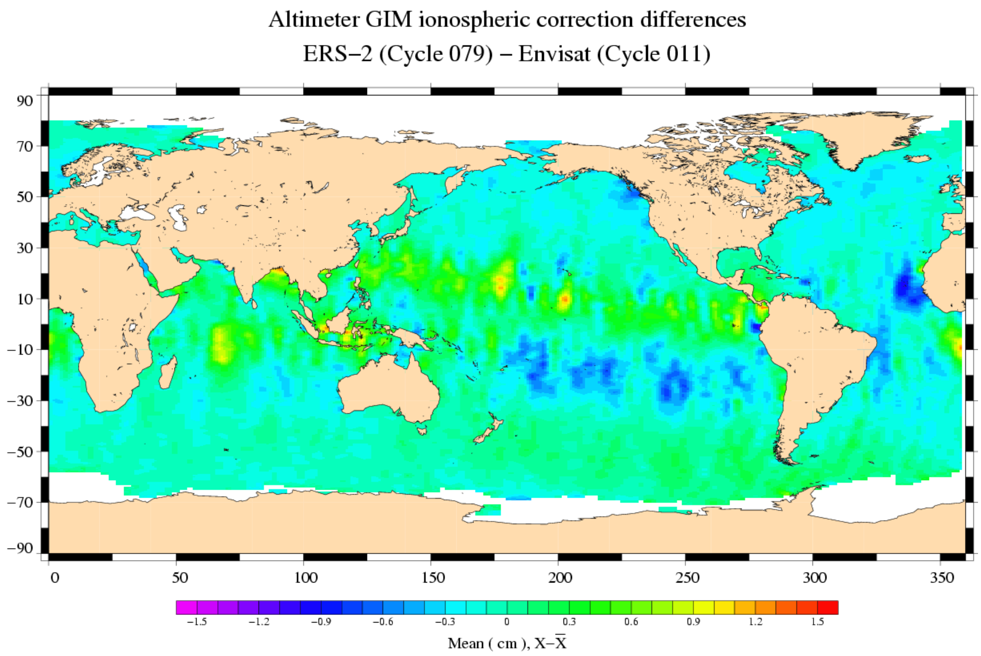

Figure 52 : GIM (ERS-2 – ENVISAT) ionosphere correction differences (cm). Values are centred about the mean.

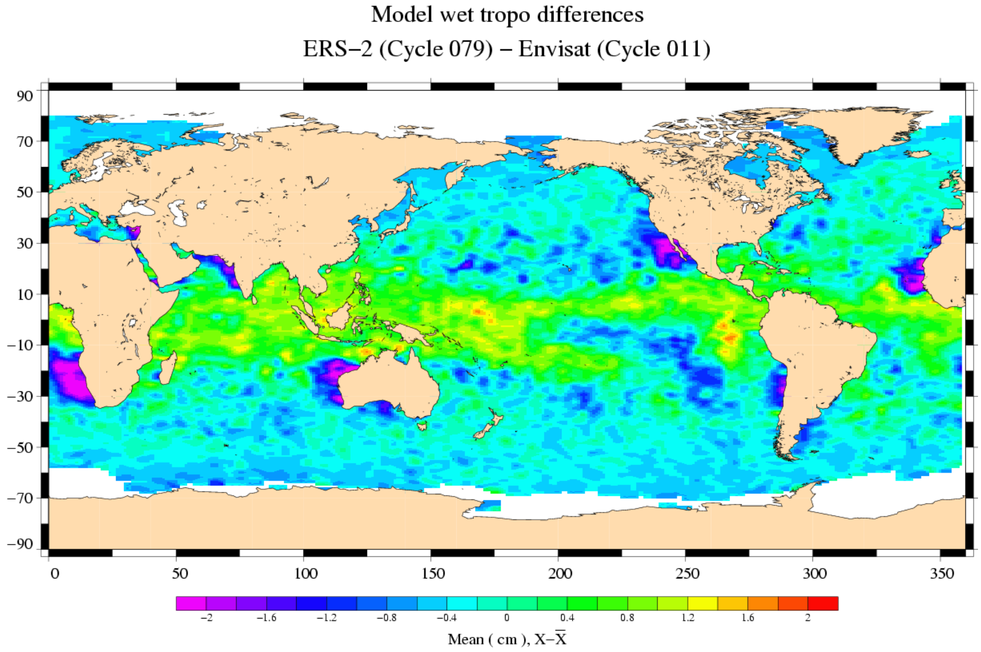

Figure 53: Map of (ESR-2 – ENVISAT) ECMWF wet troposphere correction differences (cm). Values are centred about the mean.

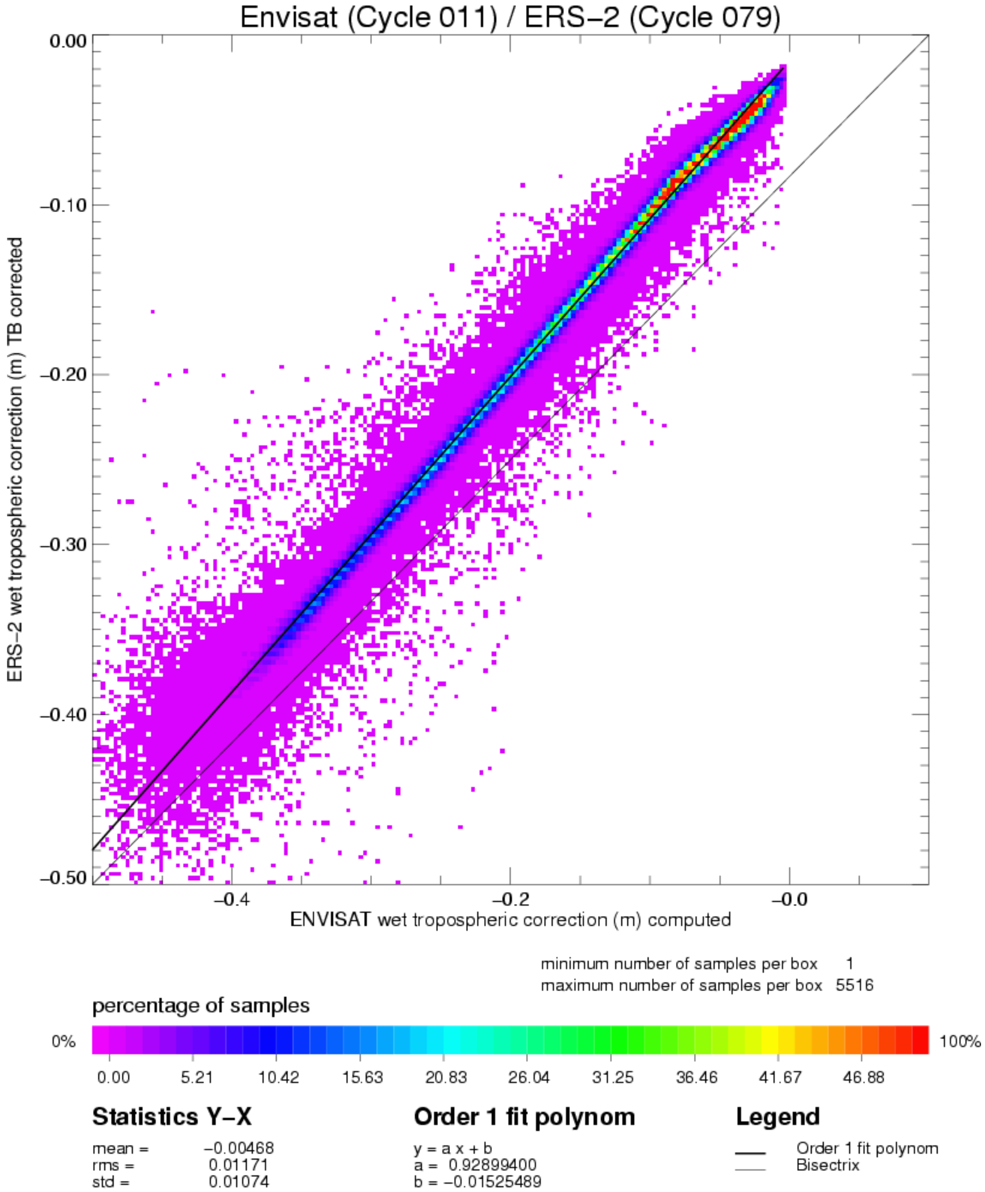

Figure 54: Scatter plot of ESR-2 radiometer correction versus ENVISAT radiometer correction (m).

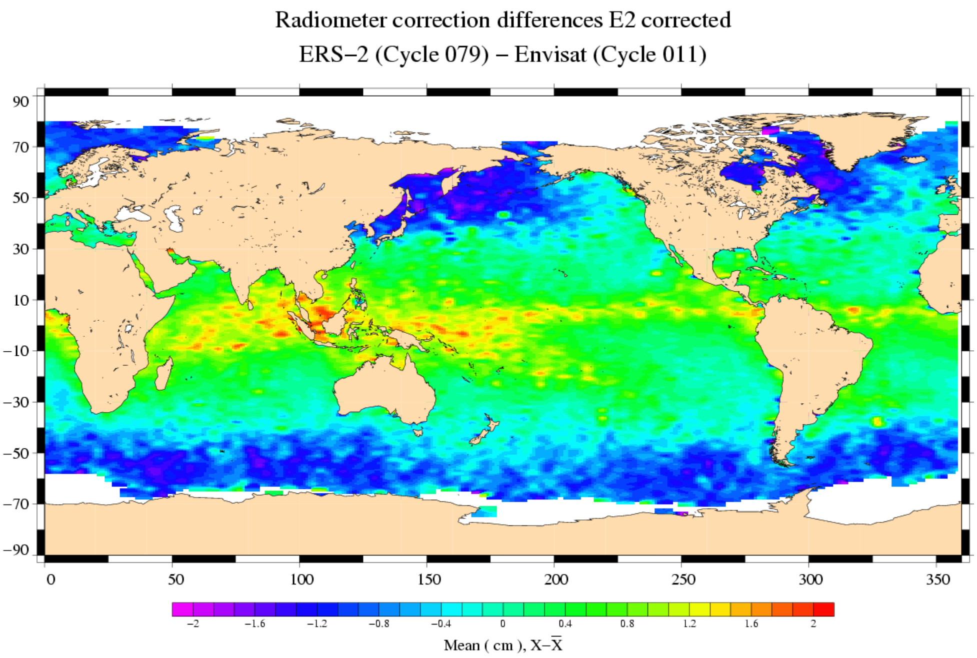

Figure 55 : Map of (ERS-2 – ENVISAT) radiometer correction differences (cm). Values are centred about the mean.

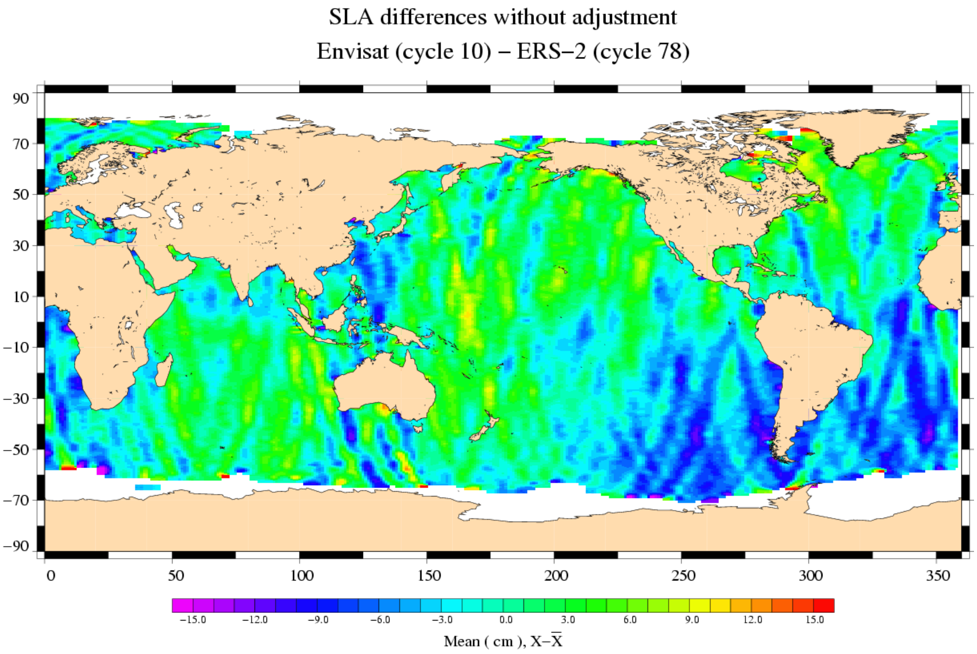

Figure 56 : Map of (ENVISAT – ERS-2) SSH differences (cm). Values are centred about the mean.

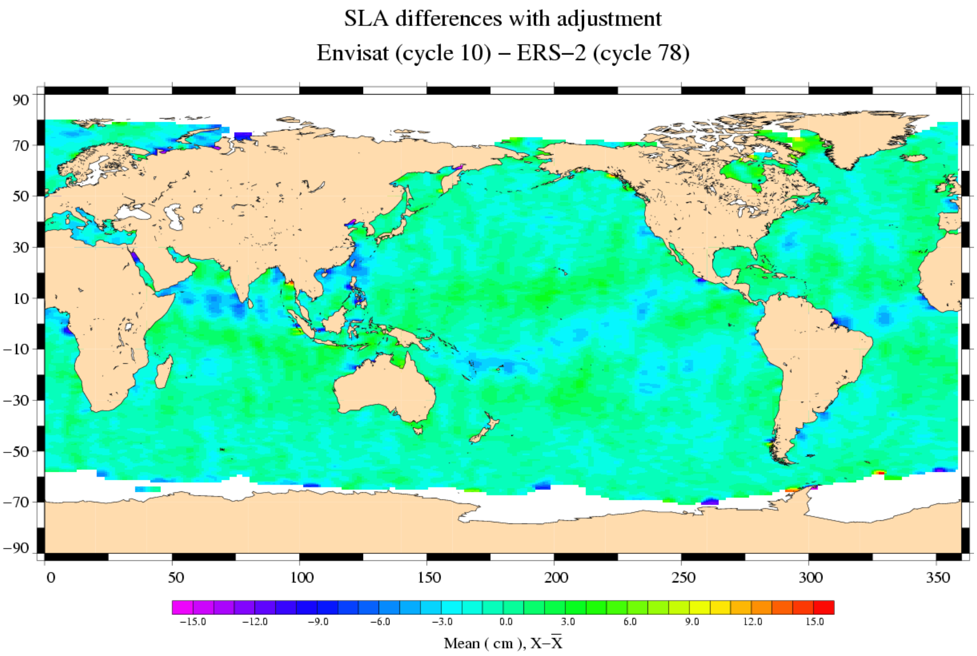

Figure 57 : Map of (ENVISAT – ERS-2) SSH differences (cm) after adjustment of orbit errors using Jason-1 data.

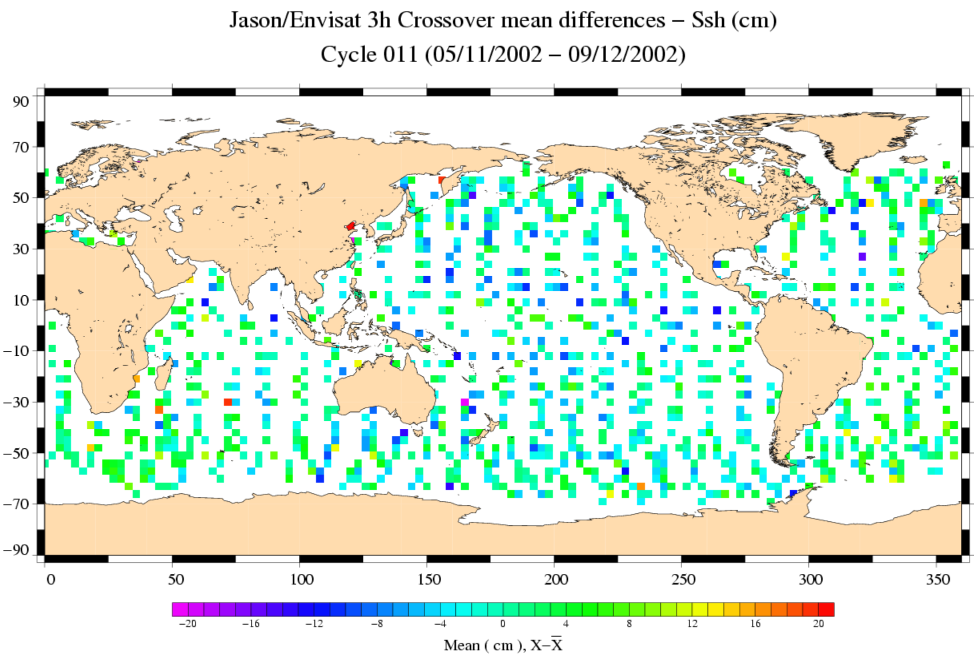

Figure 58 : ENVISAT/Jason-1 crossovers pattern, with 3-hour time lag.

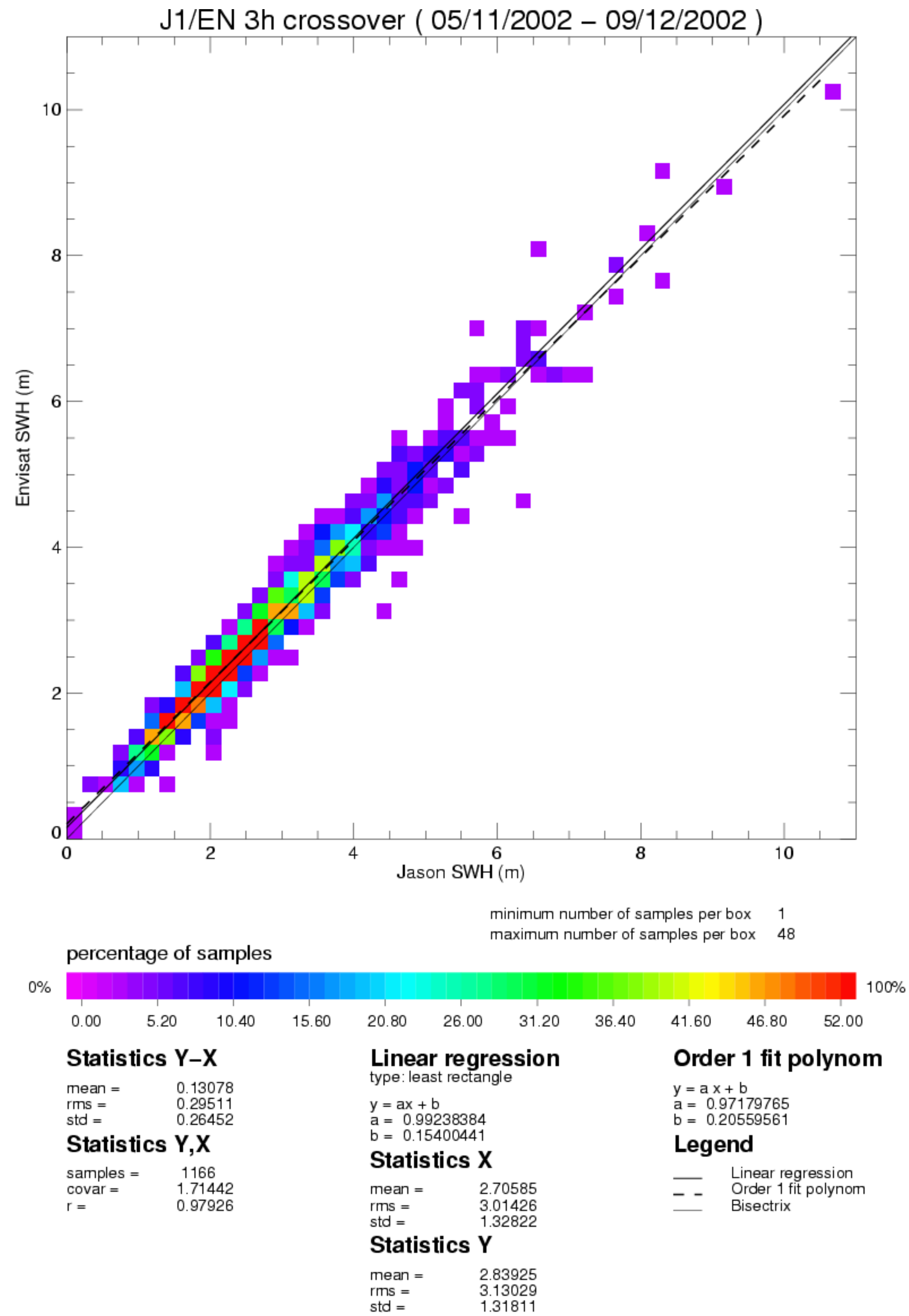

Figure 59 : Scatter plot of ENVISAT/Jason-1 SWH crossover differences (m), 3-hour time lag.

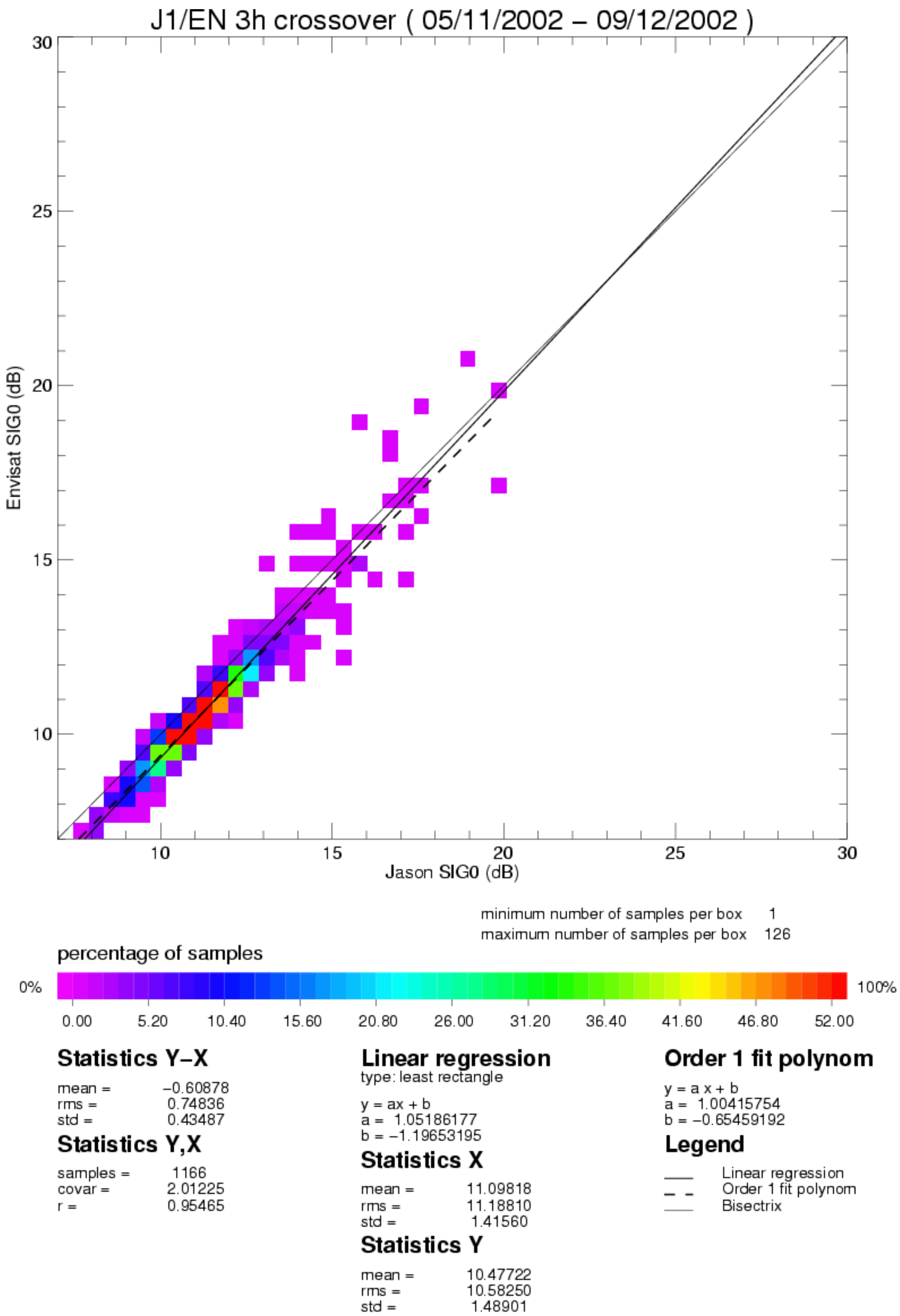

Figure 60 : Scatter plot of ENVISAT/Jason-1 Sigma0 crossover differences (dB), with 3-hour time lag.

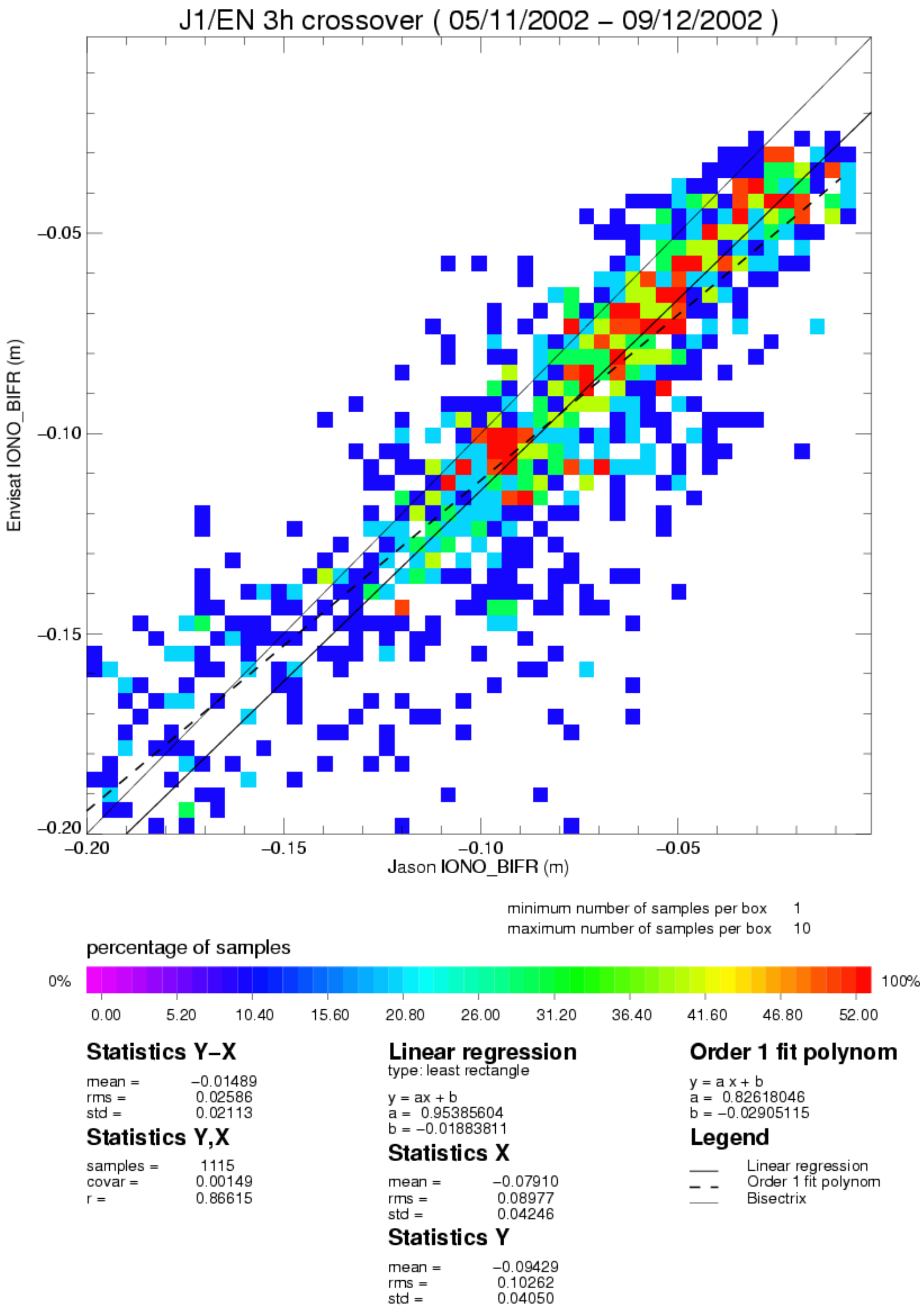

Figure 61 : Scatter plot of ENVISAT/Jason-1 Dual-Frequency ionosphere corrections (m) at crossovers (3-hour time lag).

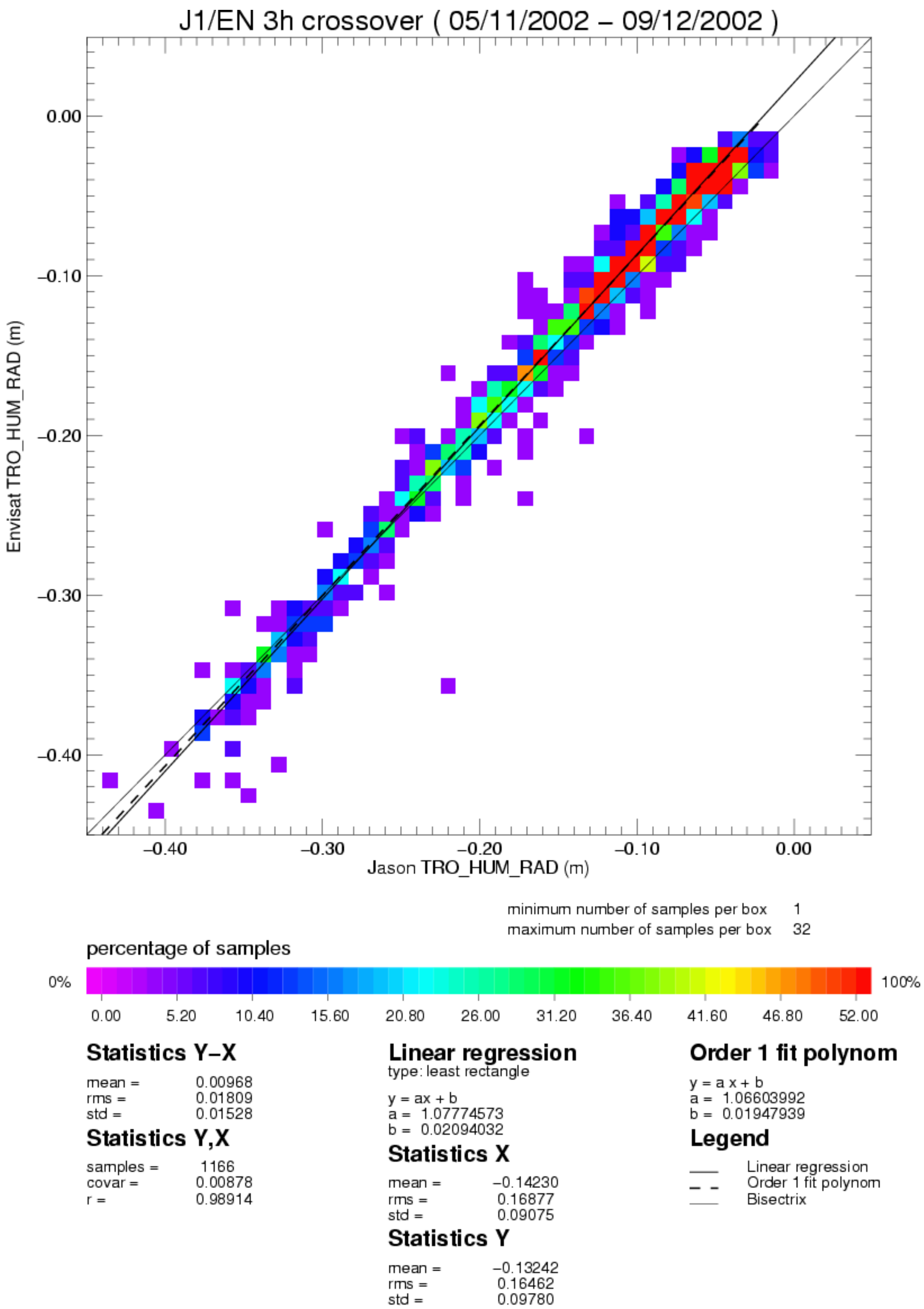

Figure 62 : Scatter plot of ENVISAT/Jason-1 radiometer wet troposphere corrections (m) at crossovers (3-hour time lag).

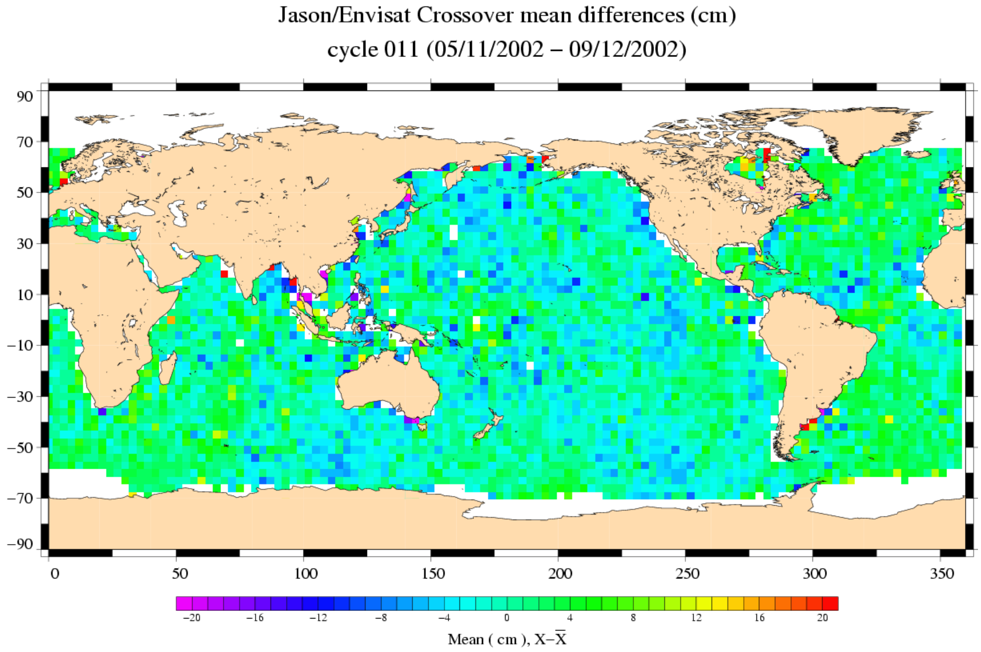

Figure 63 : ENVISAT/Jason-1 SSH crossover differences (cm), with 10-day time lag. Values are centred about the mean.

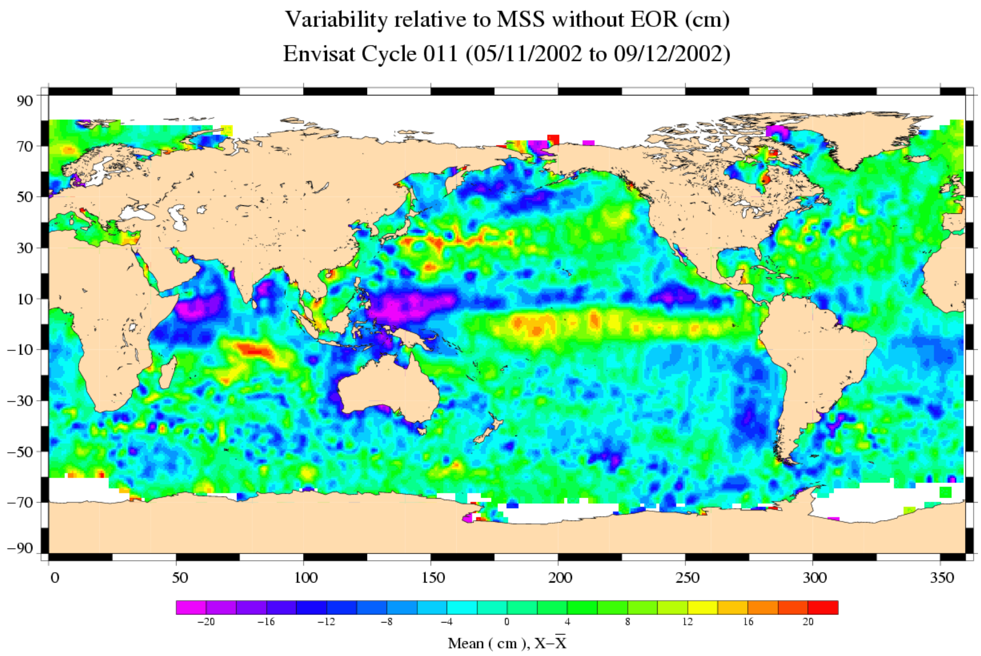

Figure 64 : ENVISAT Sea Level Anomaly (cm) relative to CLS01 MSS.

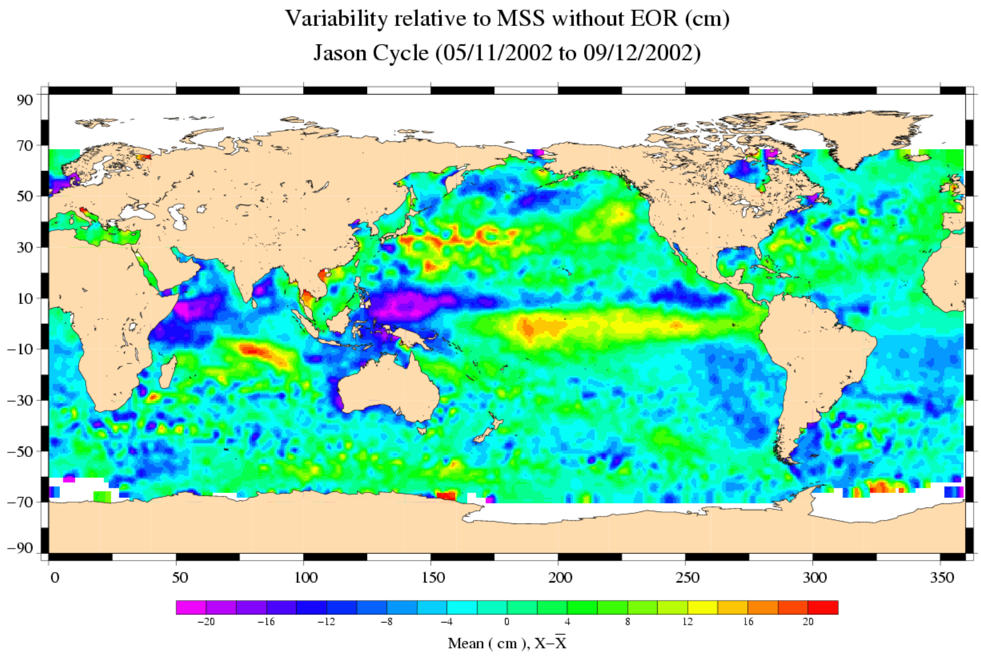

Figure 65 : Jason-1 Sea Level Anomaly (cm) relative to CLS01 MSS.

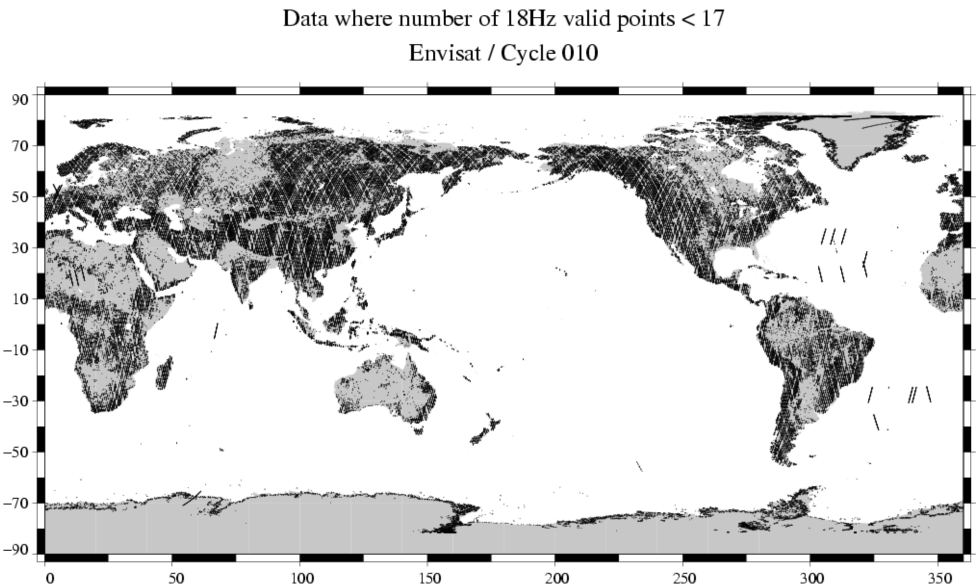

Figure 66 : Locations of measurements with number of Ku Band elementary valid ranges <17, cycle 10

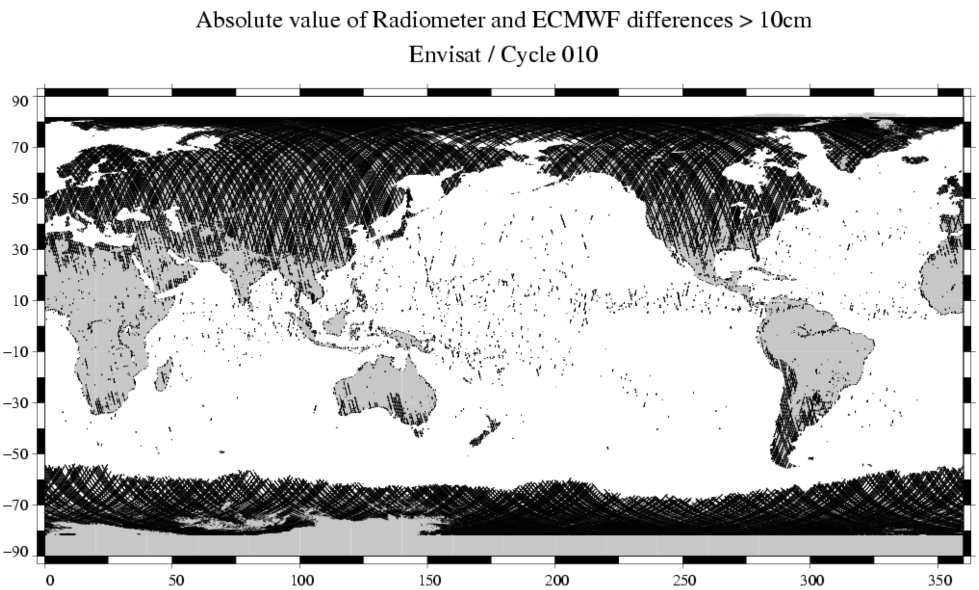

Figure 67 : Measurements for which |MWR-CMWF|>10cm, cycle 10

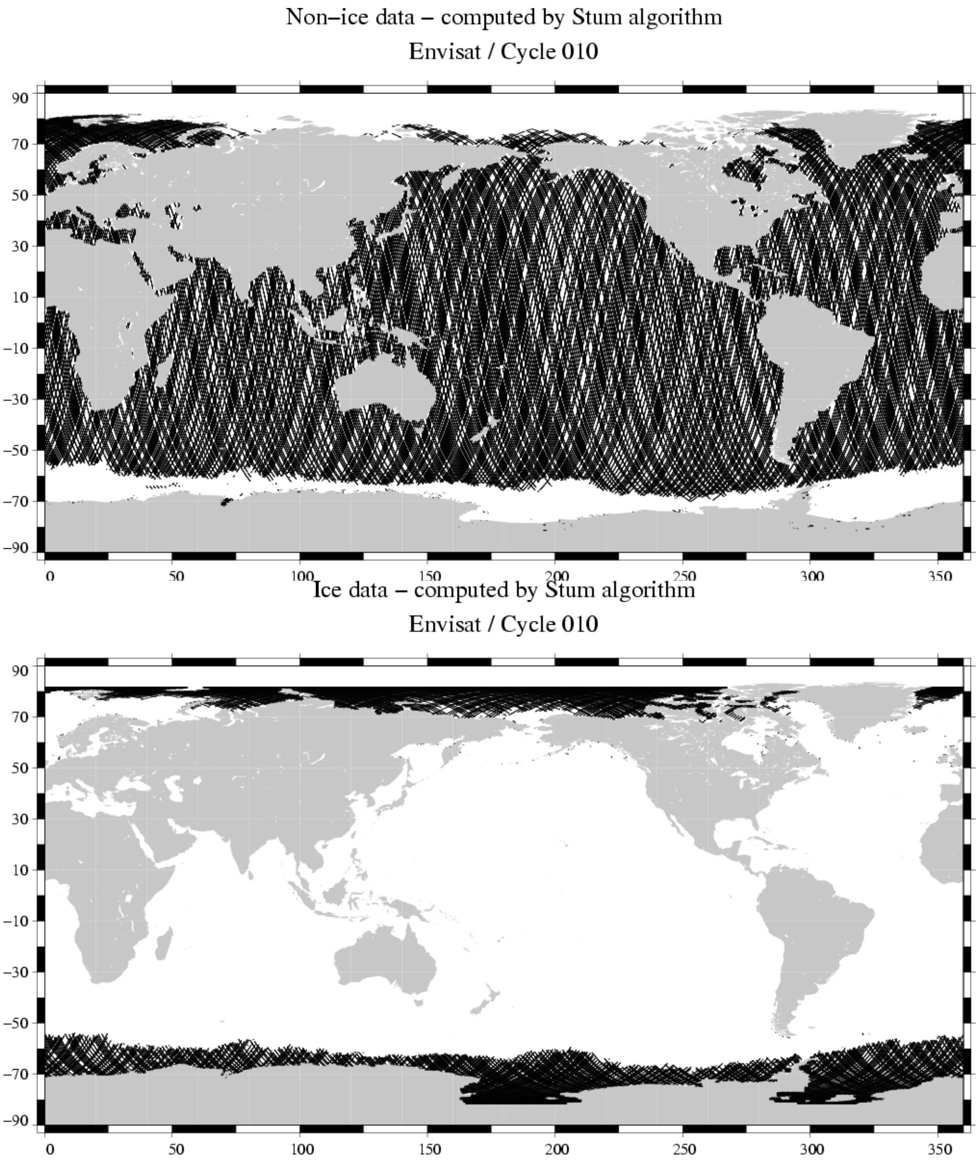

Figure 68 : Ocean (top) and ice (bottom) data using ERS-2 method, cycle 10

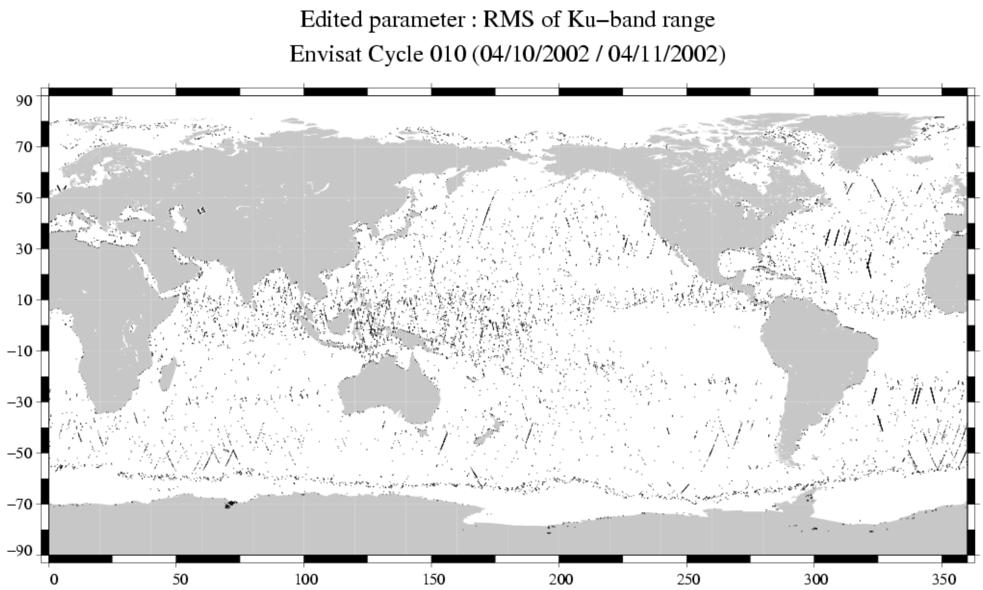

Figure 69 : RMS of Ku range>20cm over open ocean

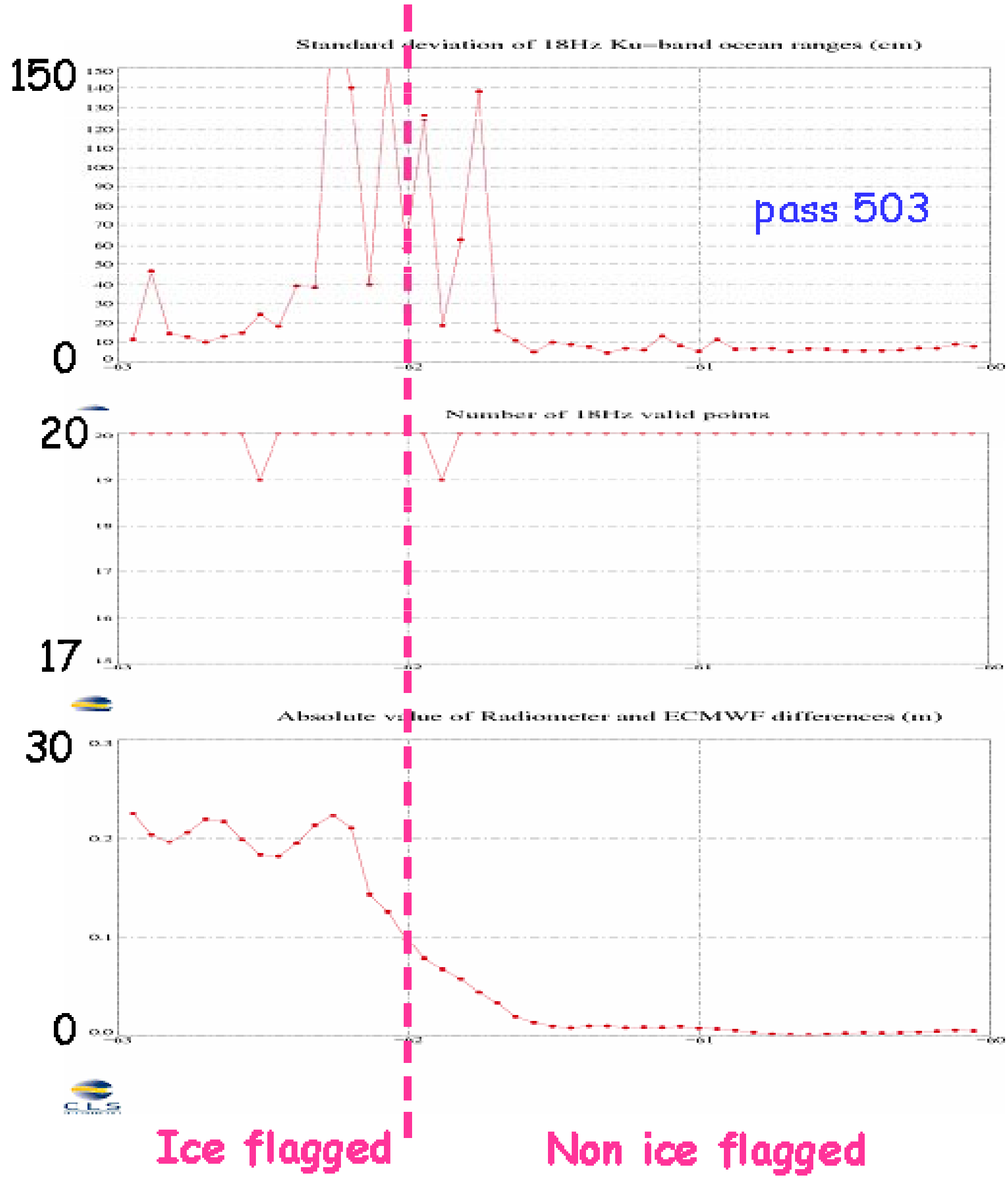

Figure 70 : RMS of Ku-band range, number of elementary measurements, and |MWR-ECMWF| on pass 503

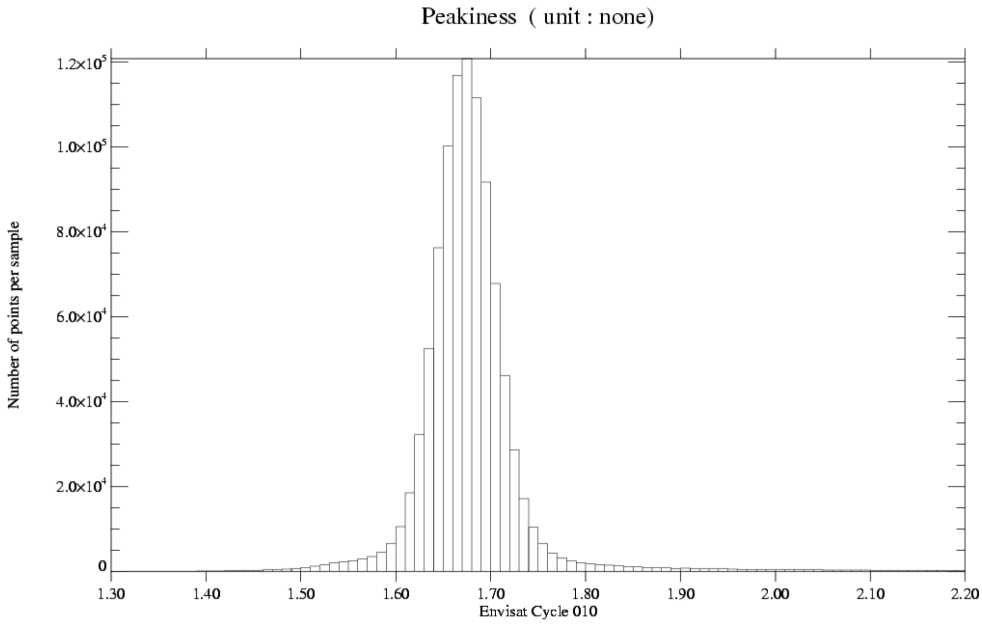

Global nb of points	:	1172316	Sel. nb of points	:	974628	Sample interval	:	0.010
Global mean	:	4.399	Selected mean	:	1.678	Maximum value	:	65.526
Global Std	:	7.647	Selected std	:	0.058	Minimum value	:	0.850

Figure 71 : Histogram of peakiness, cycle 10

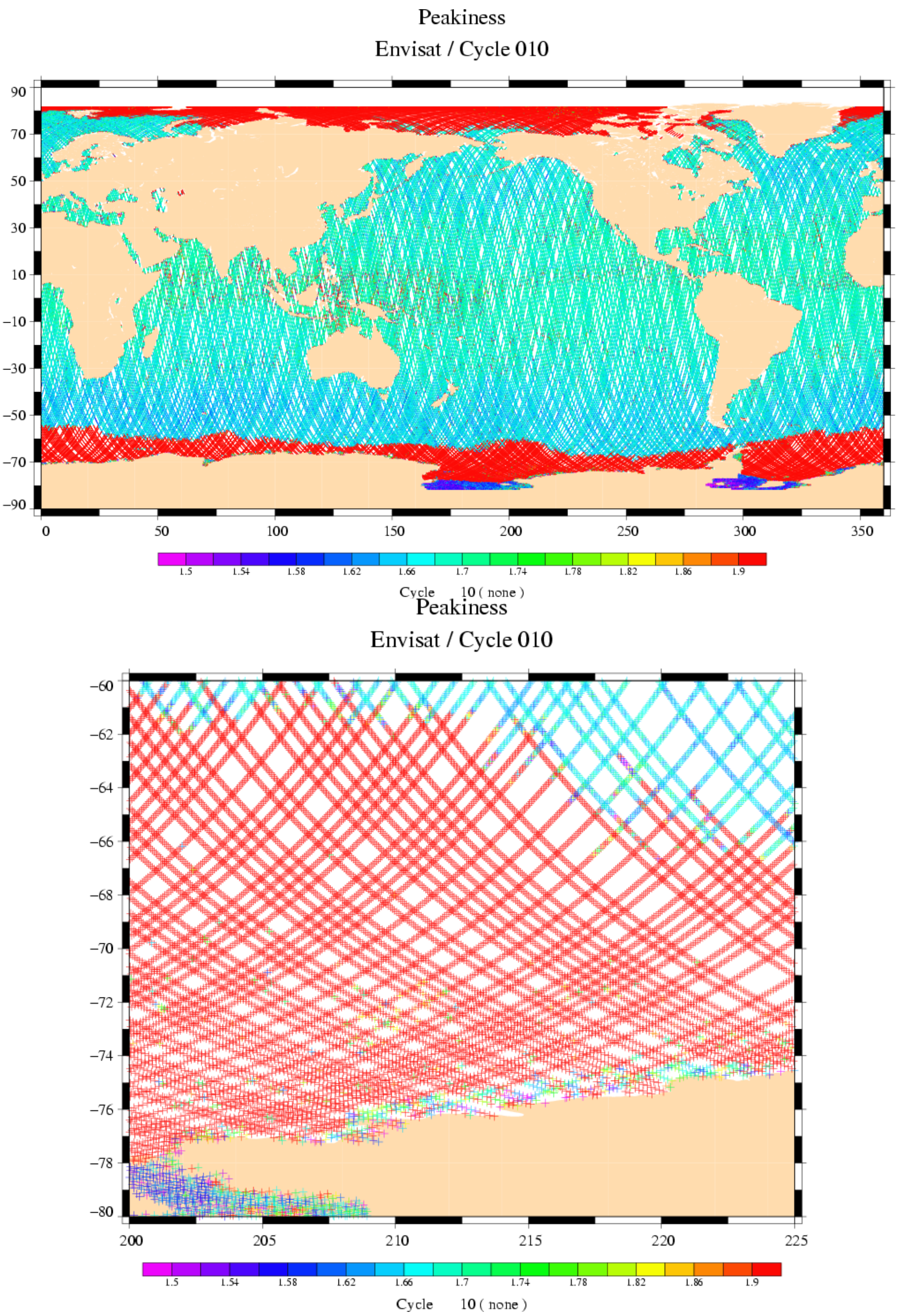

Figure 72 : Map of peakiness (top), zoom on Antarctica (bottom), cycle 10

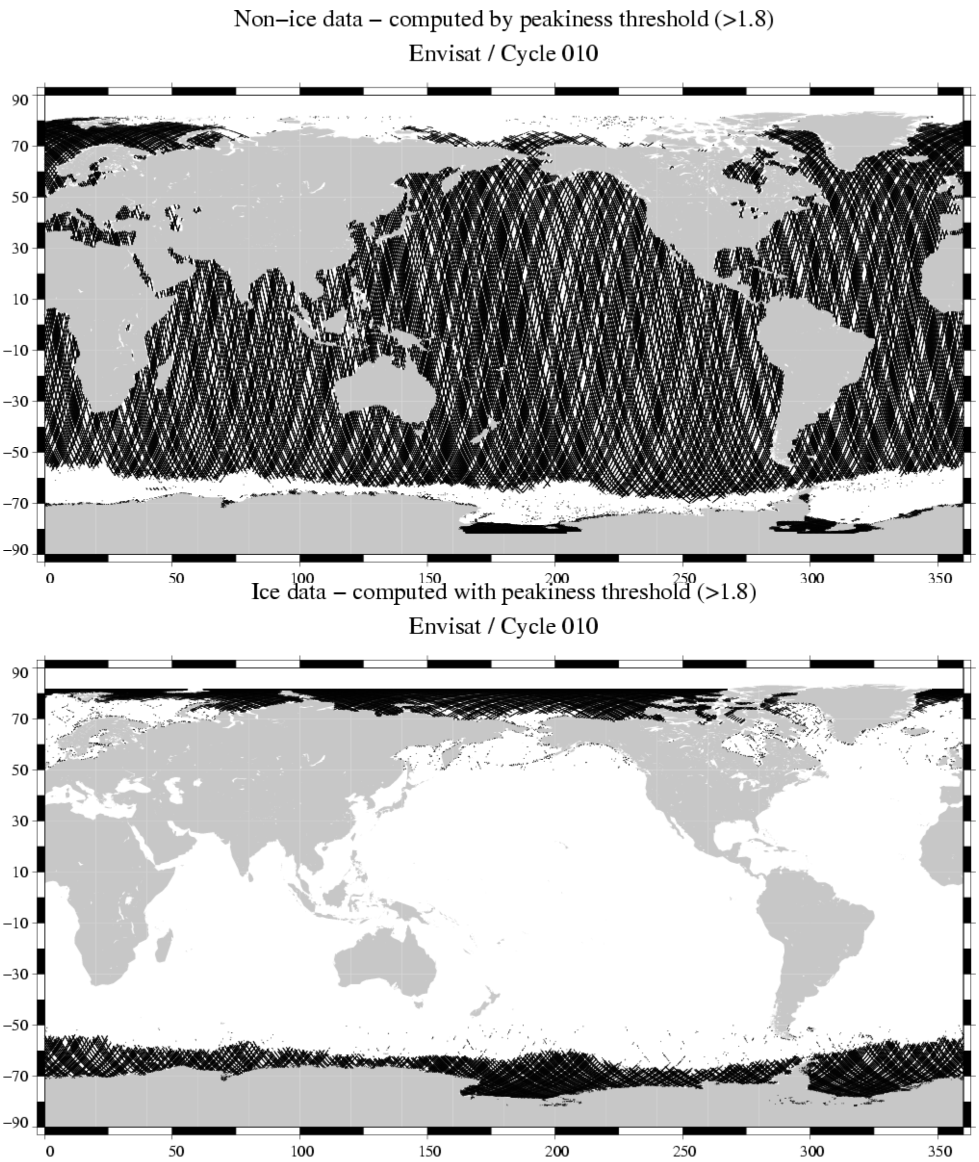

Figure 73 : Ocean (top) and ice (bottom) data using a 1.8 threshold on peakiness, cycle 10

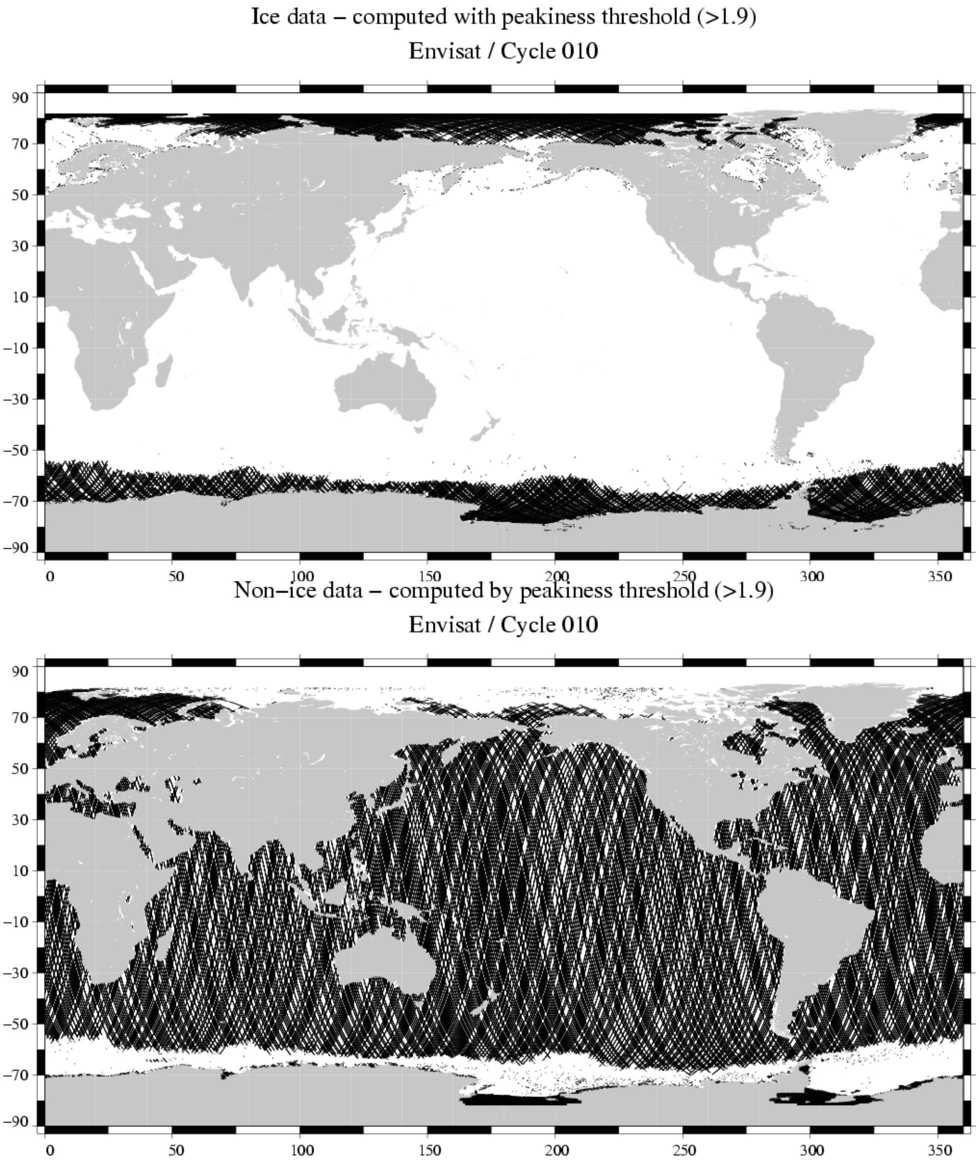

Figure 74 : Ocean (top) and ice (bottom) data using a 1.9 threshold on peakiness, cycle 10

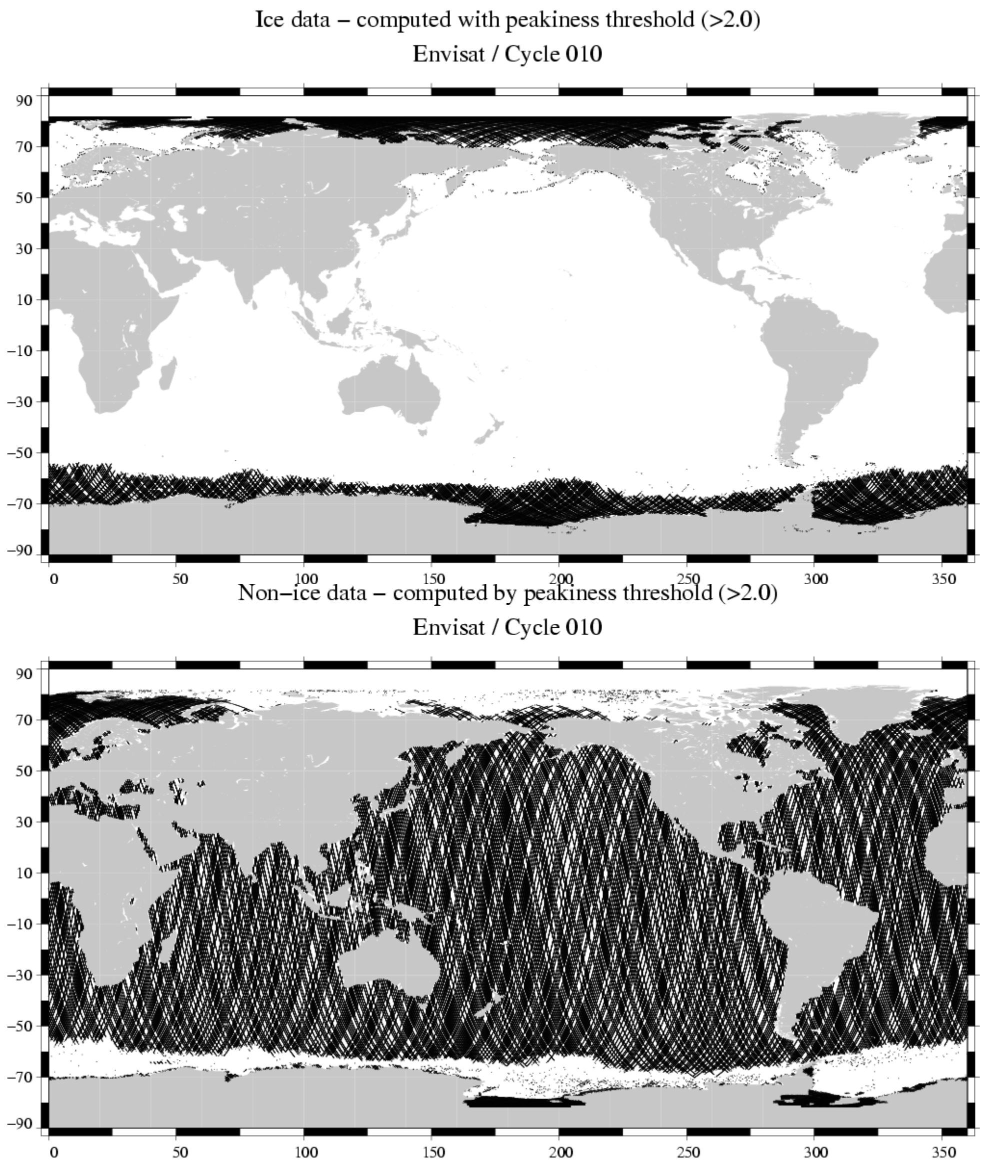

Figure 75 : Ocean (top) and ice (bottom) data using a 2.0 threshold on peakiness, cycle 10

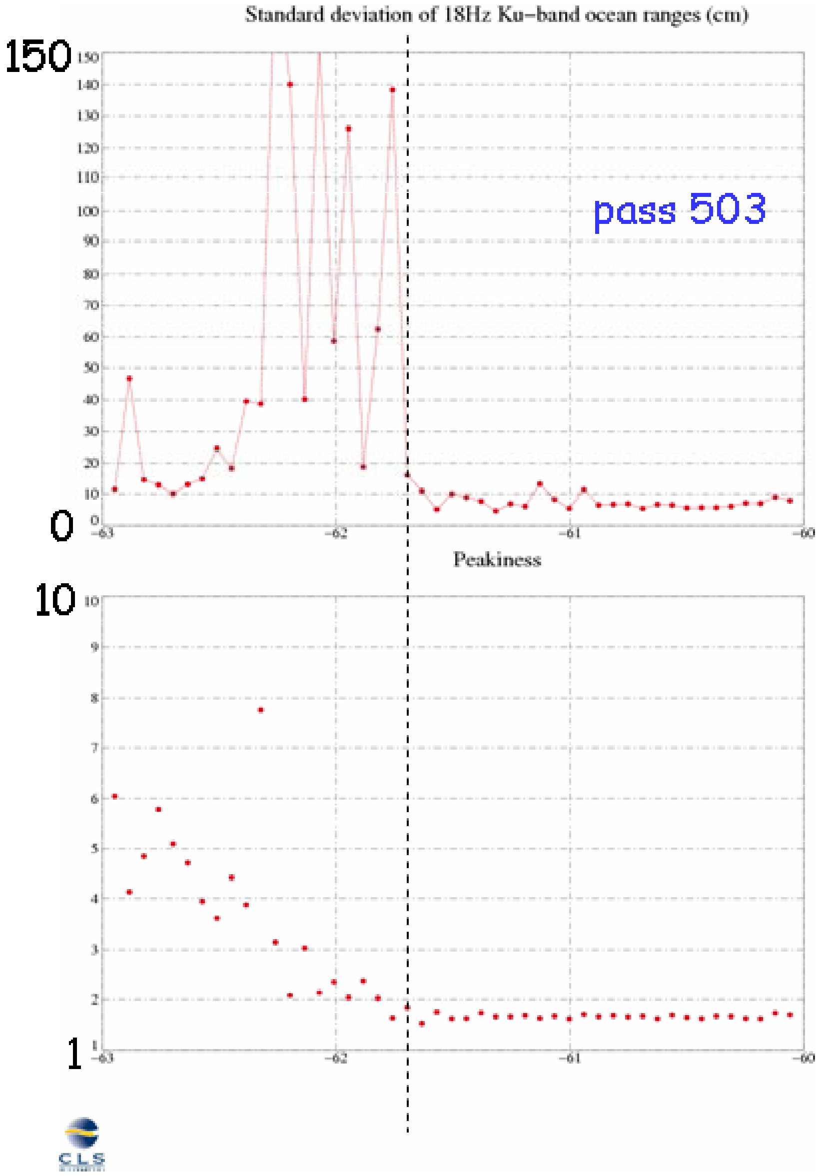

Figure 76 : RMS of Ku range, number of elementary data, |MWR-ECMWF| on pass 503

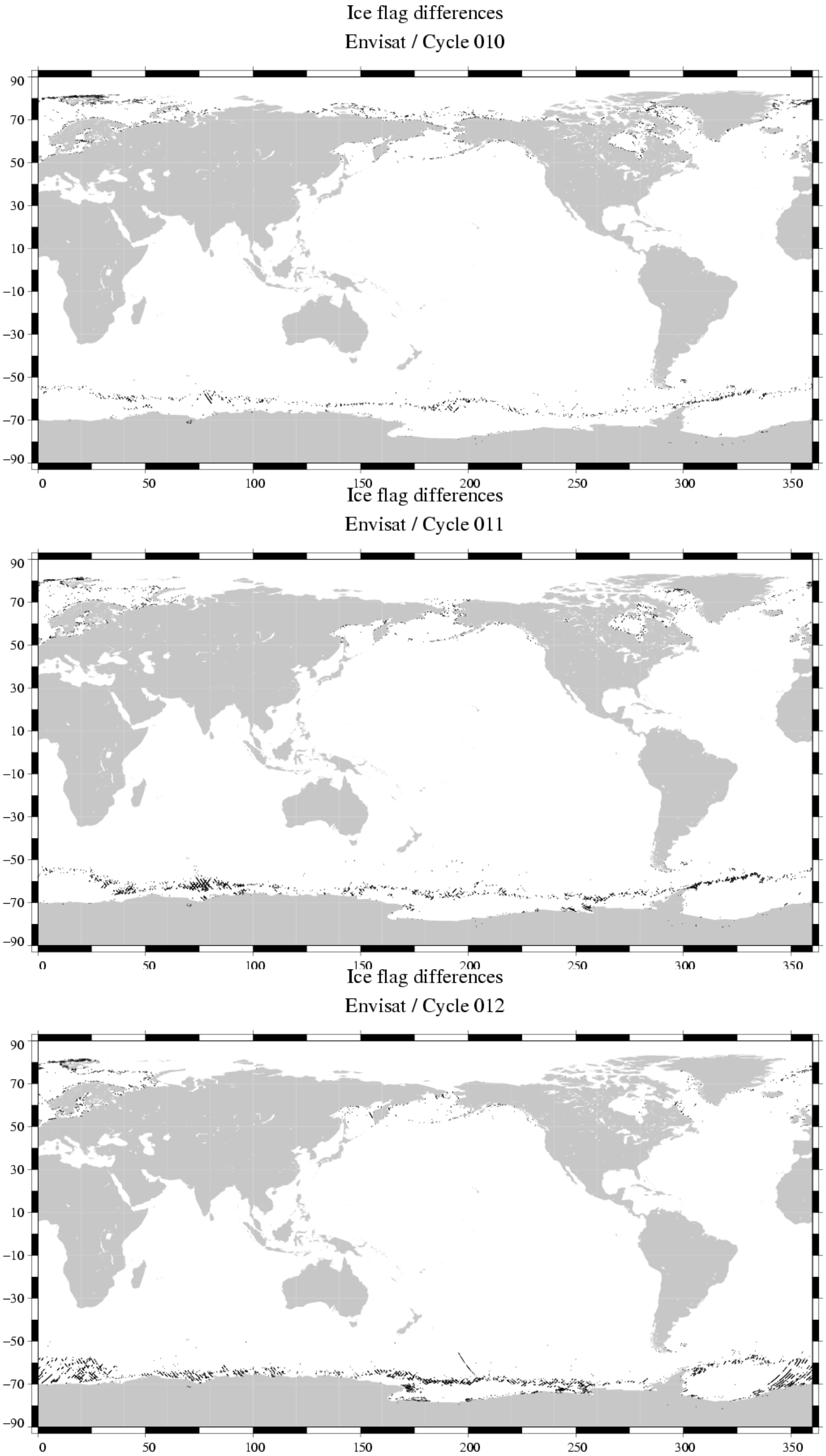

Figure 77 : Points detected as ice by a 2.0 threshold on peakiness, but seen as ocean data by the ERS-2 method, cycles 10, 11 and 12

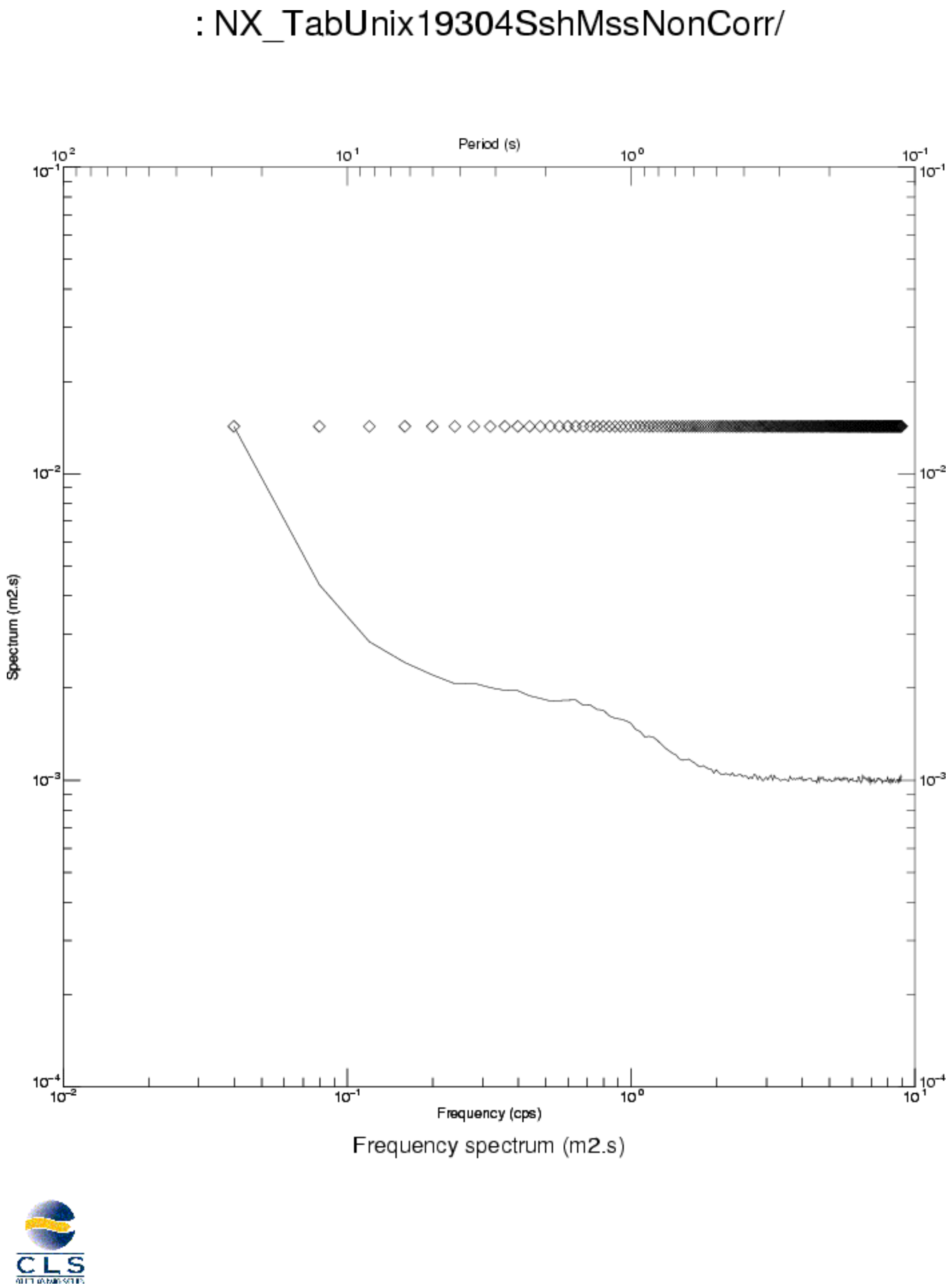

Figure 78 : Power spectrum of Envisat $SLA_{nc/mss}$ at 20Hz

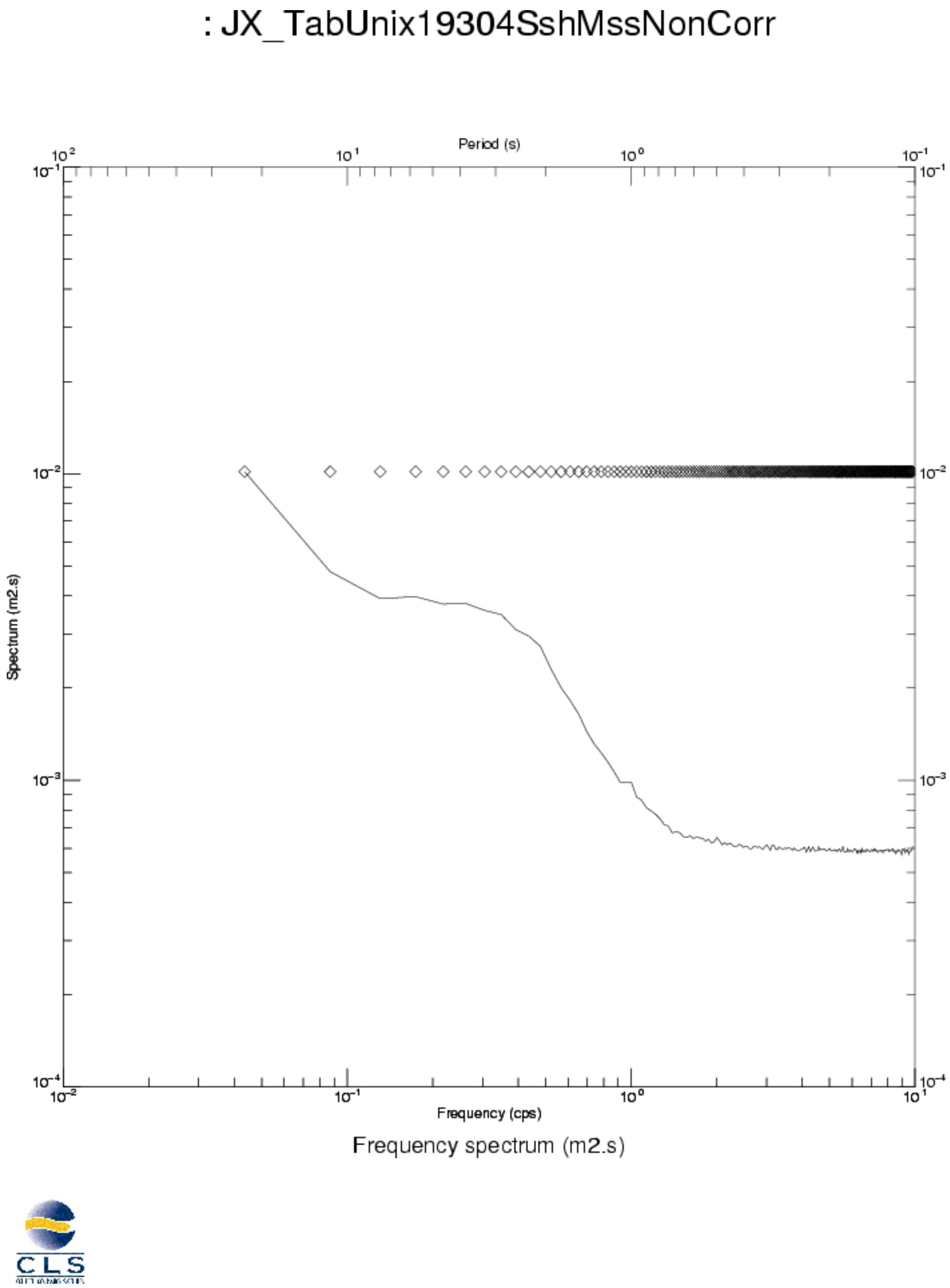

Figure 79 : Power spectrum of Jason SLA$_{nc/mss}$ at 20Hz

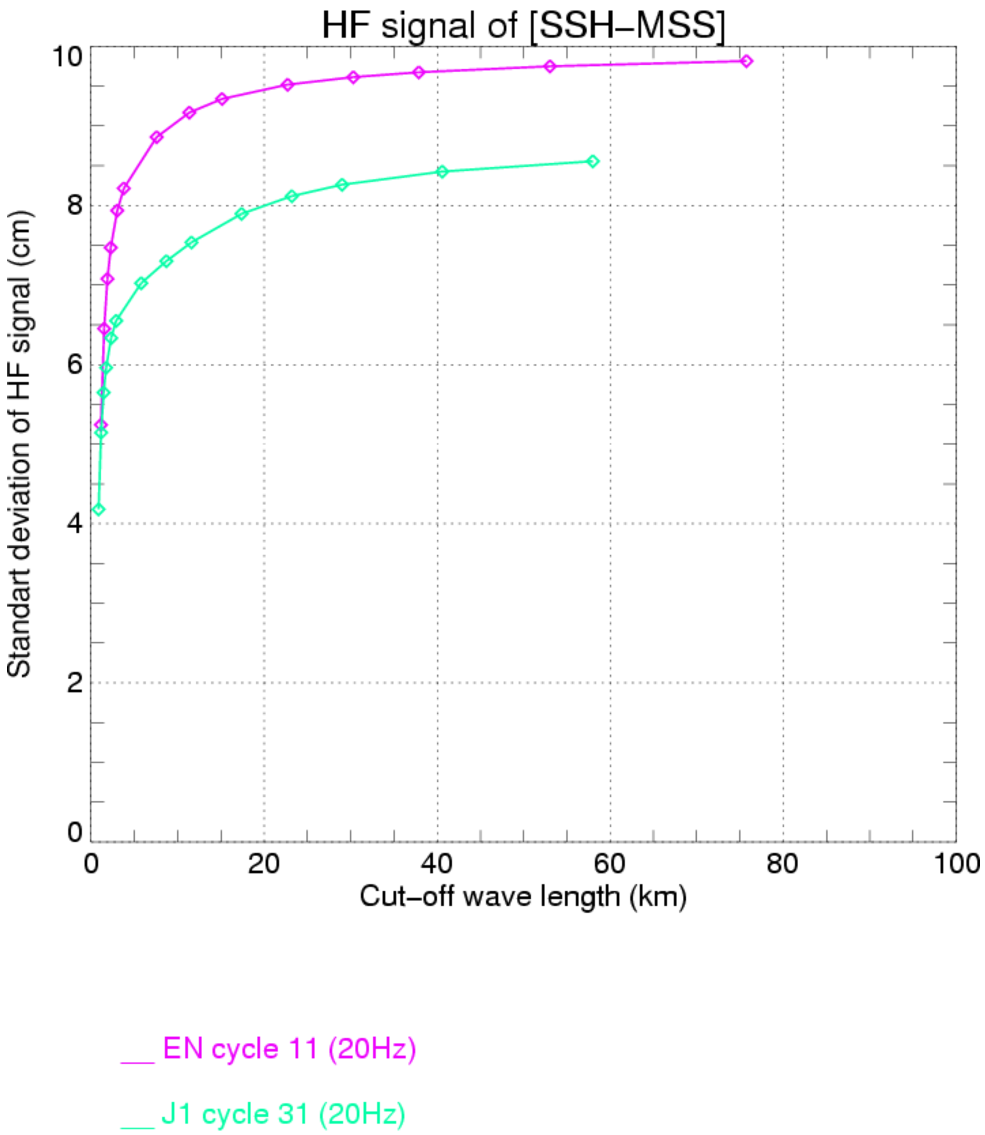

Figure 80 : Standard deviation of HF[$SLA_{nc/mss}$] at 20Hz according to cut-off wave-length

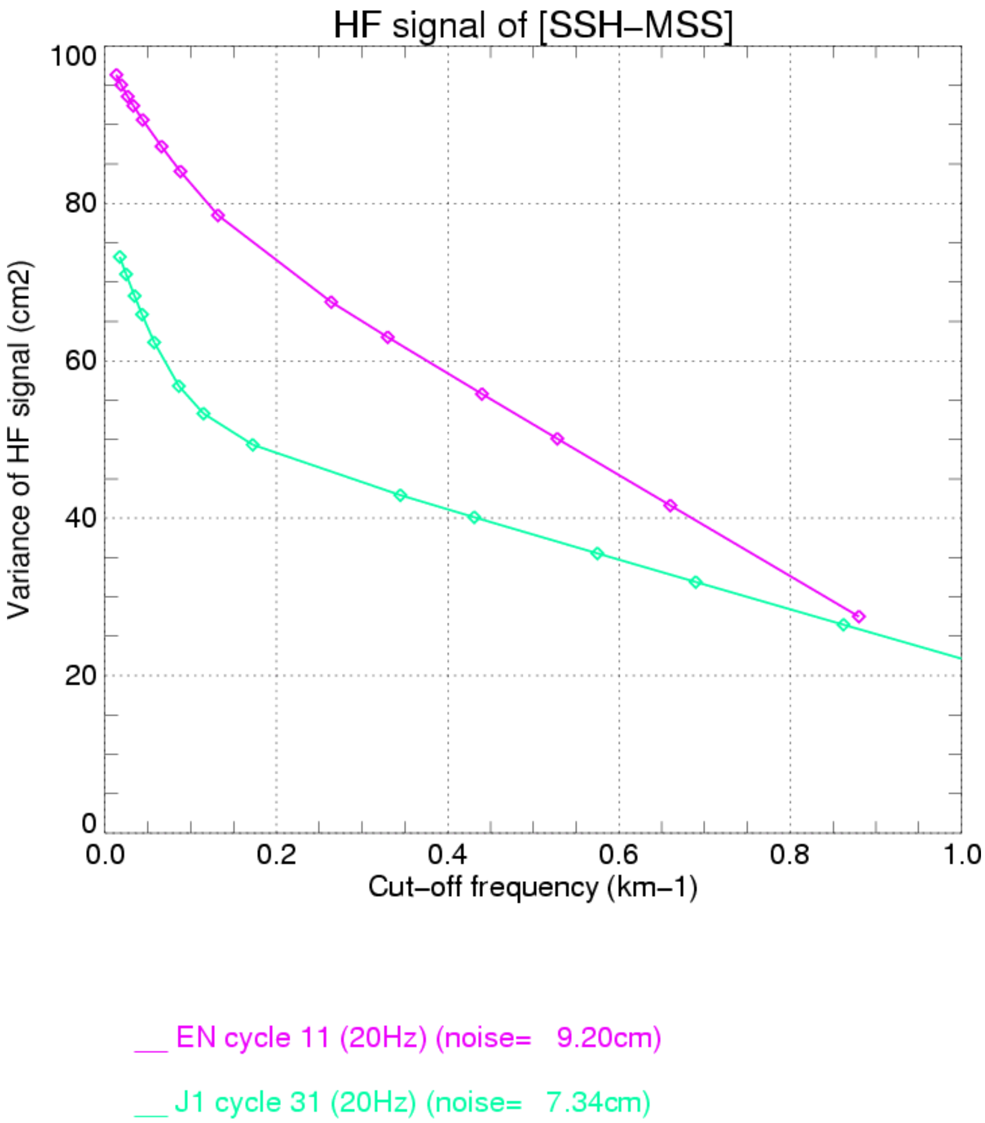

Figure 81 : Standard deviation of HF[SLA$_{nc/mss}$] at 20Hz according to the cut-off frequency

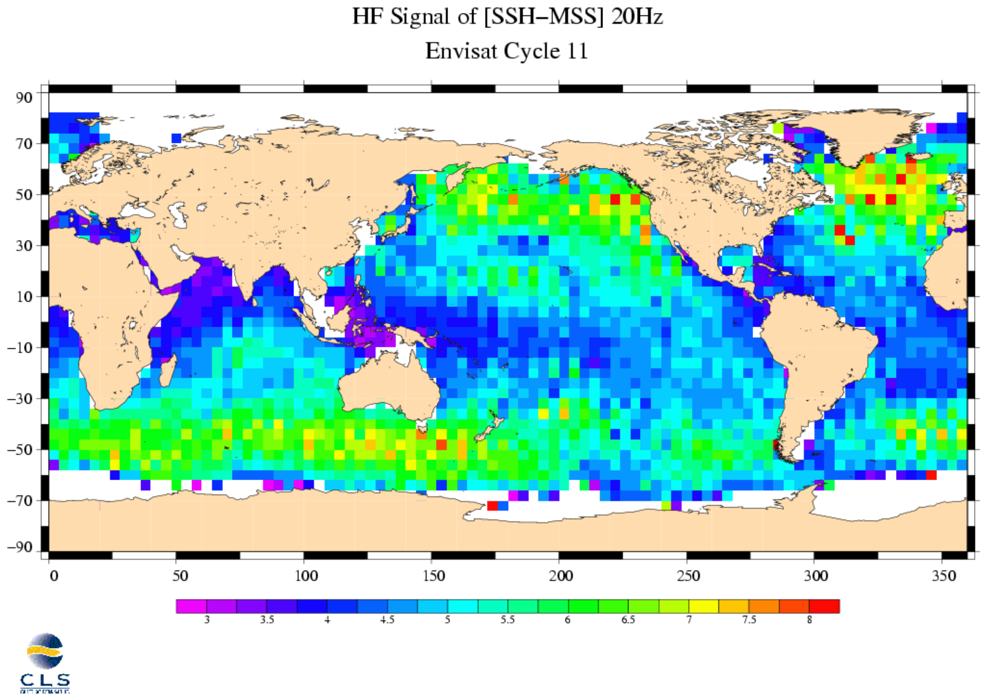

Figure 82 : Standard deviation of ENVISAT High Frequency signal, using 20Hz data

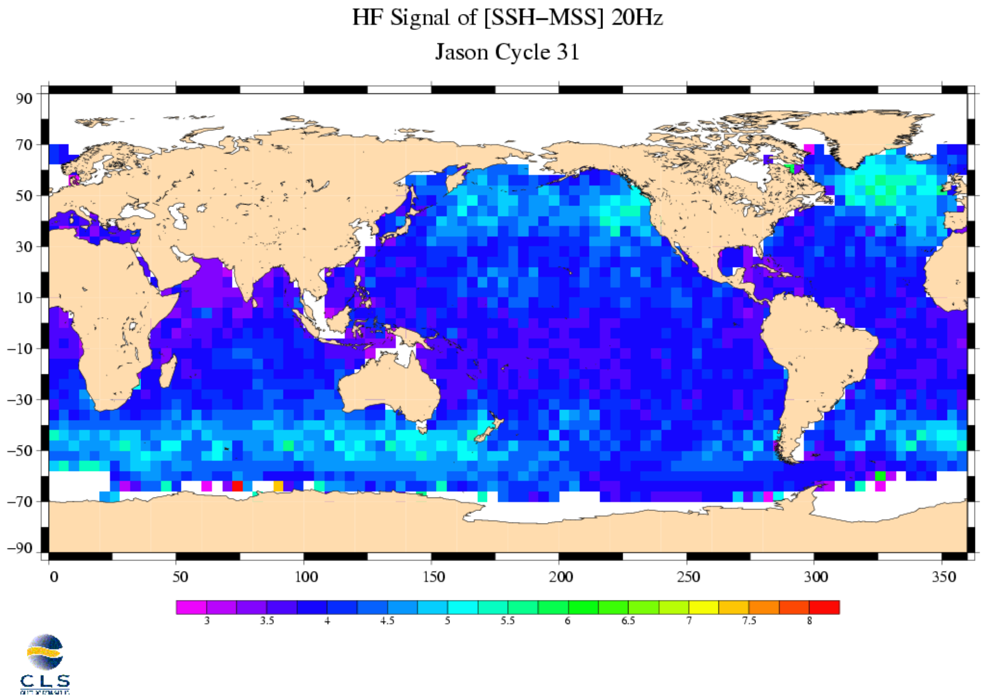

Figure 83 : Standard deviation of Jason-1 High Frequency signal, using 20Hz data

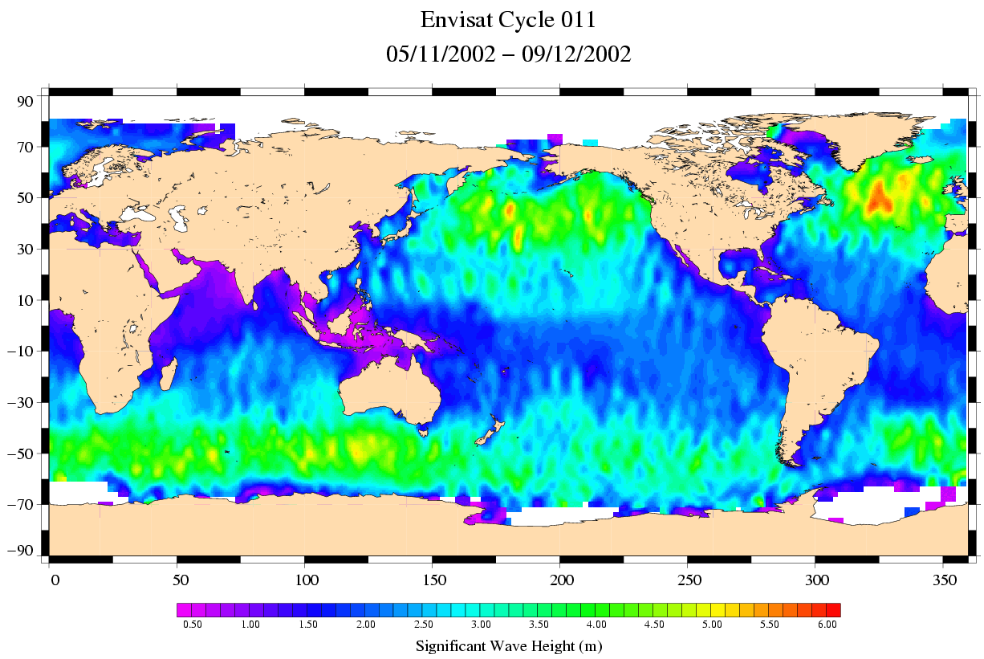

Figure 84 : ENVISAT SWH

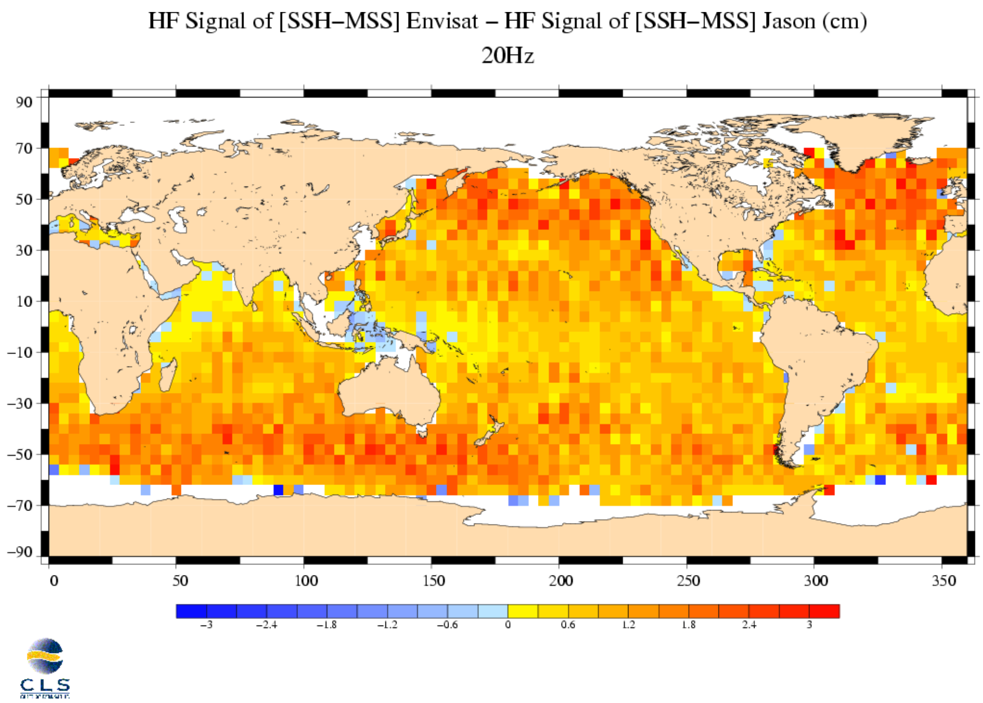

Figure 85 : Difference [Figure 83 - Figure 82]

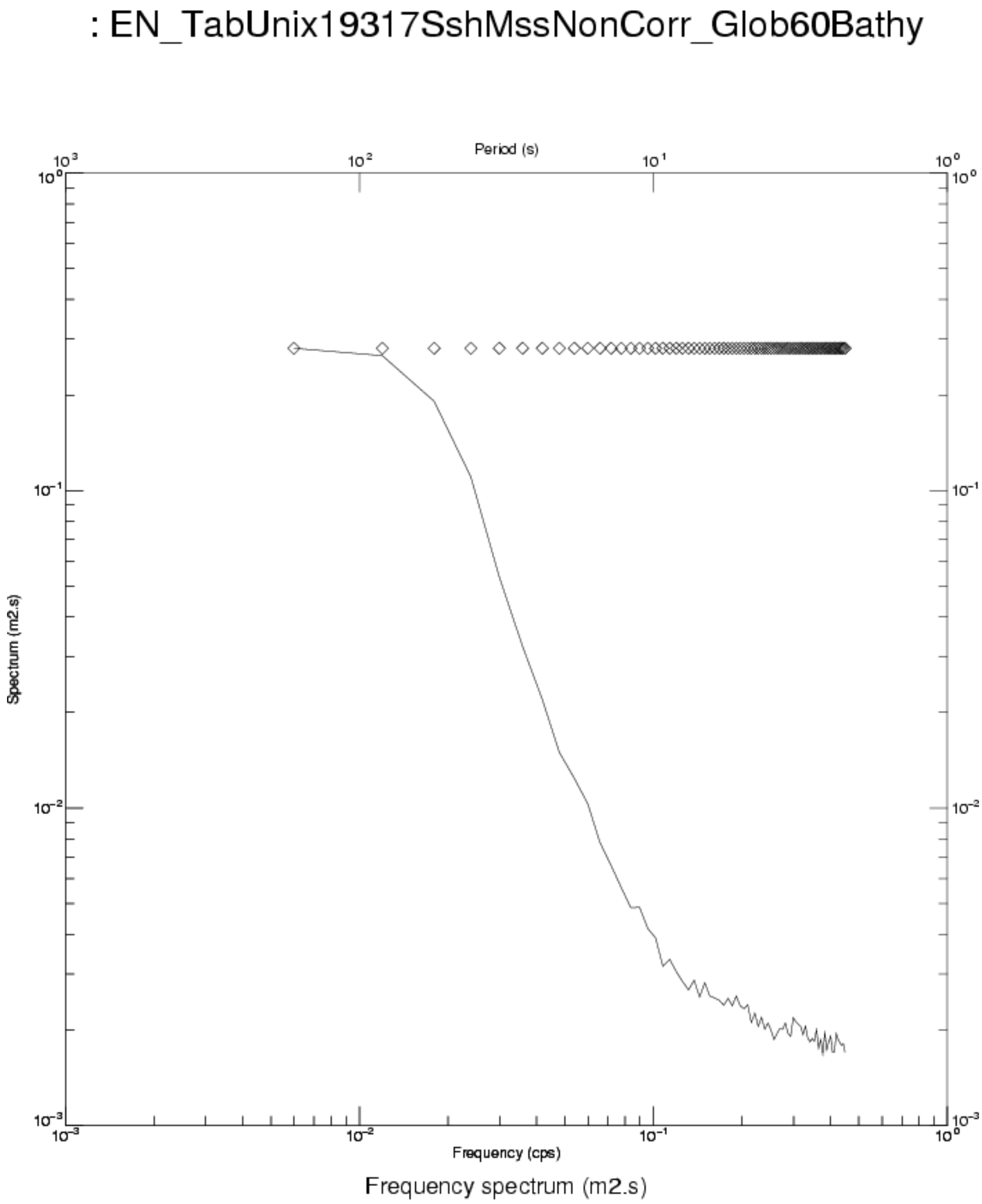

Figure 86 : Power spectrum of Envisat $SLA_{nc/mss}$, using 1Hz data

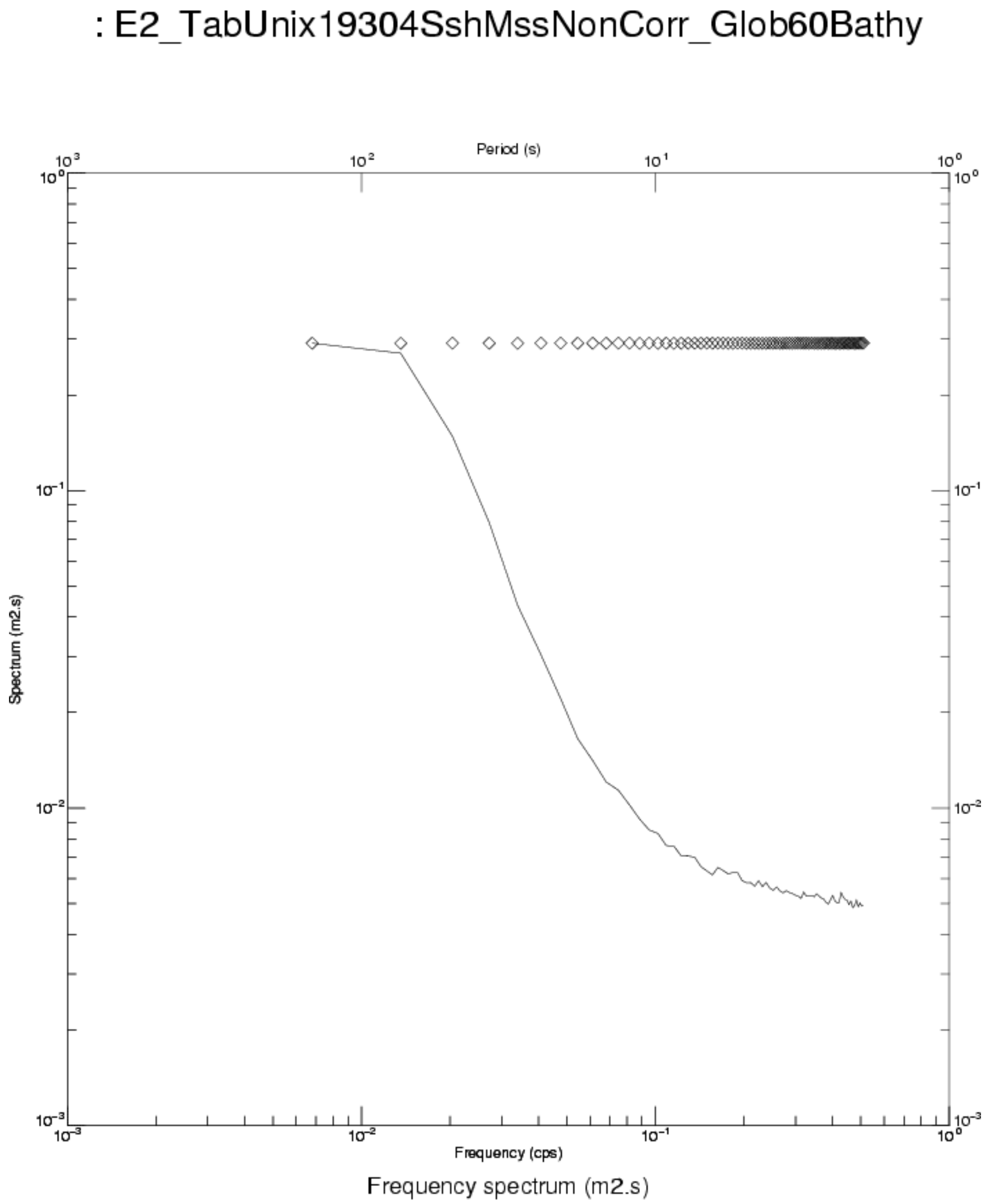

Figure 87 : Power spectrum of ERS-2 $SLA_{nc/mss}$, using 1Hz data

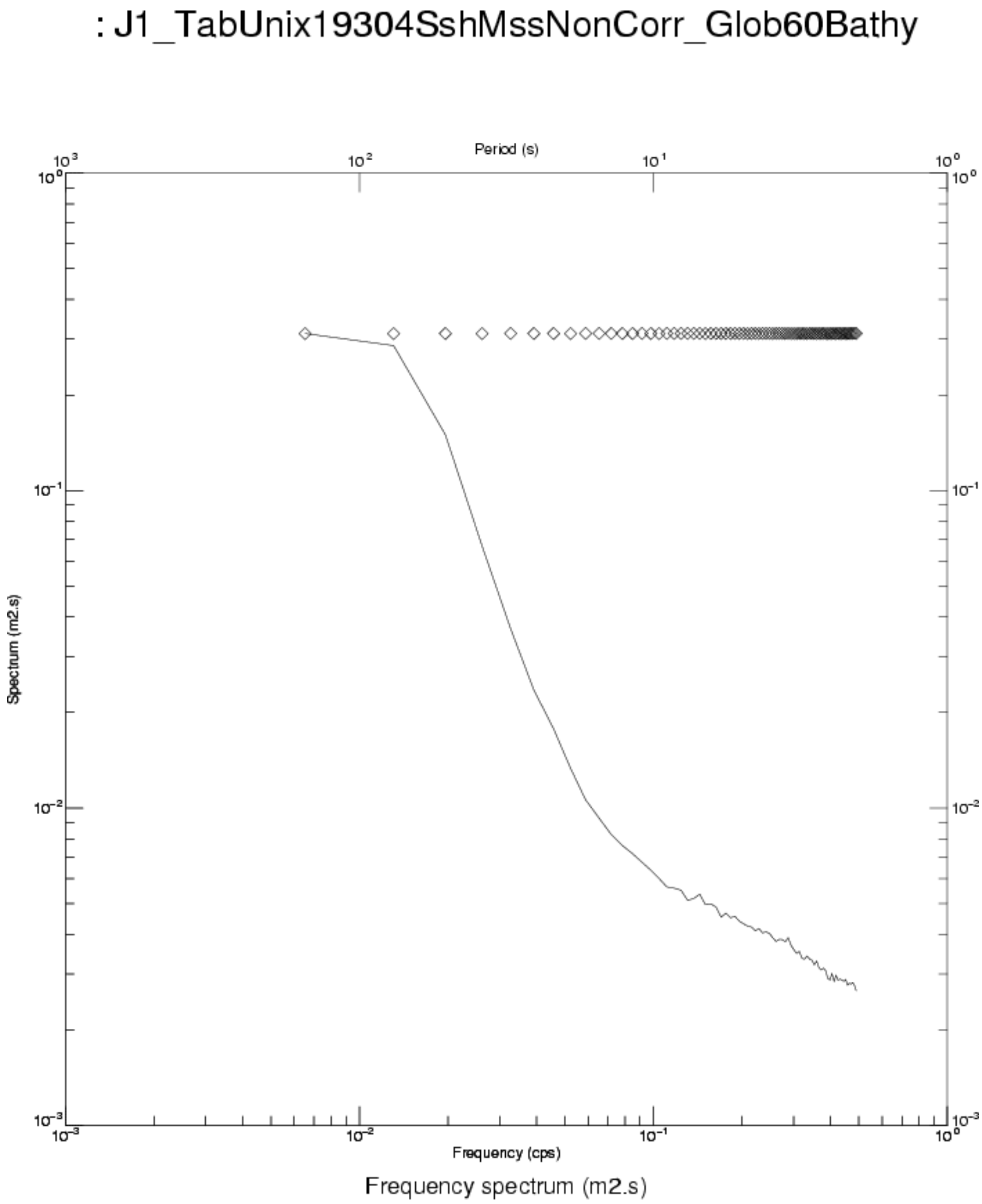

Figure 88 : Power spectrum of J1 SLA$_{nc/mss}$ using 1Hz data

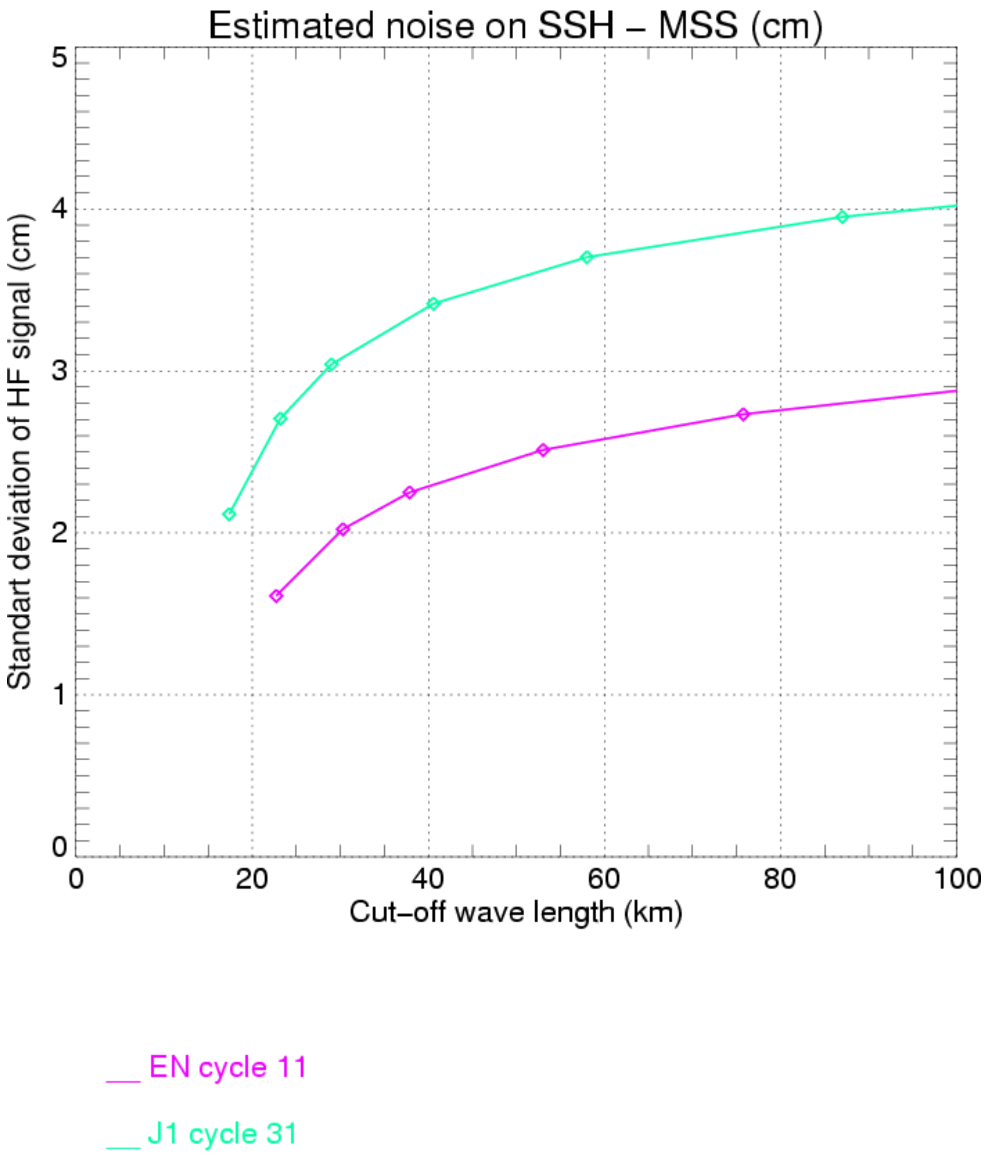

Figure 89 : Standard deviation of High Frequency signal as a function of the cut-off wave-length, using 1Hz data

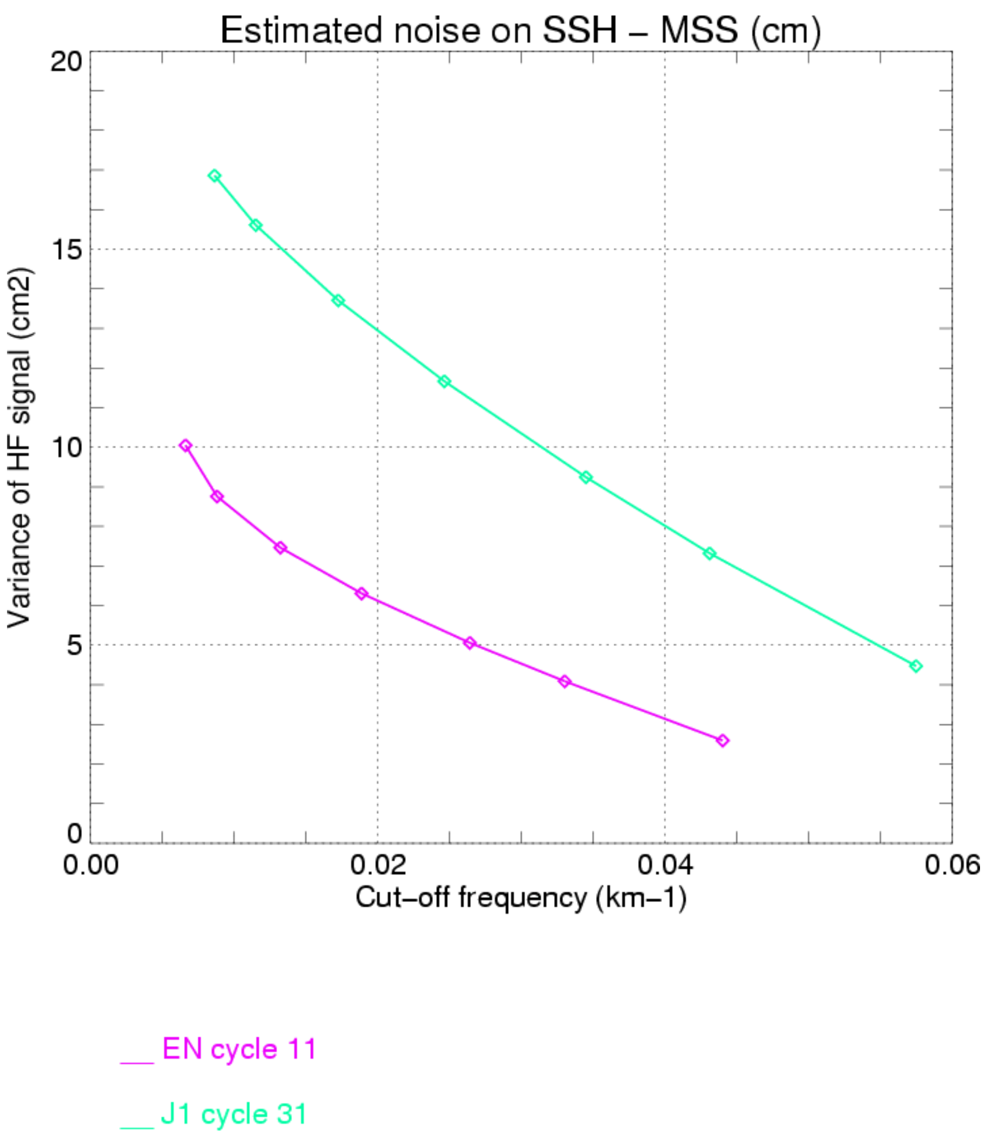

Figure 90 : Standard deviation of High Frequency signal as a function of the cut-off frequency, using 1Hz data

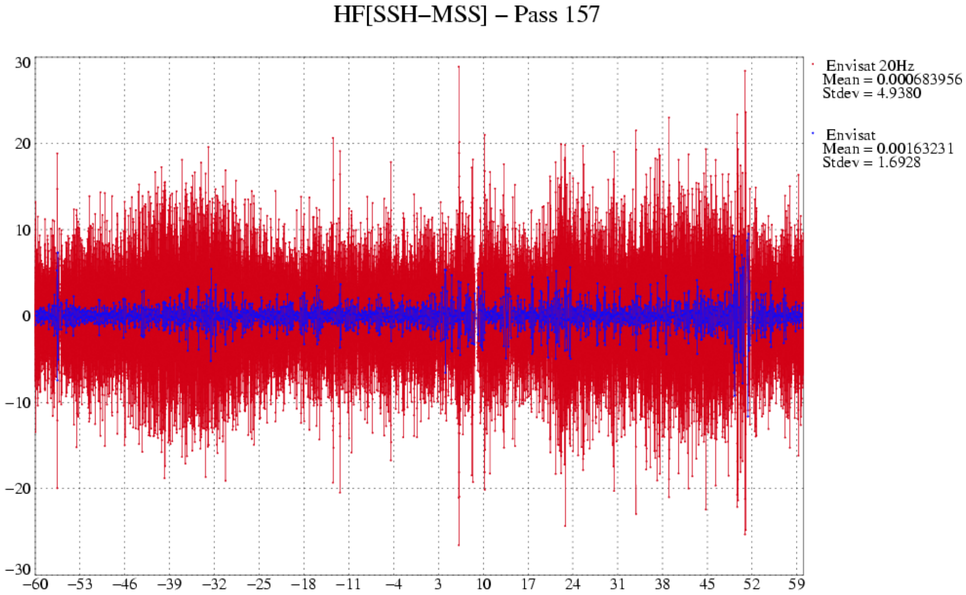

Figure 91 : HF signals, red: 20 Hz data, blue: 1 Hz data, on a particular ENVISAT pass

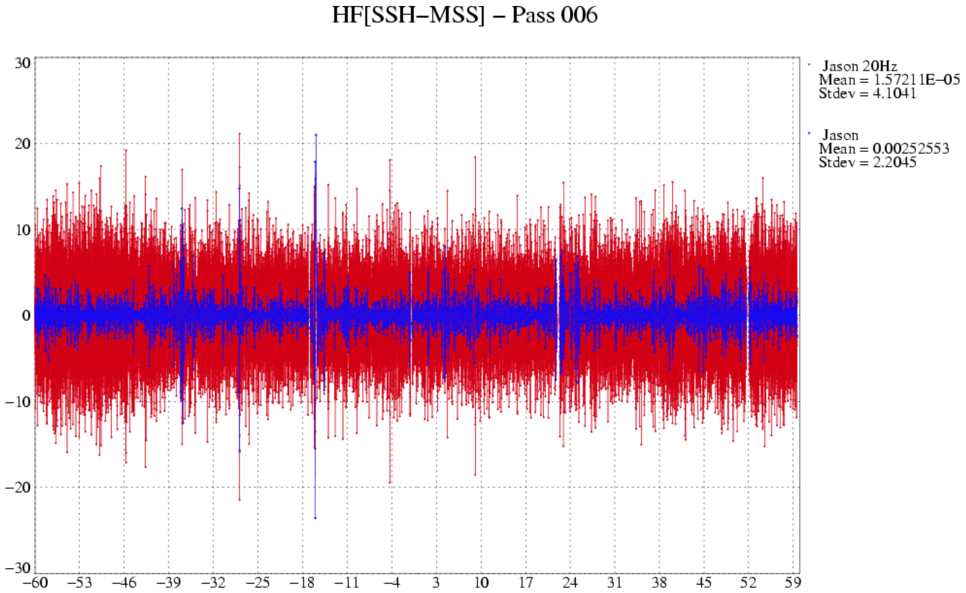

Figure 92 : HF signals, red: 20 Hz data, blue: 1 Hz data, on a particular Jason-1 pass

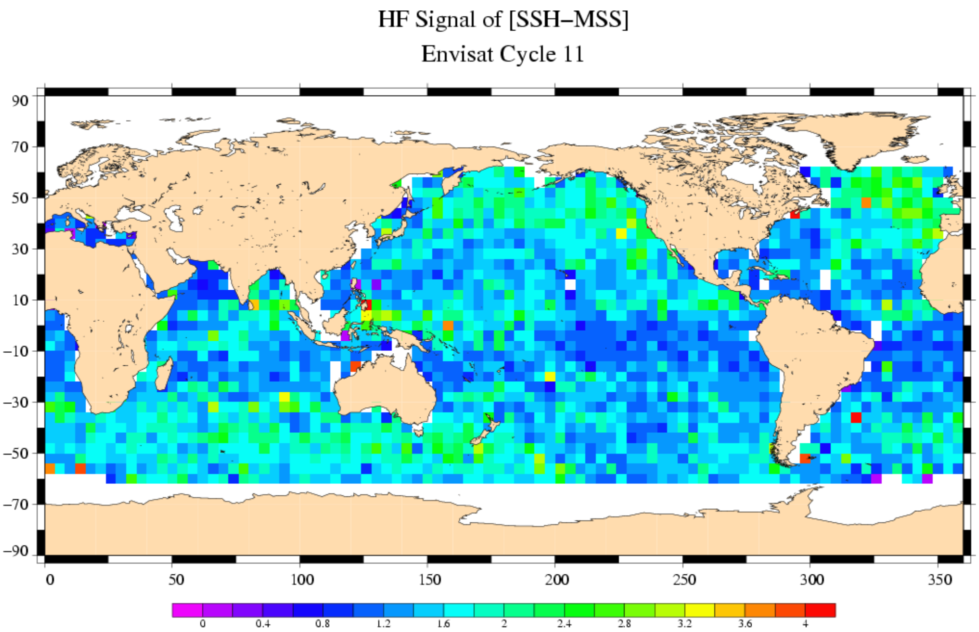

Figure 93 : Standard deviation of ENVISAT HF[$SLA_{nc/mss}$] at 1Hz

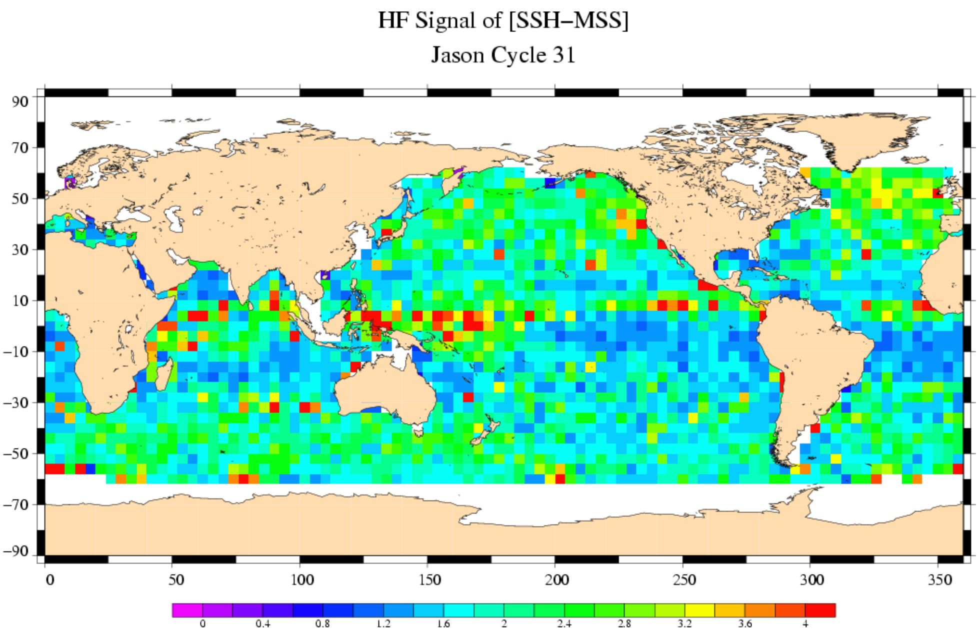

Figure 94 : Standard deviation of Jason-1 HF[$SLA_{nc/mss}$] at 1Hz

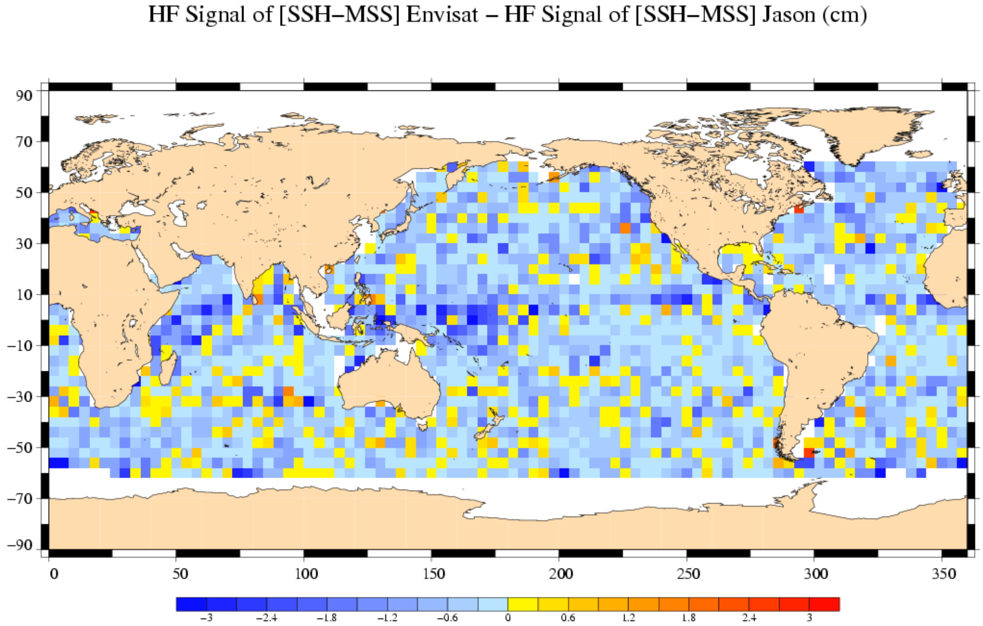

Figure 95 : Difference [Figure 94 - Figure 93]

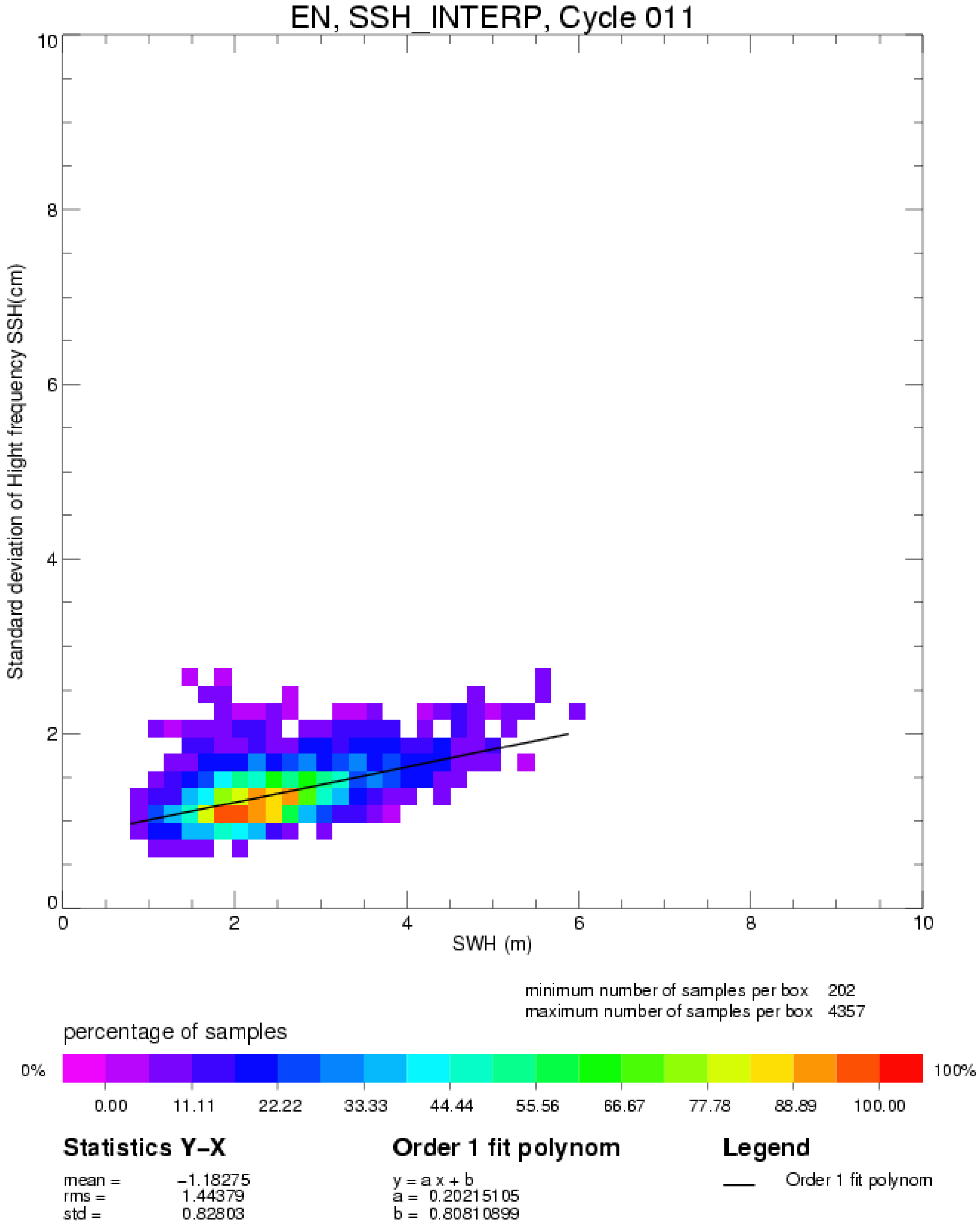

Figure 96 : Scatter plot of the standard deviation of Envisat HF[$SLA_{nc/mss}$] at 1Hz according to waves

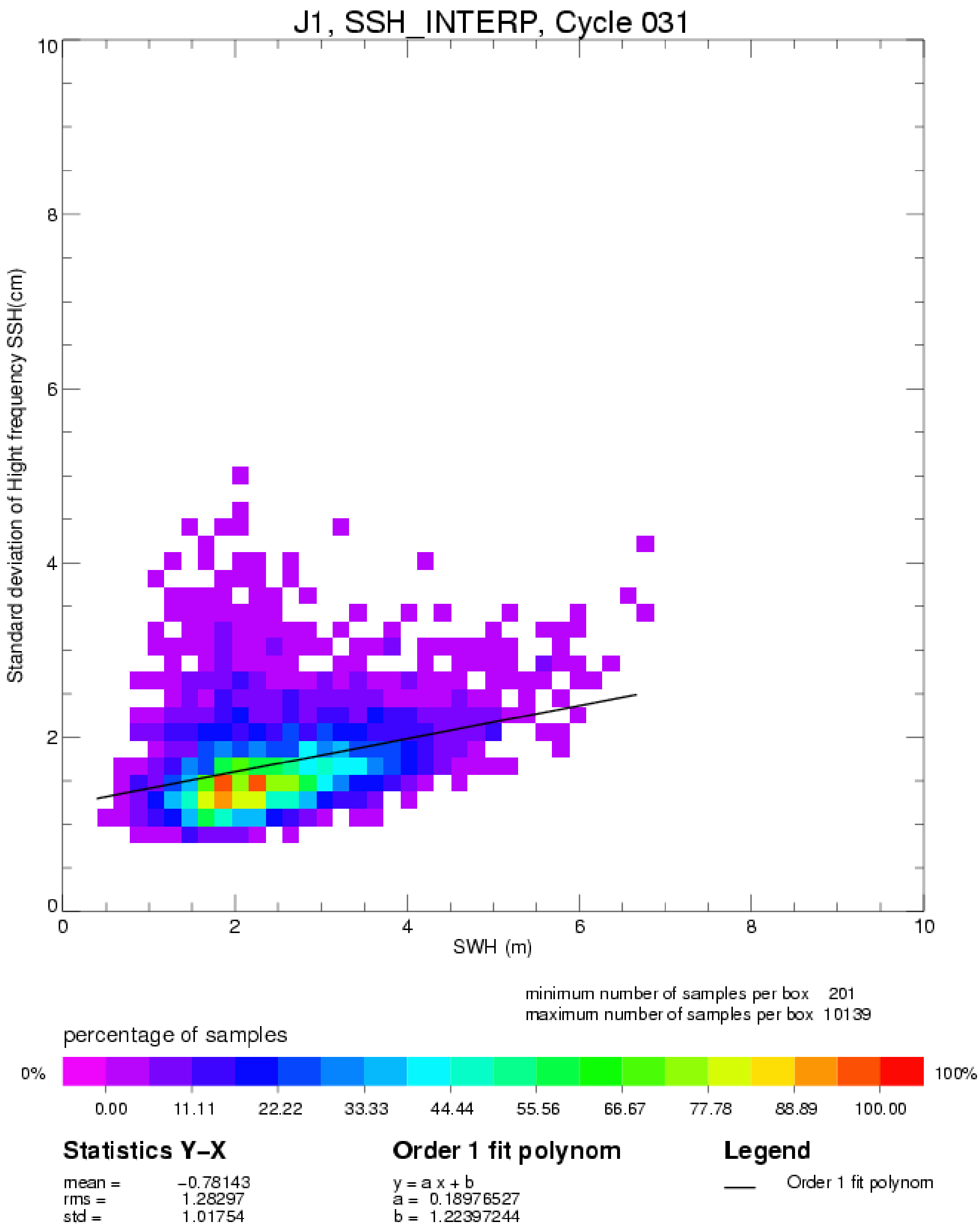

Figure 97 : Scatter plot of the standard deviation of Jason HF[$SLA_{nc/mss}$] at 1Hz according to waves